



Battelle

Columbus Laboratories
505 King Avenue
Columbus, Ohio 43201
Telephone: 614/424-4244
Telex: 24-3434

June 7, 1984

(9.a.3)

Mr. M. Silberberg
Assistant Director for Research
and Technical Support
Accident Source Term Program Office, RES
Mail Stop 1130SS
U. S. Nuclear Regulatory Commission
Washington, D.C. 20555

Dear Mel:

Enclosed for your information and use is the report summarizing our results for PWR Standard Problem Number One. The results contained in this report have been previously presented and discussed at several meetings of the Containment Loads Working Group (CLWG).

While I have found the analyses of the standard problems to be a very useful vehicle for comparing different methods for evaluating containment loads and exploring the sensitivities of these loads to input and model variations, I continue to be concerned about the application of the results of the standard problem analyses. In particular, I am troubled by statements that containment will or will not fail based on the results of the work of the CLWG. My concern with such conclusions is twofold.

First, the conditions that may lead to containment failure are not well known. Thus, any statement regarding the containment's ability to maintain its integrity must be qualified by failure criteria assumed. Just what those criteria should be are not at all clear at this time. Incidentally, the containment failure criteria need not necessarily be of a threshold nature. Second, even if the failure criteria were well defined, conclusions based on the CLWG analyses regarding containment failure would apply only over the range of conditions examined in the standard problems. While the parameters considered in PWR Standard Problem Number One are clearly in the range of interest, they are not exhaustive and may not even be bounding. For example, while the standard problem considered all the uranium dioxide and Zircaloy in the active core, the amount of steel exiting the vessel could conceivably be greater than given; one of the key factors affecting containment loads was found to be mass of debris involved. Thus, great care should be used in applying the numerical results obtained.

8507130057 850415
PDR FOIA
ALVAREZ85-110 PDR

Mr. M. Silberberg
U. S. Nuclear Regulatory Comm.

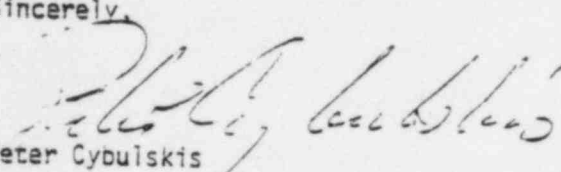
2

June 7, 1984

The above is not intended as criticism of the CLWG effort or the standard problem approach. I have found the efforts of the CLWG to be most useful. I believe the group has focused on the key issues, agreed on approaches for treating many aspects of the problem of defining containment loads, and identified some potentially important areas that have heretofore received little or no attention. My concern is with the application of specific numerical results to reach conclusions that may not be fully warranted, or that may not be supportable given the information at hand.

If I can clarify any of the above thoughts or the enclosed report, please feel free to contact me.

Sincerely,



Peter Cybulskis

PC/11j

Enclosure

~~cc: Containment Loads Working Group (18)~~

REPORT

on

PWR STANDARD PROBLEM NUMBER ONE

to

U. S. NUCLEAR REGULATORY COMMISSION

June 7, 1984

by

P. Cybulskis

BATTELLE
Columbus Laboratories
505 King Avenue
Columbus, Ohio 43201

PWR STANDARD PROBLEM NUMBER ONE

INTRODUCTION

The objective of the Containment Loads Working Group (CLWG) is to develop an updated technical position on the relatively short term (few hours duration) containment pressure-temperature loading following reactor vessel failure. A way of developing an understanding of the problem is to have a number of experts analyze well-defined situations representative of the conditions expected during the course of severe reactor accidents. Comparison of the results of such analyses would bring into focus differences in the understanding of the phenomena and methods used to treat them as well as areas of agreement among the analysts. The analysis of a series of "standard problems" was the approach selected by the CLWG.

The first of the standard problems selected was the analysis of the "steam spike" in a large dry containment PWR (Zion).

The particulars for the PWR Standard Problem Number One were given in the July 29, 1983, memorandum from M. Silberberg, NRC. This report summarizes the analyses performed at Battelle's Columbus Laboratories in conjunction with this standard problem.

APPROACH

Two types of analyses were performed at Battelle-Columbus on PWR Standard Problem Number One. The first type consisted of a series of hand calculations to consider a number of simple quenching cases; the second type consisted of a number of MARCH 2 calculations to investigate the effects of various debris-water interaction assumptions on the predicted results. Each of these sets of analyses is discussed below. Both the simple quenching analyses as well as the MARCH 2 calculations assumed adiabatic conditions in the containment, i.e., heat losses to structures were not considered. The latter condition was imposed on the standard problem to simplify the analyses and to assist in putting the several analyses on a common footing.

RESULTS

Simple Quench Analyses

A series of "hand" calculations were performed to scope the analyses, define the controlling parameters, and indicate the range of containment pressures to be expected for the conditions as defined in the standard problem. The first consideration was given to the amount of water available in relation to the mass and heat capacity of the debris. Table I summarizes the water available as given in the problem definition or inferred from other parameters. As will be shown later, if the accumulators are assumed to discharge onto the debris in the reactor cavity, there will be more than sufficient water to fully quench the core debris. For the case of the 3.2 m depth of water initially in the cavity, there will be an excess of water available. Heating of the excess water by the core debris was not considered in the simple quenching calculations.

Table II summarizes the results of the simple quenching analyses. All the results in this table are based on the quenching of 138,400 kg of debris, with the available energy going into the production of steam. The debris temperatures considered are given in the table, with the (S) and (L) denoting solid and fully liquid debris at the given temperature. The table entries for the weight of steam (WSTM) in the atmosphere correspond to the incremental steam addition for each of the individual cases considered. The first entry corresponds to the steam present in the containment prior to reactor vessel failure; the second entry gives the steam addition from the blowdown of the primary system, without any debris quenching. The last four entries in the WSTM column give the steam produced from quenching of the debris for each of the assumed debris initial conditions. Note that the maximum steam from debris quench corresponds approximately to the accumulator water inventory. The total pressure column, PTOT, gives the total pressure in the containment for each of the conditions considered, including non-condensable gases as well as steam addition. The initial pressure of 0.40 MPa was given in the problem definition; the pressure was calculated to rise to 0.48 MPa due to the release of the primary system steam inventory. The other entries

correspond to pressures resulting from the quenching of the debris for each of the conditions considered.

As noted above, the containment pressures given in Table II are based on the quenching of 138,400 kg of debris. Figure 1 presents the results of containment pressure as a function of the mass of debris quenched. As would be expected, the relationship is essentially linear. It may be noted that the latent heat of fusion assumed in these analyses corresponds roughly to 500 K of debris temperature; thus, the pressures for conditions not explicitly shown on the figure, e.g., 2033 K (L), can be easily inferred.

MARCH 2 Calculations

Following the simple quenching calculations discussed above, a number of MARCH 2 calculations were performed; the MARCH analyses duplicated some of the hand calculations as well as considering other assumptions of the debris interaction with water, as well as concrete. In the MARCH analyses, no heat losses to structures were considered, per standard problem definition, even though it could easily be accommodated. Thus, the relatively short term pressure peaks as derived from these analyses would be of principal interest, with those taking long times to develop being suspect due to the neglect of heat losses.

The MARCH calculations performed for the purpose of these standard problem analyses differ considerably from normal MARCH calculations. Rather than starting the analyses at the beginning of the accident sequence and letting the code evaluate all parameters of interest thereafter, the MARCH input was set up to deliver to the reactor cavity the quantities and conditions of core debris as specified in the standard problem. Normal MARCH runs initiated from time zero would not necessarily yield the quantities and temperatures of debris defined by the standard problem. Thus, the present set of MARCH calculations focused on the debris-water interaction model (HOTDRP) and the containment response model (MACE) in MARCH.

Table III summarizes the results of the MARCH analyses and Figures 2 - 10 give graphical presentations of selected results. The first three cases of Table III consider rapid quenching of the core debris for an assumed particle size of 5 mm and the debris temperatures indicated. These are analogous

to the simple quenching hand calculations except that the HOTDRP analyses include the effect of metal-water reactions during the quenching process. It is seen that appreciable additional clad oxidation was predicted only for the highest temperature considered, i.e., FZR goes from 0.49 at the start of quench to 0.61 when quenching is complete. The corresponding containment pressure and temperature responses for the three rapid quenching cases as shown in Figures 2 - 6. The continued increases in containment temperature following the spike due to debris quenching in Figures 3 and 5 are due to the fission product heating model in MARCH; the effect is particularly noticeable since heat losses to structures are not considered in these analyses.

Cases 4 and 5 of Table III give the results for slow debris quenching from particle beds, for two assumed particle sizes. Heat transfer from the particle bed to the overlying water is evaluated by the debris bed models in HOTDRP. In these analyses, the accumulator water was assumed to be injected on top of the particle bed and there was no further, continuing water addition. The results indicate that steam generation by the debris beds for the assumed conditions is much slower than quenching of isolated particles, as would be expected. It is interesting to note that in the case of the small particle size, substantial oxidation of the metals in the debris is predicted, indicating poor coolability and thus high particle temperatures during bed dryout. For the larger particle size considered, the quenching of the bed appears to be fast enough to preclude extensive additional reactions. Figures 7 and 8 show the containment pressure histories for these two cases.

Cases 6 and 7 of Table III consider minimal interaction between the core debris and water, but address the direct attack of the concrete; limestone and basalt concrete types are considered. The containment pressure histories for the two cases are illustrated in Figures 9 and 10. Containment pressurization due to concrete decomposition is seen to be much slower than that due to water quenching of debris. The penetration of the basalt concrete is seen to be greater than that of the limestone type. Since heat losses to structures are not included in these calculations, containment pressurization as presented here is expected to be overestimated.

DISCUSSION OF RESULTS

The hand calculations and the HOTDRP analyses of rapid debris quenching yield very similar results. This is to be expected for the simplified conditions assumed for both sets of calculations. The neglect of heat losses to structures is not expected to be a serious limitation for the short quench times predicted. Except for extremes in particle sizes, the containment pressure from debris quench would be expected to be proportional to the stored energy in the debris. For extremely small particle sizes, the reaction of the metals in the debris may be significant; for extremely large debris particle sizes, quench times may be long enough that heat losses to structures should be considered.

For the cases of slow debris quenching via particle bed, the two cases considered show a dependence on the assumed size of the particles in the bed. It will be recalled that for the cases considered, the particle beds had initial overlying water layers with no further addition of water; thus, whether the beds were intrinsically coolable or not, they would eventually heat up due to the evaporation of the coolant. For the case of the larger particle size considered, the bed quenched fast enough to preclude substantial additional metal-water reaction; the peak containment pressure in this case is largely due to steam generation from the debris quench. The rate of bed quenching is, of course, much slower than quenching of isolated particles. In the case of the small particle size considered, the bed did not quench rapidly, staying at an elevated temperature, and led to substantial additional reaction of the metals with steam. For the particular set of parameters considered, all the Zircaloy cladding, as well as a substantial portion of the steel in the debris, was predicted to have reacted with steam to generate hydrogen. While these calculations are by no means definitive, they do indicate that for marginally coolable debris beds, or beds that are subjected to dryout, considerable hydrogen production beyond that occurring in-vessel can be encountered. While this additional hydrogen does not pose a threat to large dry containments by overpressurization due to the buildup of non-condensables, its role in the event of hydrogen burning

may need further consideration. Also, the significance of such additional hydrogen could be substantially different in other containment designs.

For limited interaction of the core debris with water in the reactor cavity, early concrete attack would be encountered. The cases considered under these assumptions show that the pressurization of large dry containments due to concrete decomposition is much slower than that from water quenching of the debris. This is, of course, an expected result. The erosion of the basalt concrete was faster than that of the limestone concrete. This, again, is an known result.

While the standard problem specified both low pressure and high pressure meltdowns, only the high pressure cases were explicitly considered in these analyses. For the same debris-water interaction assumptions, the difference between the high and low pressure cases would be expected to be the pressurization due to the release of high pressure steam, or about 0.08 MPa for the present case. However, for high pressure meltdowns, there may be a significant likelihood that the core debris would be ejected from the reactor cavity following vessel failure. In the latter case, the debris escaping the cavity would in all likelihood be quenched by the water on the containment floor. For the low pressure meltdowns, there would be less likelihood of debris ejection from the cavity. Further, in the low pressure cases, the rate of debris quenching may be limited by the ability of the steam to leave the cavity and/or the ability of water to enter the cavity. The above questions of debris ejection and countercurrent flow limitations on the rate of debris quenching were not explicitly addressed in the present study.

CONCLUSIONS

The analyses discussed above have addressed the question of the steam spike loading due to debris-water interactions in a large dry containment design. The analyses show that the process of rapid debris quenching can be adequately approximated by a simple thermodynamic analysis. Slower debris quenching, such as may take place in a particle bed, may involve significant chemical reactions in addition to the heat transfer processes

and may thus require more elaborate consideration. For the range of conditions and modeling assumptions considered, peak containment pressures following vessel breach were found to range from 0.48 to 0.81 MPa, starting from the given initial pressure of 0.40 MPa. The 0.48 MPa pressure corresponds to just the release of high pressure steam from the primary system to the containment with no contribution from debris quenching. The 0.81 MPa pressure was calculated for a bed of 5 mm particles and included substantial hydrogen generation during the bed dryout process. Based on the analyses performed, and assuming that all of the core debris as defined in the problem interact with water, it is inferred that 0.5 MPa would represent a low containment pressure loading, 0.8 MPa the high loading, and 0.7 MPa the nominal loading. If less than the entire debris is assumed to participate, the loadings would be correspondingly lower. These pressure loadings assume that the energy in the debris goes into generating steam and/or decomposing concrete, including appropriate chemical reactions. These containment loadings do not include consideration of the direct heating of the containment atmosphere by the debris, nor the air oxidation of the metallic components of the debris. Such considerations may increase the containment pressures above those calculated in the present analyses. The most significant parameters with regard to the predicted containment pressure loads were found to be the mass and temperature of the debris that undergo interaction with water.

PWR Standard Problem Number One was posed to examine the so-called "steam spike" loadings in a representative large dry containment. The problem did not include consideration of hydrogen burning. It is not clear that questions of containment loads due to hydrogen burning should be excluded from consideration for these types of containments. In the cases involving rapid steam generation, hydrogen burning would be precluded by high partial pressures of steam. In the absence of large steam spikes, or in cases where the steam generation takes place over extended periods of time, hydrogen burning may not be precluded. Since the standard problem as posed did not include heat losses (steam condensation) to structures, it is not possible to draw conclusions regarding the likelihood and magnitude of possible hydrogen burns under the conditions considered.

WATER AVAILABLE

ACCUMULATOR	90,000 KG
0.5 M DEPTH	17,812 KG
3.2 M DEPTH	113,979 KG

TABLE 1.

<u>TDBR, K</u>	<u>WSTM, KG</u>	<u>PTOT, MPa</u>
---	133,357	0.40
---	40,560	0.48
2533(S)	60,770	0.67
2533(L)	76,630	0.71
2033(S)	46,464	0.63
3033(L)	90,904	0.74

WDBR = 138,400 KG

TABLE 11.

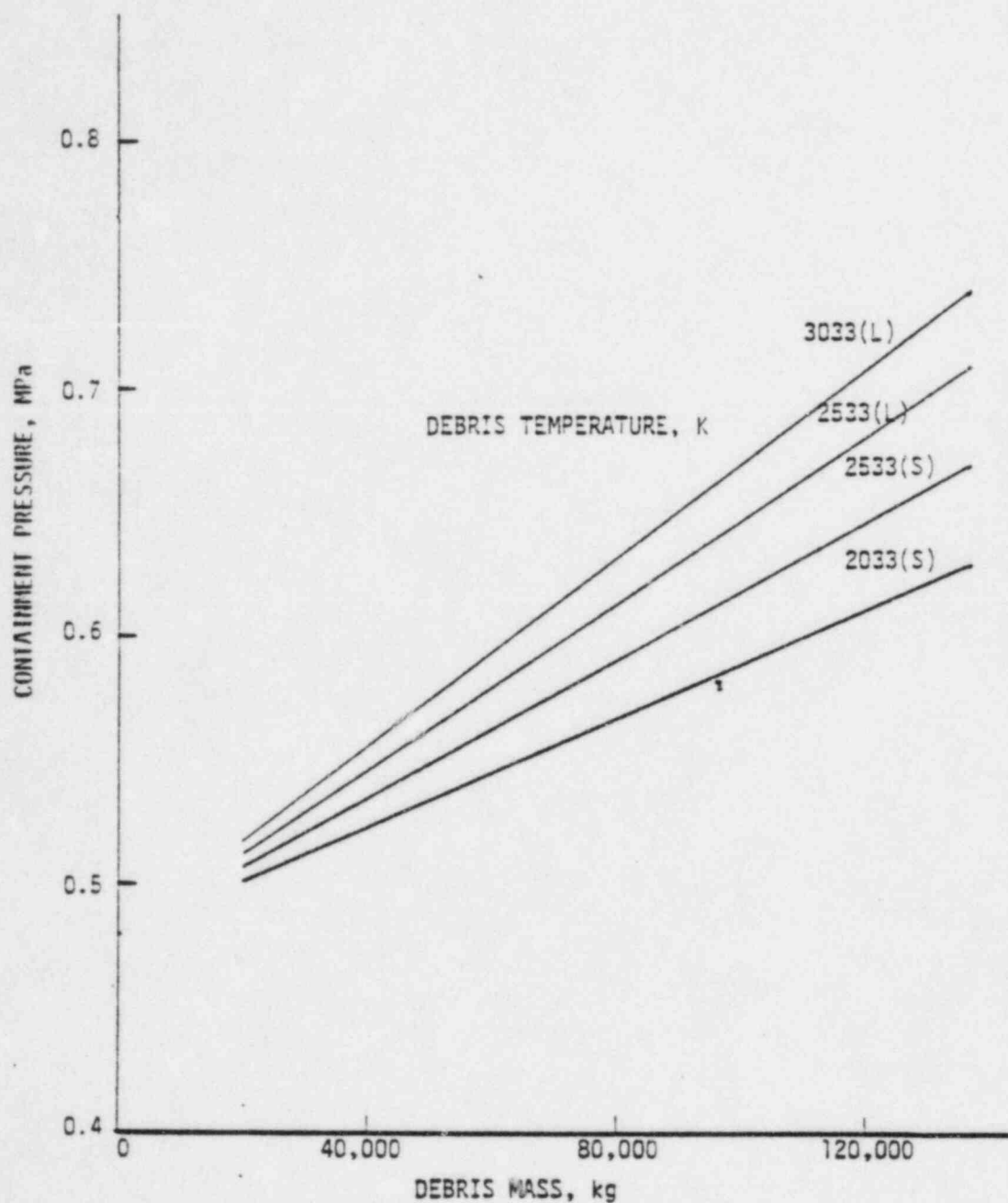


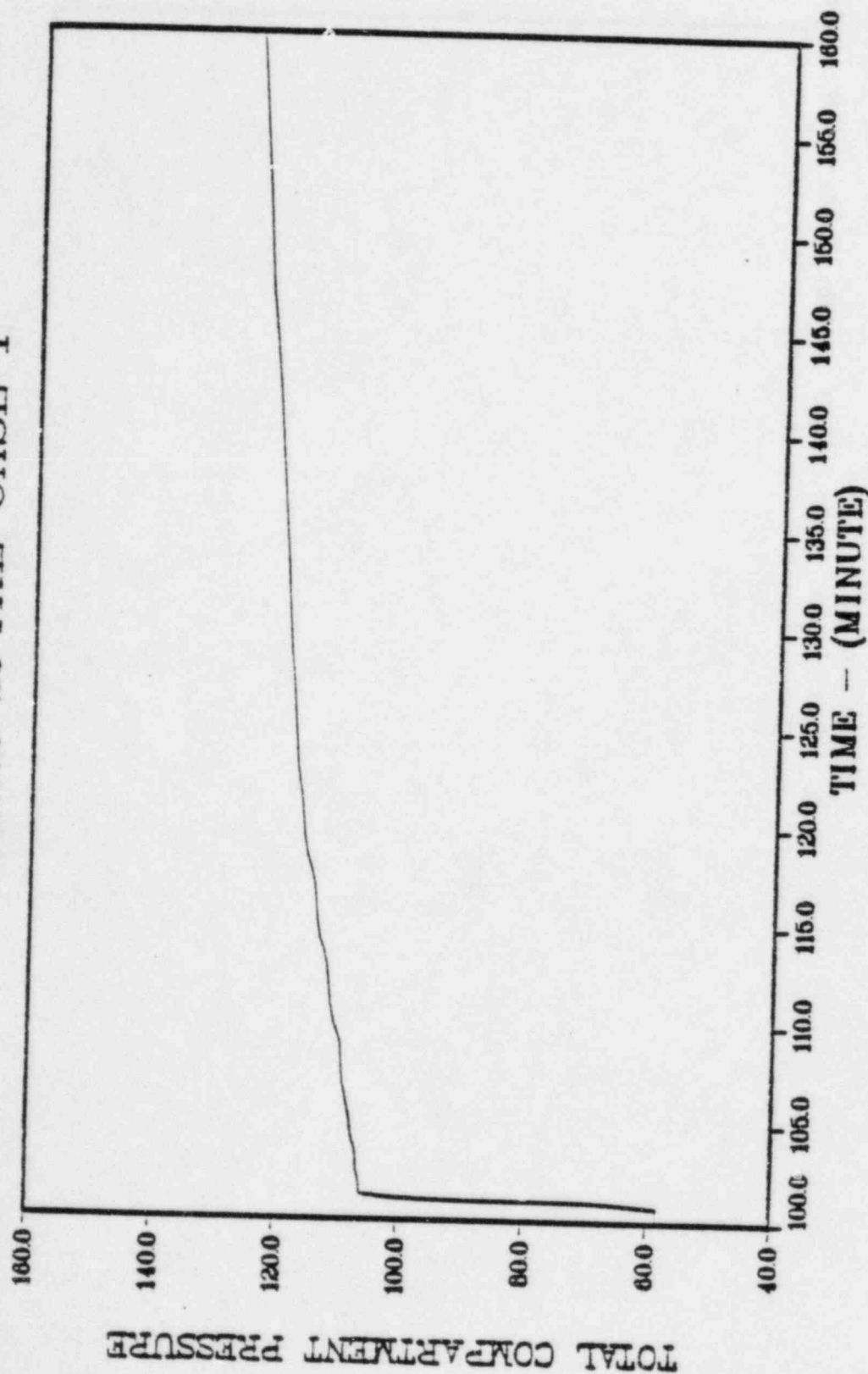
FIGURE 1.

CASE	TDBR, K	WSTM, kg	PRESSURES, MPa			DT, sec	REMARKS
			PNCB	PSIM	PTOT		
RAPID QUENCH							
2	2533(S)	58,469	0.12	0.54	0.66	17	FZR = 0.49
1	2533(L)	75,615	0.13	0.60	0.73	16	FZR = 0.53
3	3033(L)	89,994	0.13	0.65	0.79	12	FZR = 0.61
SLOW (DEBRIS BED) QUENCH							
4	2533(S)	88,543	0.17	0.64	0.81	1060	DP = 5 mm, FZR = 1.0, FFE = 0.86
5	2533(S)	79,606	0.13	0.59	0.72	770	DP = 25 mm, FZR = 0.63, FFE = 0.09
DIRECT CONCRETE ATTACK							
6	2533(S)	36,252	0.13	0.49	0.61	3600	FZR = 0.47, DZ = 12 cm, DR = 10 cm Limestone Concrete
7	2533(S)	57,250	0.14	0.56	0.70	3600	FZR = 0.96, DZ = 44 cm, DR = 23 cm Basalt Concrete

WDBR = 137,644 kg

TABLE III.

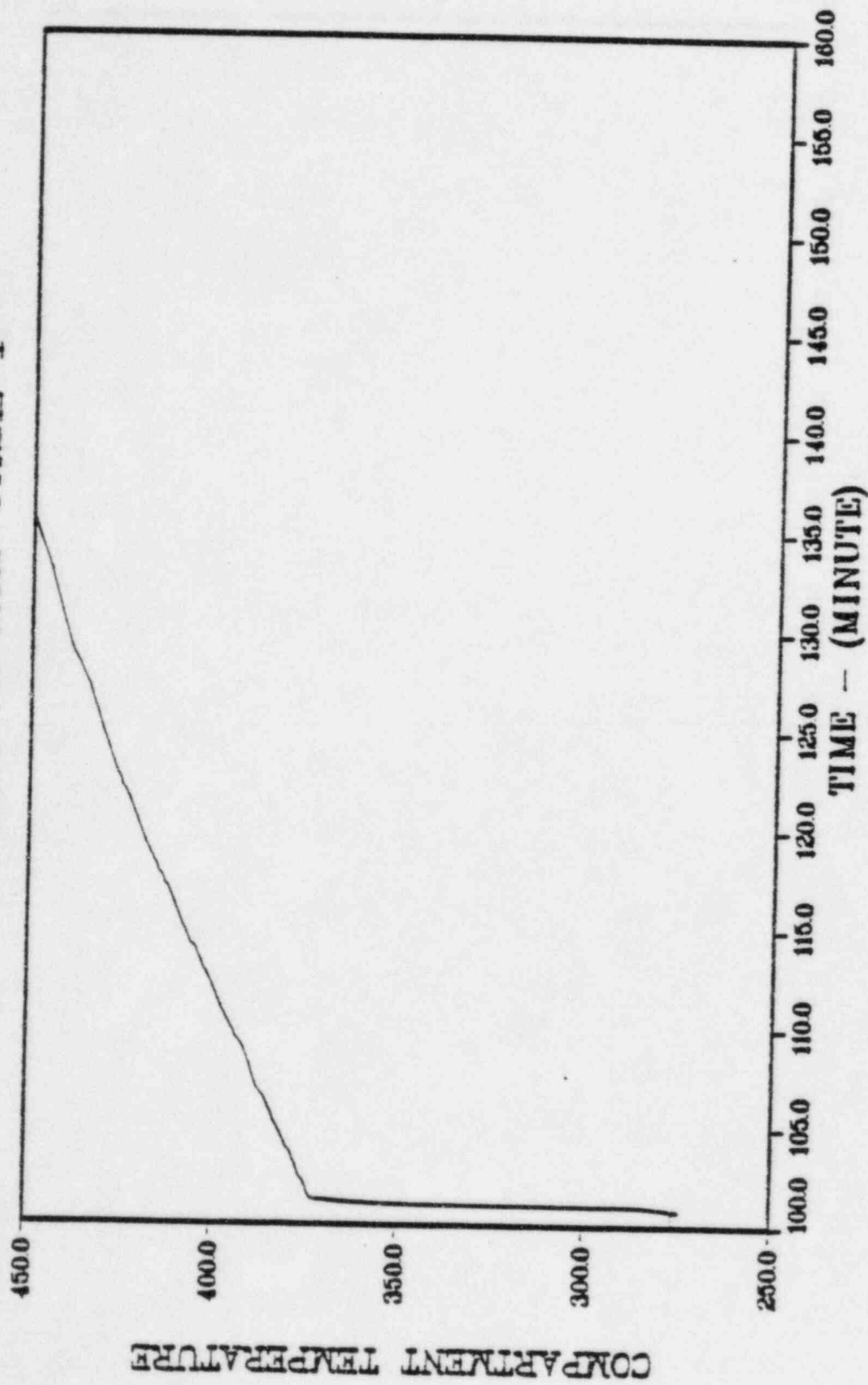
STEAM SPIKE CASE 1



VOLUME NO. 1

FIGURE 2.

STEAM SPIKE CASE 1



VOLUME NO. 1

FIGURE 3.

STEAM SPIKE CASE 2

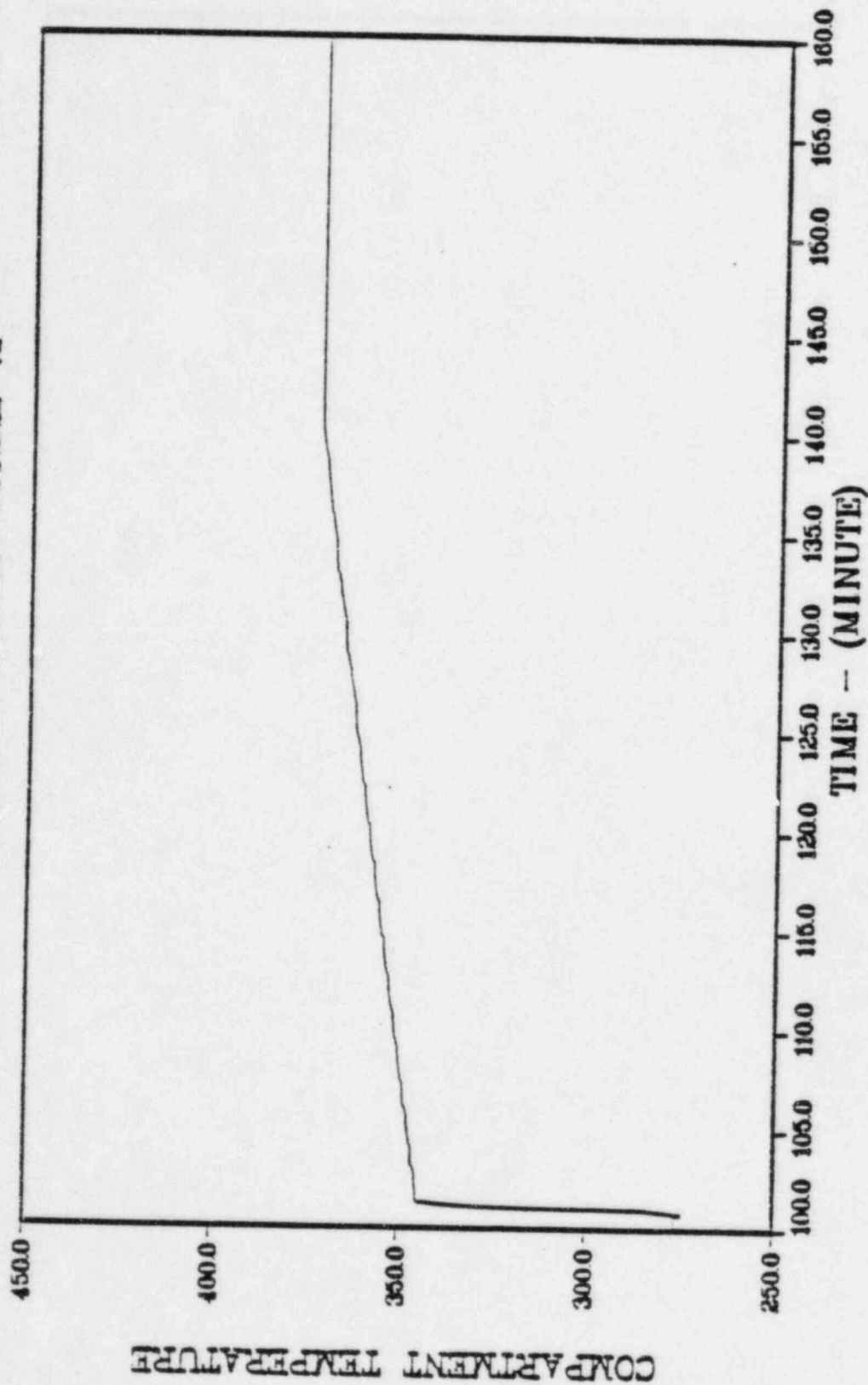


FIGURE 5.

VOLUME NO. 1

STEAM SPIKE CASE 3

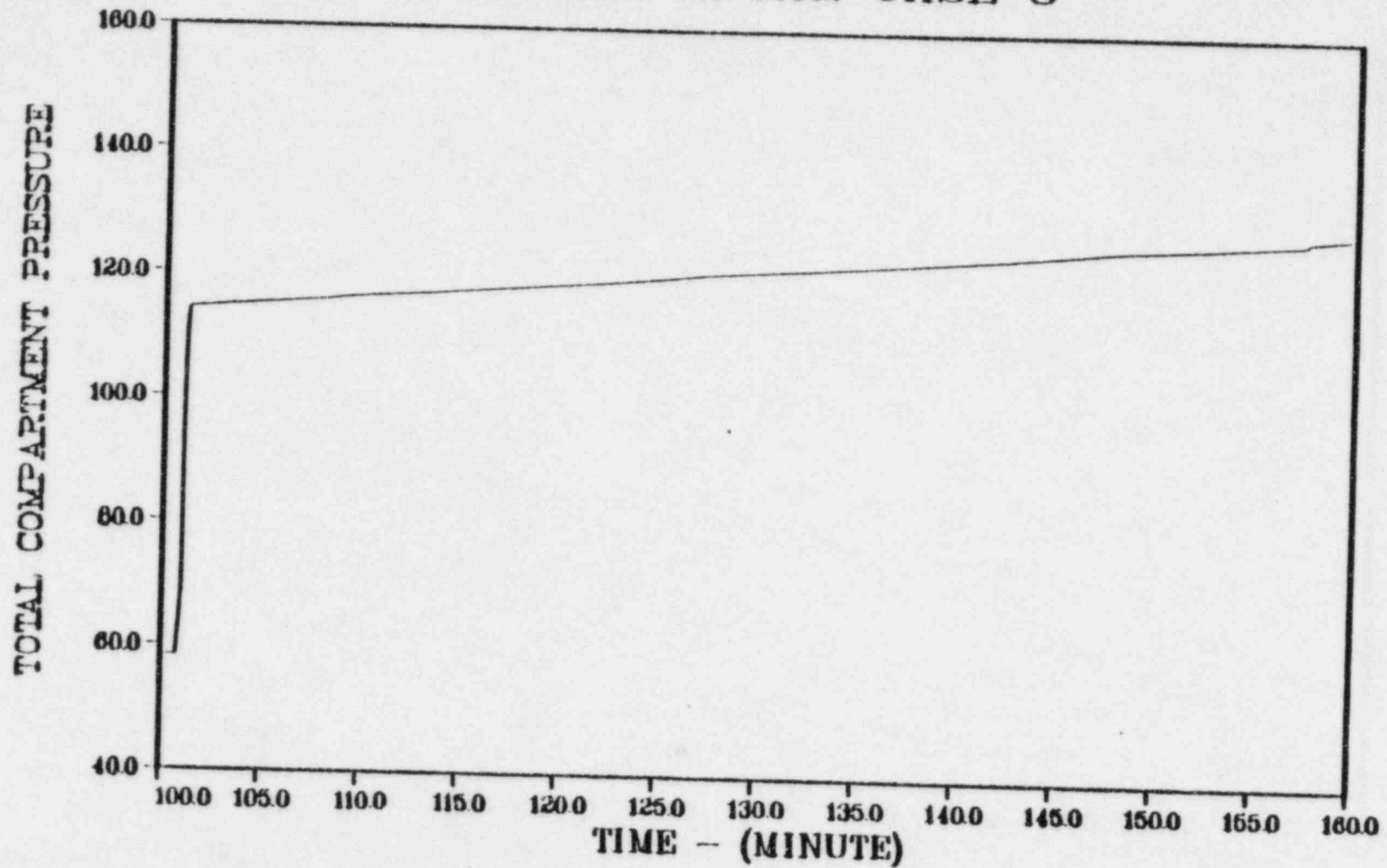
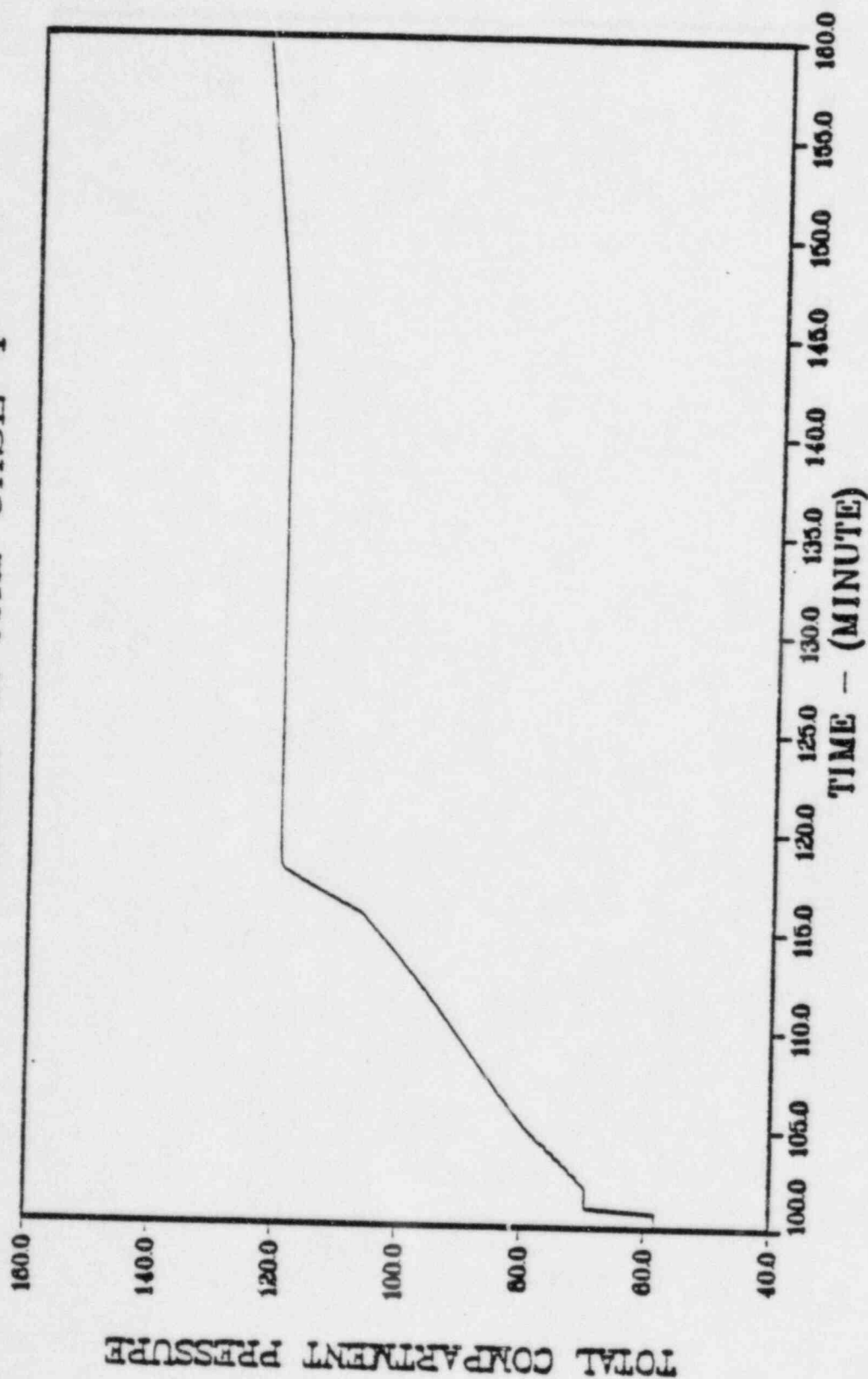


FIGURE 6.

VOLUME NO. 1

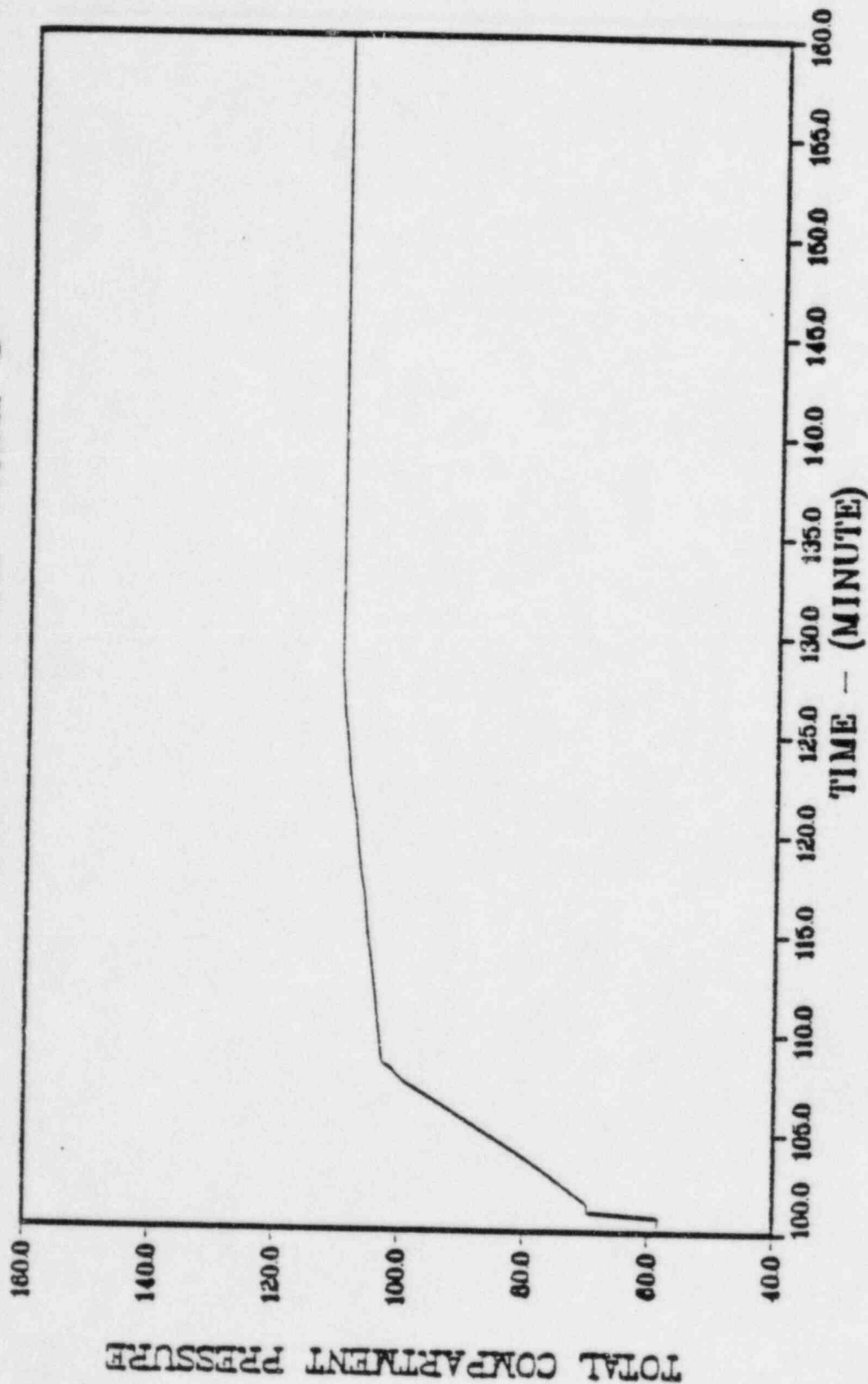
STEAM SPIKE CASE 4



VOLUME NO. 1

FIGURE 7.

STEAM SPIKE CASE 5



VOLUME NO. 1

FIGURE 8.

STEAM SPIKE CASE 6

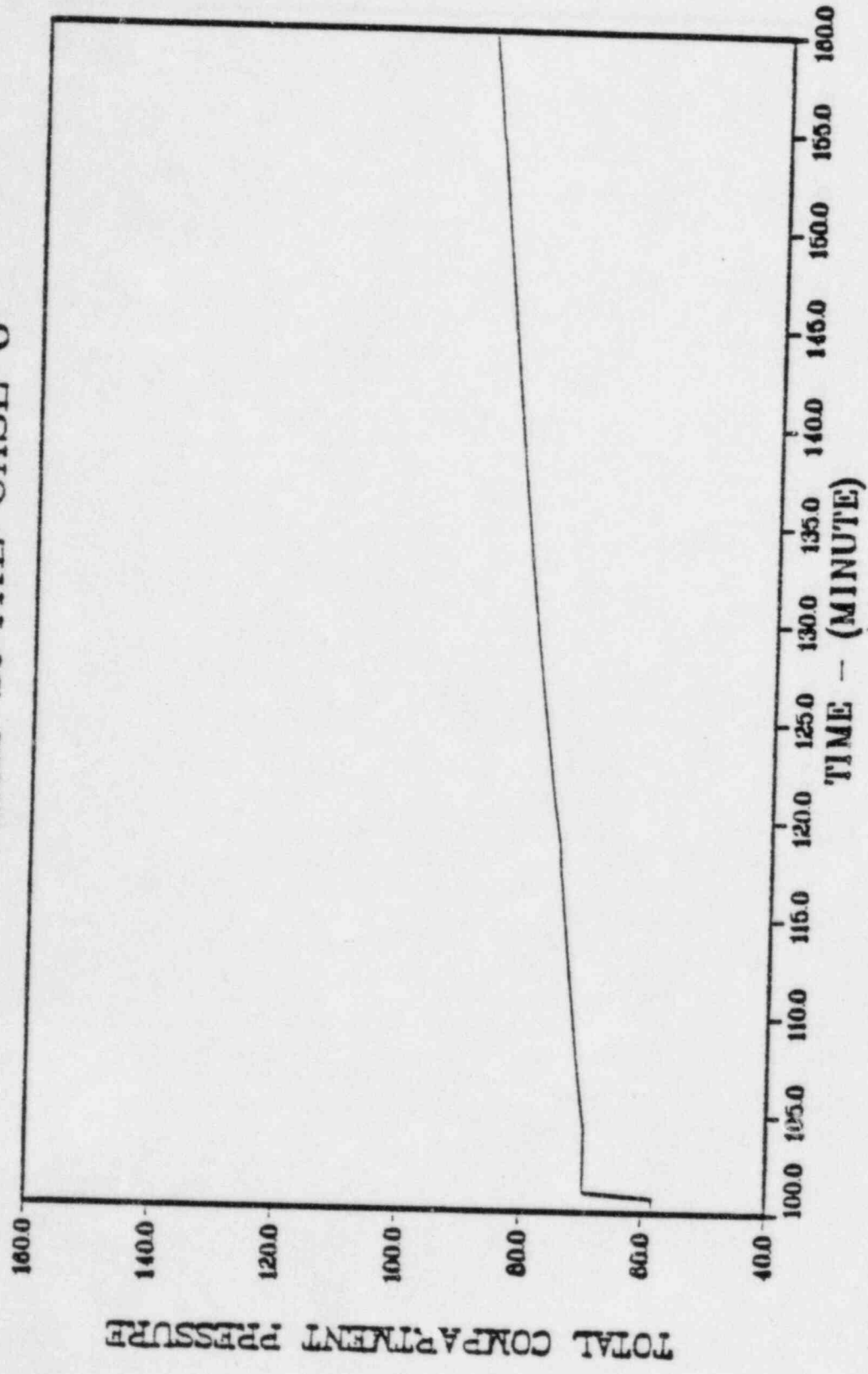


FIGURE 9. VOLUME NO. 1

STEAM SPIKE CASE 7

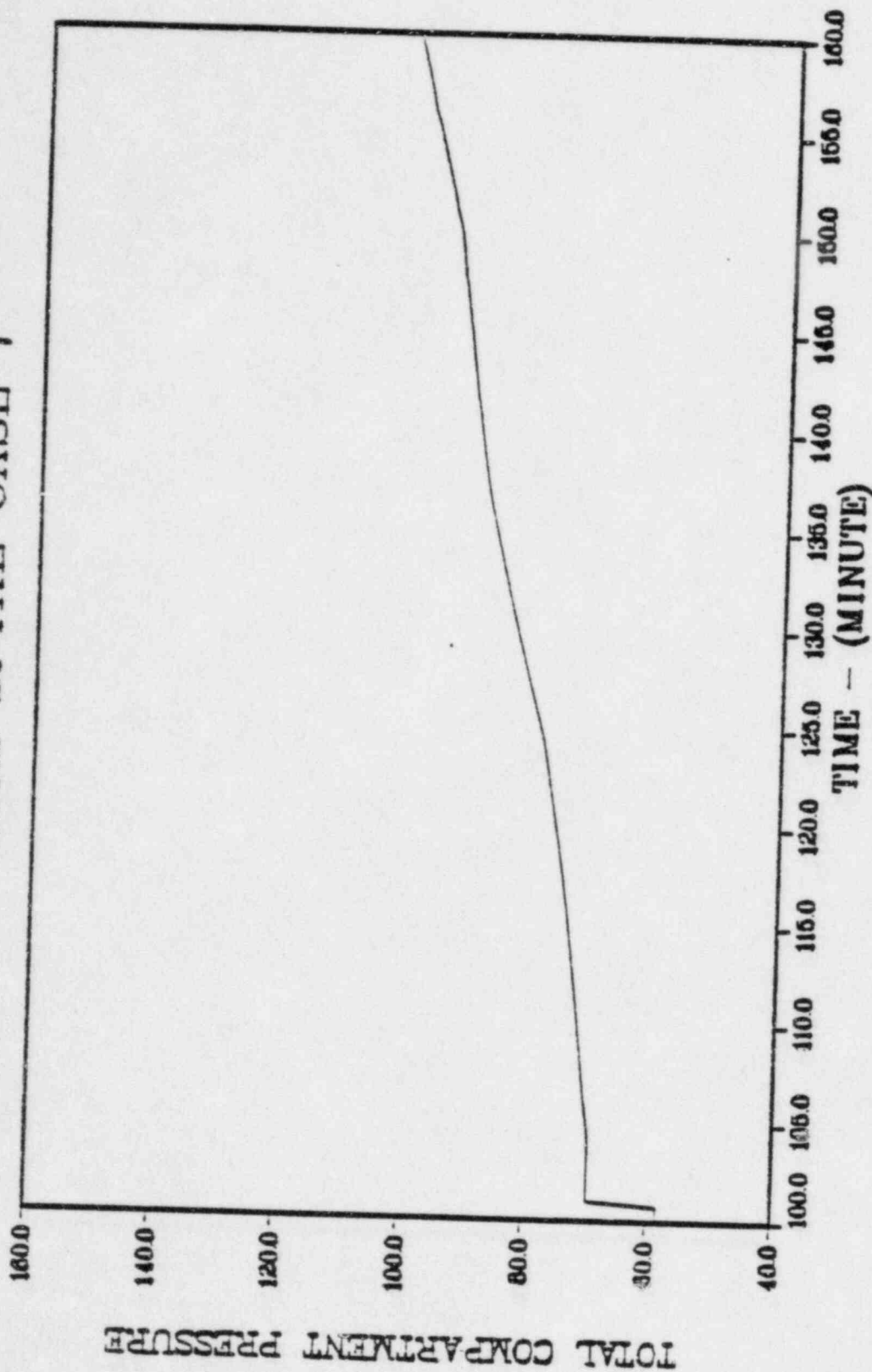


FIGURE 10.

VOLUME NO. 1

25.4.

SNL
MK I
II

June 7, 1984

(9.d.3)
(9.e.3)

Dr. Trevor Pratt
Building 130
Brookhaven National Laboratory
Upton, N.Y. 11973

Dear Trevor:

Attached you will find the letter report which details Sandia's MARCON analysis of the EWR MARK I and II Standard Problems as outlined in the January 20, 1984 Memorandum from Melvin Silberburg, "Completion of EWR MARK I, MARK II Standard Problems." In general, we have retained the case numbers used in that memo with one exception. The Case 1 results with zero upward pool radiative heat transfer has been labeled Case 1C.

You will find a fairly complete description in Section I of the assumptions used in the analysis as well as the important physical properties. The results for the MARK I calculations are found in Section II while those for the MARK II are located in Section III. Appendix A contains a brief description of the MARCON modeling used in these calculations. Please note that the MARCON modeling for the EWR analysis was developed AD HOC for that specific purpose and that the modeling is still in a developmental phase. A listing of the updates for "hardwiring" the initial conditions and a listing of the MARCH and CORCON input decks for MARK I Case 1 and MARK II Case 5 are included in Appendix B.

An attempt has been made to address the problem which was discussed at the May 10, 1984 Chicago working meeting regarding the effective concrete heat capacity during concrete degassing. The heat of vaporization for the free water content together with the heat of reaction for decomposition of the bound water have been added to the heat capacity over the assumed temperature range. The effect is an increase (over the dehydration-temperature range, 200-500°F) in Cp of approximately a factor of 3. In terms of containment response, the pressures are lower by 35 to 50 psi (for Case 1) and the temperatures were

reduced by nearly 200°F. It should be noted that, although the higher value of Cp should apply only to the temperature range over which degassing occurs and only to the spacial nodes that are within that temperature range the current MARCH code modeling does not allow for a temperature or positional dependence in thermo-physical property. As a result, the constant Cp used should over-predict the heat absorbing capacity of the concrete.

If you have any questions, please contact me at (505) 846-2486.

Sincerely,



R. D. Gasser
Reactor Safety Technology
Division 6411

RDG:6411:cgt
Attachment
243B

Copy to:

BCL	P. Cybulskis, w/att	6410	J. W. Hickman
BNL	G. A. Greene, w/att	6411	A. S. Benjamin, w/att
VRB	M. A. Cunningham	6411	V. L. Behr, w/att
NRC	M. Silberburg	6411	A. L. Camp
NRC	T. J. Walker	6411	R. D. Gasser
ORNL	S. A. Hodge, w/att	6422	D. A. Powers
Purdue	T. Theofanous	6440	D. A. Dahlgren
RMA	C. J. Shaffer, w/att	6442	C. V. Subramanian
SAI	L. N. Smith, w/att	6444	R. K. Cole

MARCON Results for Mark I & II
Containment Standard Problems

R. D. Gasser
F. E. Haskin
V. L. Behr
C. Shaffer
L. Smith

May 1984

I. INTRODUCTION

The series of seven cases outlined in Table 2 of Reference 1 for the BWR Mark I standard problem together with seven of the nine cases identified for the Mark II standard problem have been run at Sandia utilizing the MARCON code. These cases nominally consist of a baseline case (Case 1 for the Mark I and Case 5 for the Mark II) and a number of additional cases in which key parameters have been varied (see Tables I.1 and I.2) to determine the sensitivity of the containment response to those selected parameters. The term "baseline" here refers to the case against which other cases in the current analysis are being compared. It does not imply a higher probability. An additional case was inserted in both the Mark I and Mark II matrices in which radiation from the top surface of the molten pool was "switched off" with a view to assessing the relative effects of drywell heating due to radiation and gas generation.

This report is organized into three main sections: an introductory section, a section covering the Mark I standard problem, and the last section which treats the Mark II standard problem. In addition, a brief description of the MARCON modelling is included in Appendix A. Appendix B contains a listing of the input for the baseline cases.

The primary tool used in the Sandia analysis of the BWR standard problems was the MARCON code. For a detailed description of the MARCON code, see Appendix A. In brief, however, the MARCON code consists of a composite "hard link" of the MARCH 2.0 (Version 111) and CORCON MOD2 codes. The CORCON code has been utilized in MARCON to supplant the INTER subroutine in MARCH. Both INTER and CORCON calculate the source terms which emanate from the thermal and chemical interaction of molten core debris with concrete in the reactor cavity, but CORCON is considered to be significantly more sophisticated than the older INTER code. In the version of MARCON, which was utilized in the present analysis, the CORCON code delivers energy to the drywell atmosphere in two ways. First, the gases generated in the attack of molten debris upon concrete convectively transfer heat from the pool to the atmosphere. And secondly, heat is transferred from the molten pool surface directly to the atmosphere by radiation. The assumption is made in the latter mechanism that sufficient aerosols, steam, and CO_2 are present in the atmosphere to render it opaque to radiation. In addition, it is assumed that the drywell atmosphere is well mixed by natural convection and by the gases generated in the molten pool, and that the aerosol particles are in thermal equilibrium with the atmosphere. The code has been modified to include radiative heat transfer from the drywell atmosphere to the containment passive heat structures as well.

A rather simplistic model was developed and included in the MARCON code in an attempt to assess the magnitude of the contribution to containment response due to degassing of the concrete heat structures in containment (see Appendix A for a description of the model). The model allows for the outgassing of both steam and CO₂, depending on concrete composition. To allow for diffusional delays, the steam, (from free and bound water) for example is assumed to come out of the concrete linearly over a specified (input) temperature range. In this analysis, it was assumed that steam begins to outgas at 200°F and is completely removed by 500°F (to allow for the presence of bound water). The model has some inherent problems, the most serious one being the difficulty of accounting for the energy involved in phase changes and chemical reactions. Without completely removing the finite difference solution used for the heat structures in MARCH and incorporating a solution that includes volumetric heat sources and sinks and convective terms, the problem cannot be solved rigorously. However, an approximation can be made by adjusting the concrete heat capacity to account for these effects.

It should be emphasized that the accident scenario which has been analyzed in the present exercise must not be construed to be one that we necessarily believe to be realistic or credible. The object of these exercises was to compare results obtained at a number of laboratories and to identify areas of uncertainty in phenomenology and methodology that may require more detailed study. It is felt, for example, that a high pressure failure of the primary system is not consistent with the rather limited distribution of core debris (three to five meters) that has been specified in both Mark I and Mark II standard problems. Similarly, although such questions as direct heating effects and the possible energetic relocation of core debris into the Mark II wetwell have been treated separately, these effects have not been directly factored into the assessment of containment response.

Table I.3 contains some of the physical properties and compositions of the concrete heat structures. Table I.4 shows the composition of type 304 stainless steel together with chemical reactions by which the steel is believed to be oxidized during the core melt phase. These reactions are used to estimate the quantity of hydrogen generated in-vessel and to establish the initial composition of the molten debris at the time of vessel failure for the various conditions defined in Tables I.1 and I.2. The quantities of the chemical species present in the debris at vessel failure are given in Table I.5.

TABLE I.1: Mark I Standard Problem Definitions

Case	1	1A	1B	2	3	3A	4
Corium Spread, m	5	5	5	3	5	5	3
Debris Temperature, F	4130	4130	4130	2700	4130	4130	2700
Concrete Type	L	L	L	L	B	B	B
Free H ₂ O, %	3	6	3	3	4	8	4
Steel in Corium, lb _m	140K	140K	85K	140K	140K	140K	140K
Pool Losses, %	0	0	0	0	0	0	0

KEY

L - Limestone
B - Basalt

TABLE I.2: Mark II Standard Problem Definitions

Case	5	5A	5B	6	7	7A	8
Corium Spread, m	5	5	5	3	5	5	3
Debris Temperature, F	4130	4130	4130	2700	4130	4130	2700
Concrete Type	L	L	L	L	B	B	B
Free H ₂ O, %	3	6	3	3	4	8	4
Steel in Corium, lb _m	140K	140K	85K	140K	140K	140K	140K
Pool Losses, %	0	0	0	0	0	0	0

KEY

L - Limestone
B - Basalt

Table I.3

Material Properties for Different Concrete Types

<u>Property</u>	<u>Limestone(L)</u>		<u>Basalt(B)</u>	
Thermal Conductivity (W/cm/K)	0.01385		0.015	
Specific Heat (J/gm/K)	0.996		1.7	
Density (g/cm ³)	2.52		2.4	
Weight Fractions: 8%	3%	6%	4%	
CaCO ₃	0.80	0.77	0.01	0.01
Ca(OH) ₂	0.15	0.15	0.18	0.18
SiO ₂	0.01	0.01	0.57	0.53
Free H ₂ O	0.03	0.06	0.04	0.08
Al ₂ O ₃	0.01	0.01	0.20	0.20
Solidus Temp. (k)	1690		1350	
Ablation Temp. (k)	1750		1450	
Liquidus Temp. (k)	1875		1650	
Emissivities				
Concrete Surface	0.5		0.5	
Oxidic Phase	0.5		0.5	
Metalic Phase	0.5		0.5	
Surroundings	0.7		0.7	
Rebar (kgFE/kgCONC)	0.135		0.135	

Table I.4

Chemistry and Debris Composition

304 Stainless Steel	Cr	19%
	Ni	9.5%
	Mn	2%
	Si	1%
	Fe	68.5%
	C	<.1%

15% Steel Oxidation According to:



Excess Fe According to:



In-vessel Oxidation of Zr for Equivalent Oxidation
of 13% Zr + 15% Steel for 140,000 and 85,000 lb.

140,000 Lb. FDCR = .2778

85,000 Lb. FDCR = .2197

Table I.5
Debris Composition at Melt-through

STEEL -----		140,000 Lb.		85,000 lb.	
		Lb.	Kg	Lb.	Kg
UO ₂	=	280,000	127,000	280,000	127,000
Zr	=	100,050	45,382	100,050	45,382
Fe	=	81,515	36,974	49,491	22,449
Cr	=	22,610	10,256	13,727	6,226
Ni	=	13,330	6,033	8,075	3,663
ZrO ₂	=	20,194	9,160	20,194	9,160
Cr ₂ O ₃	=	5,832	2,645	3,541	1,606
FeO	=	18,506	8,394	11,236	5,096
NiO	=	0.0	0.0	0.0	0.0

II. MARK I RESULTS

As indicated in Table I.1, there are five parameters that are allowed to vary in the Mark I standard problem matrix. These include the area of deposition of the core debris, the initial debris temperature, the concrete composition, the quantity of free water in the concrete, and the quantity of steel that comes with the debris at vessel failure. Of these five parameters only four have been allowed to vary independently. The deposition area and the debris temperature were varied together. The following are the general conclusions regarding these four independent modes of variation:

1. Free Water Content - Doubling the free water content resulted in more severe drywell condition with pressures 10% higher for limestone and 30% higher for basalt concrete.
2. Steel in Corium - Decreasing the quantity of steel resulted in only marginally lower pressures and temperatures.
3. Debris Temperature and Deposition - The combination of lower initial debris temperature and larger area of deposition was, by a wide margin, the most sensitive parameter combination. At three hours the pressure was 35% lower for limestone and nearly 40% lower for basalt concrete. Peak drywell temperatures were reduced by 100°F and 200°F for limestone and basalt concretes, respectively.
4. Concrete Type - As expected, the large quantities of non-condensibles evolved from the decomposition of limestone concrete resulted in significantly higher drywell pressures (33% higher) while producing only marginally higher drywell temperatures.

In general it appears that, although the containment was not allowed to fail in these calculations, there is a high probability that it would fail within two hours. The steel structures within containment heat up to 700°F by two hours. This is well beyond the design criterion for valves and penetrations. Pressures are clearly beyond currently estimated failure thresholds at two hours. It is not clear which loading would initiate failure. It seems likely that since both temperature and pressure loading reach critical magnitude at roughly the same time, the two loadings would combine to produce a breach of containment.

Baseline Case (Case 1)

The baseline case for the Mark I standard problem is Case 1. Results for this case together with the tabular results for all the cases identified in Table I.1 are presented in Table II.1.

The sequence as defined in standard problem Case 1 leads to core melt and vessel breach. Since the standard problems calls for 80% of the core to participate in the molten core/concrete interaction, the power level in MARCH (QZZRO) was reduced to 80% of full power. The result is that vessel failure (257.5 min) is delayed beyond the point that it would normally occur, but the specific power level in the ex-vessel phase should properly match the quantity of core debris present. The core debris is assumed to spread over a circular area with a radius of five meters, and begin thermally attacking the limestone concrete basemat.

The drywell pressure and temperature traces are shown in Figures II.1 and II.2, respectively. The temperature plot, however, appears to more strongly indicate what is occurring in the core/concrete interaction phase so that reference should be made to it during the following discussion of the results. Initially the debris enters the drywell at a high temperature (4130°F) and the rate of convective and radiative heat transfer from the pool to the atmosphere is quite high. The second temperature spike in Figure II.2 (after vessel failure, 257.7 min) corresponds to the direct heating of the atmosphere as the core debris radiates. The high heat fluxes quickly result in a crust which builds at the top surface of the debris and begins to inhibit upward radiation. As a result, heat transfer from the atmosphere to the heat structures reduces atmospheric temperature from an early peak of 545°F down to 460°F at about 265 minutes. By this time the generating of hot gases from the decomposition of the concrete basemat becomes a significant heat source and the drywell temperature again begins to increase. A general upward trend continues until about 295 minutes at which time the temperature is 660°F. At this point the metallic zirconium is depleted. With the loss of the highly exothermic zirconium reactions, the pool temperature drops rapidly with a resulting drop in upward energy transfer and a slight decline in drywell temperature. At 305 minutes the density of the heavy oxide layer has been reduced to the point at which it is less dense than the metallic layer. A layer inversion occurs at this point. The metallic layer sinks to the bottom and the heavy oxide layer is mixed with the light oxide layer at the top. The result is that the crust, having been composed, of solidified light oxides, remelts into the hotter composite oxide layer. With removal of the crust, heat is again radiated directly from the molten pool surface, and gases bubble directly through the hot oxide layer rather than being routed around the layer as

occurs in the presence of a crust. Again, with the increase heating rate, the atmosphere responds with a sharp increase in temperature. The drywell temperature continues to increase for an additional 30 minutes until at 338 minutes (about 80 minutes after vessel failure) the oxide layer solidifies forming a thick crust over the top of the still molten metallic layer. Radiation from the pool surface is again inhibited and, although gases continue to be generated at the interface between the concrete and the molten metal layer, the heat addition rate to the atmosphere is less than the heat transfer rate to the passive heat sinks. Consequently, the atmospheric temperature declines from a maximum temperature of 820°F (at 338 min) and appears to be approaching a steady state temperature of about 710°F.

Clearly, given the loads imposed on the containment structure (220 psia at two hours and 246 psia at three hours), and assuming a failure pressure on the order of 140 psia, it would have either failed prior to two hours (after vessel failure), or perhaps developed leakage pathways out of containment of sufficient magnitude to stabilize the pressure below the point of catastrophic failure.

To establish the relative effect of radiative heat transfer from the top of the molten pool, the baseline case was re-run setting the pool surface thermal diffusivity to zero effectively "switching off" upward radiative energy transfer. In addition, for the MARCON case (labeled Case 1C in Table II.1), the wall concrete degassing model was disconnected so that a more direct comparison could be established with the results obtained at other laboratories.

Elimination of upward radiative heat transfer resulted in somewhat more rapid concrete penetration, and, therefore, higher gas generation rates. This is clearly seen in the radial and axial penetration shown for Cases 1C in Table II.1. However, in the MARCON results, the increased gas generation-rate does not offset the loss of radiative heating, so that the pressures at both two hours and three hours are more than 30 psi lower than the baseline case, while the peak temperature is reduced by 260°F (from 820°F to 560°F). The time histories of the pressures and temperatures for Case 1C is shown in Figures II.3 and II.4.

Case 1A

This is the first of the parametric cases. It is the same as the baseline case except that the concentration of free water in the concrete is increased by a factor of two (from 3% to 6% by weight). The effect that is seen in the MARCON analysis is probably more dramatic than would be seen in a MARCH code calculation. This is not only because the steam source term in the core/concrete reaction increased, but the steam source term in

the MARCON degassing model is also increased. The latter effect is somewhat damped by the correspondingly increased concrete heat capacity due to the presence of additional free water, but the overall effect is a net increase in pressure ranging from 20 to nearly 30 PSI (at two and three hours, respectively). Drywell temperatures remain substantially the same. Drywell pressure and temperature graphs for Case 1A are given in Figures II.5 and II.6.

Case 1B

In this case the quantity of steel assumed to be in the core debris was reduced to 85,000 lb (140,000 lb was assumed in Case 1). Otherwise, the case is the same as Case 1. Figures II.7 and II.8 give the containment response for Case 1B. Apparently the results are not sensitive over the range of the parameter variation. The pressure was only a few psi lower while the peak drywell temperature was reduced by about 50°F to 775°F.

Case 2

Case 2 is significantly different from the previous cases in that two rather sensitive parameters were varied, the extent of basemat surface area over which the debris is deposited (three meter radius rather than a five meter radius) and the initial temperature of the core debris (2700°F rather than 4130°F). Both of these changes would be expected to reduce the severity of the containment conditions. The smaller pool surface area and the lower temperature both lower radiative heat transfer to the atmosphere, and this has already been demonstrated to be an important consideration in regard to drywell heating. The containment pressure and temperature for Case 2 are substantially lower than those obtained for the Case 1. The peak temperature is 100°F lower, and the pressure is lower by nearly 90 psi at 3 hours. Pressure and temperature plots for Case 2 are given in Figures II.9 and II.10.

Case 3

Case 3 is the same as Case 1 except that the concrete aggregate is assumed to be basalt rather than limestone. The free water content is also slightly higher (4% versus 3%). The difference in containment responses (see Figures II.11 and II.12) between Case 1 and Case 3 is due to the absence of the large quantities of CO₂ and CO that are present in the baseline case due to the decomposition of limestone.

Three hours after melt-through, for example, a comparison of the partial pressures of the various constituents in the drywell and wet well for cases 1 and 3 are as follows:

Case 3A

In this case, the concentration of free water in the basalt concrete has been increased to 8% from the 4% which was used in Case 3. The net result is somewhat higher drywell pressures and temperature (see Table II.1, and Figures II.13 and II.14). These are due to enhanced steam flowrates out of the concrete and the fact that penetration rates were more rapid for this case.

Case 4

Case 4 (Figure II.15 and II.16) is the same as Case 2, except that basalt concrete was employed rather than limestone. The debris temperature at core melt is assumed to be 2700°F and the debris is spread on the drywell floor out to a radius of 3 meters. The same sort of comments that were applied to the comparison of Cases 1 and 2 can be restated with regard to Cases 3 and 4. It was concluded from the earlier comparison that the combination of initial debris temperature and the area of debris spread out were particularly significant factors in the containment response. The same effects are observed in Case 4. The drywell pressures at 3 hours for Case 4 is only 112 psia as opposed to 158 psia for Case 2 while the peak temperature is down to 533°F compared to 720°F in Case 2.

There is apparently some disagreement between Sandia and Brookhaven on the results obtained for the MARK I standard problem. The case which should give the closest comparison with an equivalent Brookhaven case is Case 1C. A comparison of the differential pressure at 3 hours reveals the Sandia results to be about 50 PSI higher than Brookhaven's results. In an effort to identify the parameters in the MARCON analysis that most strongly effect the results, some additional cases were run and compared with Case 1 and Case 1C. Figures II.17 and II.18 show these comparisons. The solid line on these plots represents the configuration for Case 1C in which the correction has been made to the concrete heat capacity to account for the heat of vaporization of free water and the heat of decomposition of bound water. In addition, degassing and upward radiation heat transfer were "turned off". Clearly, the largest effect results from failing to adjust the concrete heat capacity (dashed line). Using a more appropriate heat capacity (hyphenated line) without upward radiation yields slightly higher drywell pressures with no change in temperature. Finally, adding in upward radiation (dotted line) yields what is believed to be an appropriate result. This curve corresponds to Case 1 in Table II.1 and shows pressures about 40 PSI higher than the case with no degassing and no radiation. Figure II.18 clearly shows the strong effect of upward radiation on drywell temperature.

TABLE II.1
SANDIA RESULTS FOR OUR MARK I STANDARD PROBLEM

CASE	P ₂	P ₃	T ₂	T ₃	T _P	T _{CON2}	T _{CON3}	T _{st2}	T _{st3}	AR ₂	AR ₃	AZ ₂	AZ ₃	F _{st2}	F _{st3}
1	220	246	726	709	820	508	526	735	710	37.8	37.9	37.9	42.7	.45	.50
1A	242	275	738	714	820	502	521	745	716	37.0	37.0	38.4	43.7	.49	.54
1B	213	241	693	686	775	467	496	698	686	37.7	37.8	40.4	45.6	.39	.45
1C	187	210	519	523	558	328	352	517	523	49.7	54.9	46.7	55.6	.15	.14
2	102	158	593	650	720	329	415	541	660	33.6	53.8	32.1	54.1	.42	.40
3	158	184	695	729	729	424	503	687	727	32.5	33.8	46.8	52.2	.58	.67
3A	201	243	742	771	771	462	532	736	769	39.4	43.4	53.5	60.8	.56	.67
4	95	112	474	533	533	279	327	445	521	36.7	51.6	37.3	64.0	.41	.44

P - Containment Pressure (psia)
T - Containment Temperature (°F)
T_{CON} - Concrete Surface Temperature (°F)
T_{st} - Steel Surface Temperature (°F)
AR - Radial Concrete Penetration (cm)
AZ - Axial Concrete Penetration (cm)
F_{st} - Mole Fraction of Steam

Subscripts - 2 - Evaluated at 2 Hours
 - 3 - Evaluated at 3 Hours
 - P - Peak Value

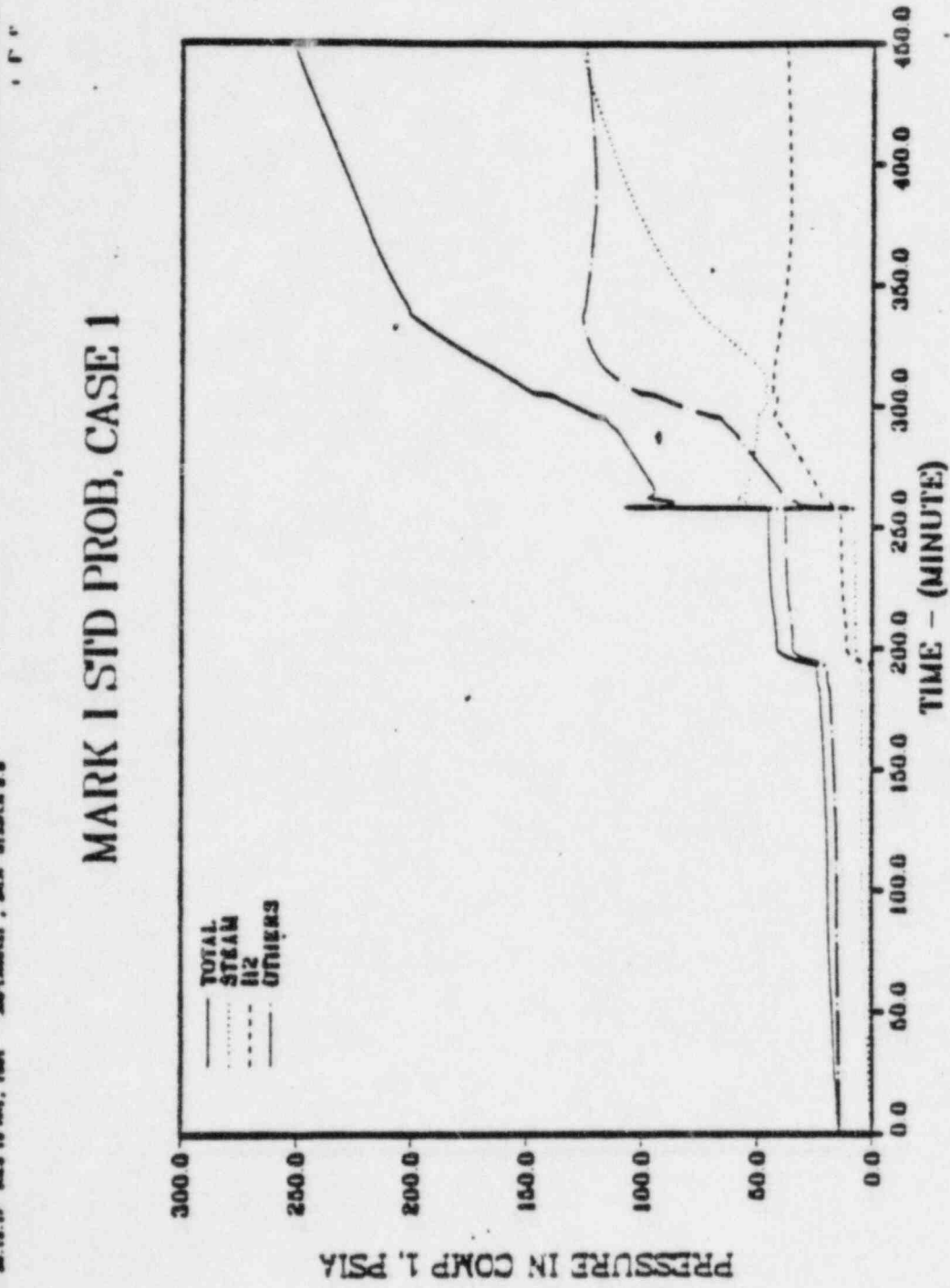


Figure 11.1

NAME: M.15.36 MES 15 NOV. 1964 JOB: 110017, SGA 8150A B B

MARK I STD PROB, CASE 1

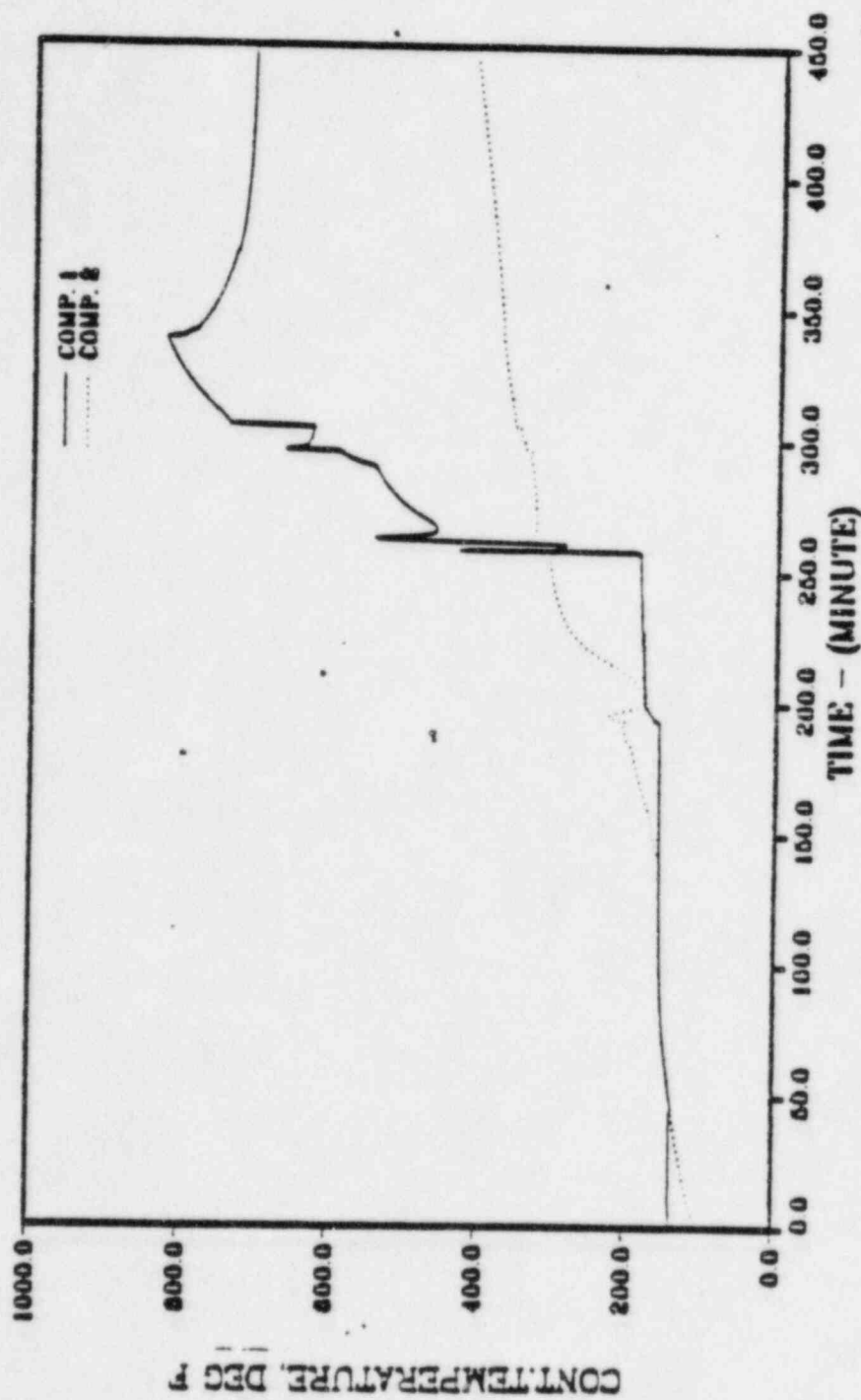


Figure 11.2

MARK I STD PROB, CASE 1A

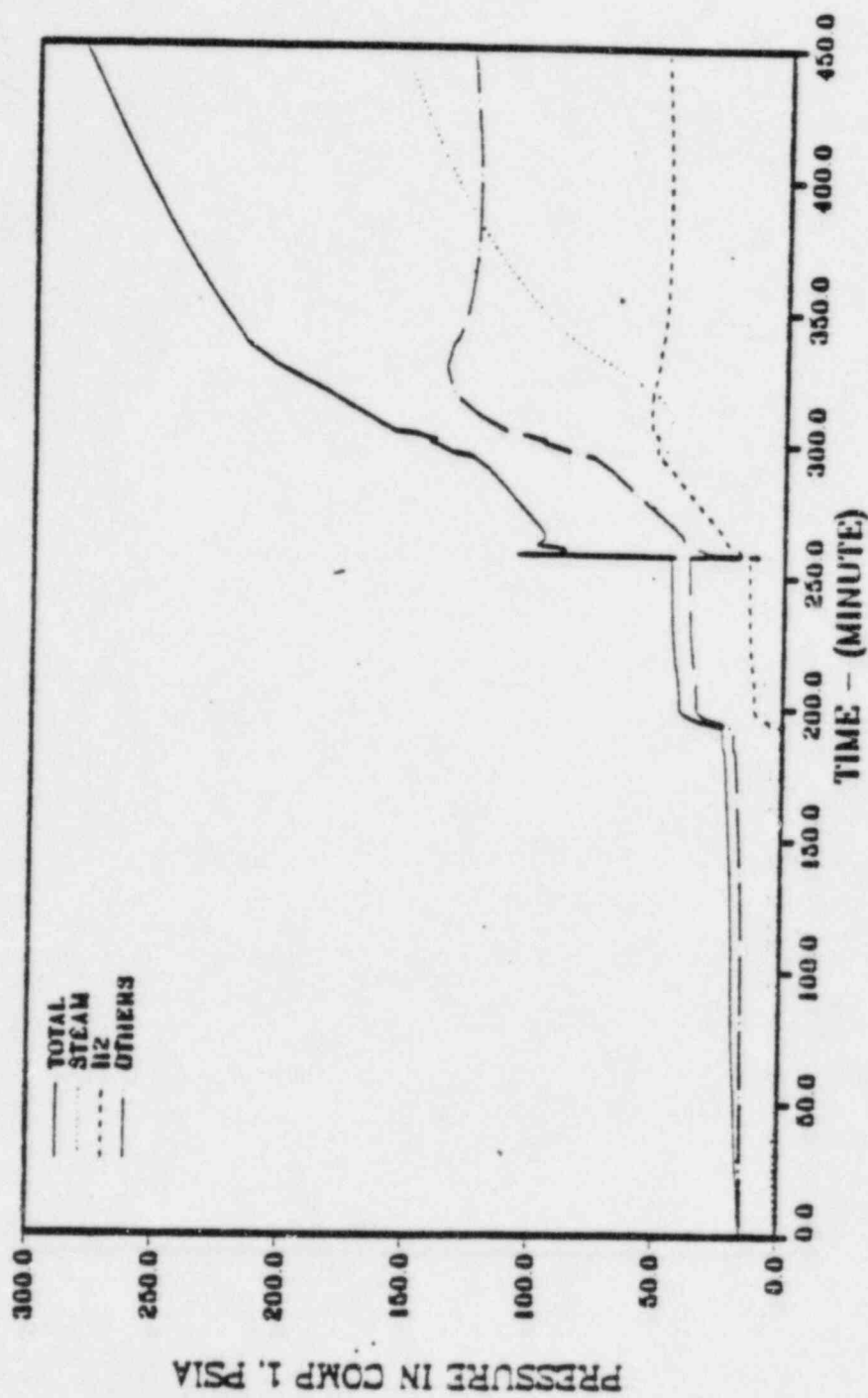


Figure 11.3

Run 3 17.08.56 MSB 10 MW, 1801 20-1000000, 20.10.1956

MARK I STD PROB, CASE 1A

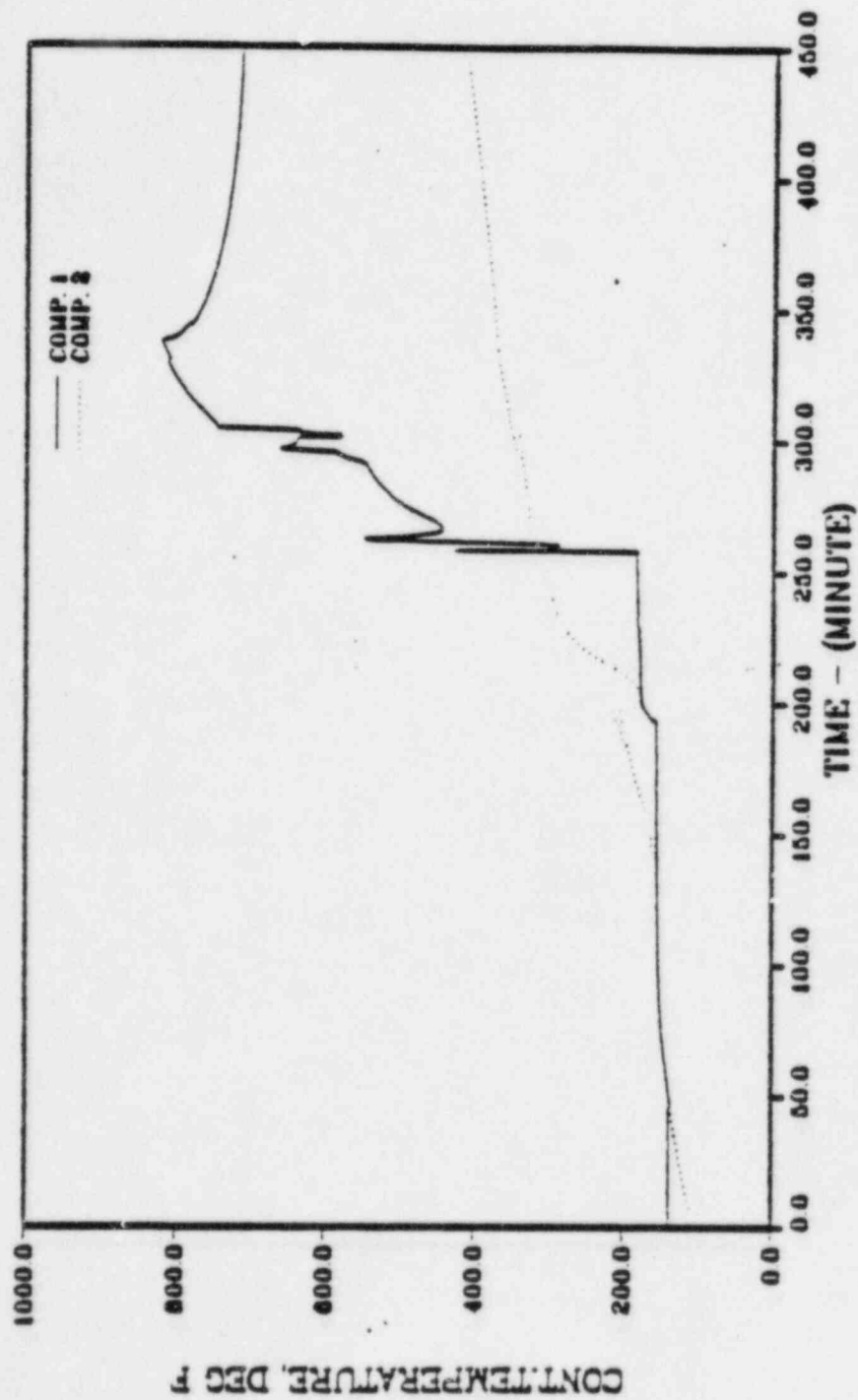


Figure II.4

MARK I STD PROB, CASE 1B

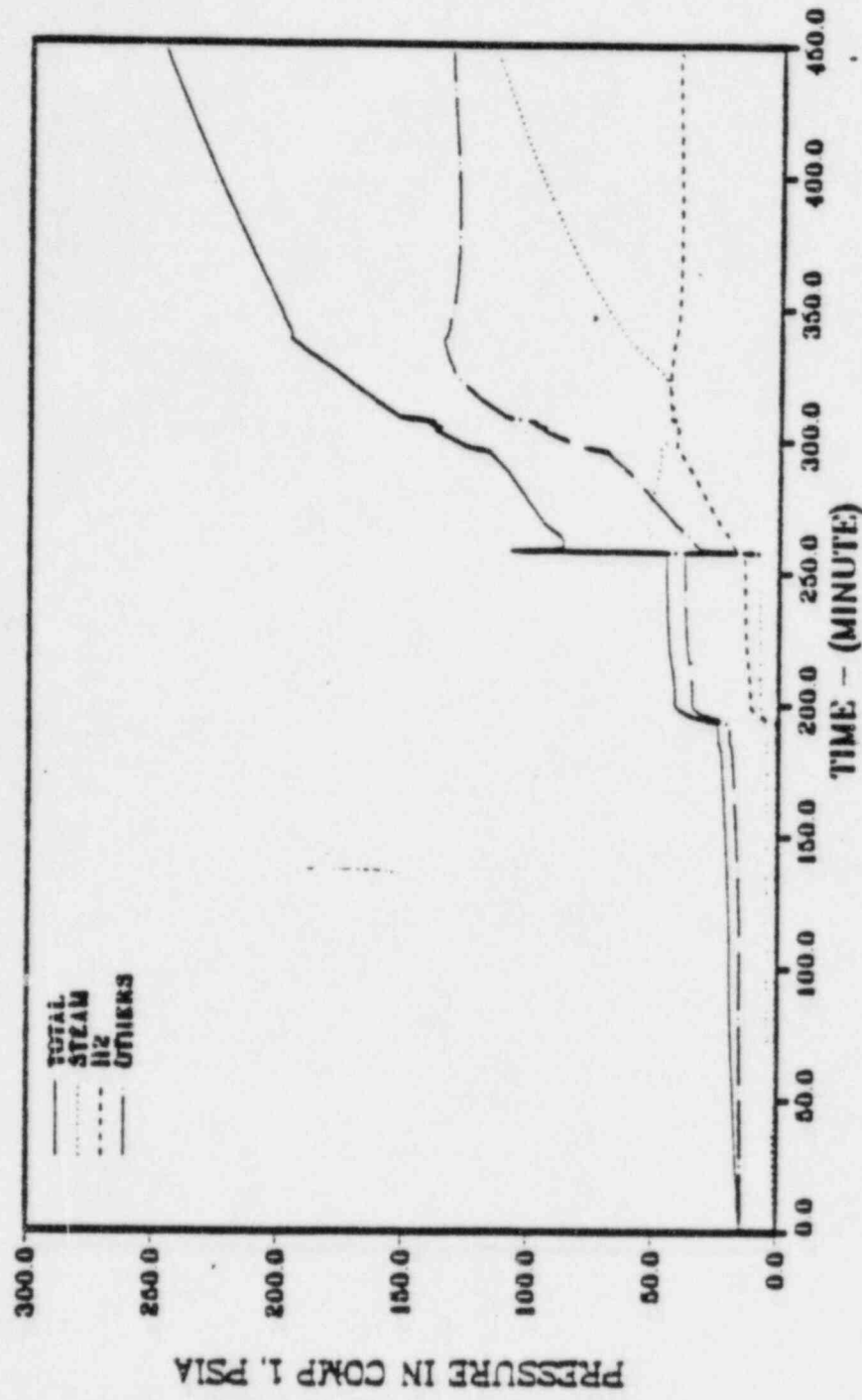


Figure 11.5

MARK I STD PROB, CASE 1B

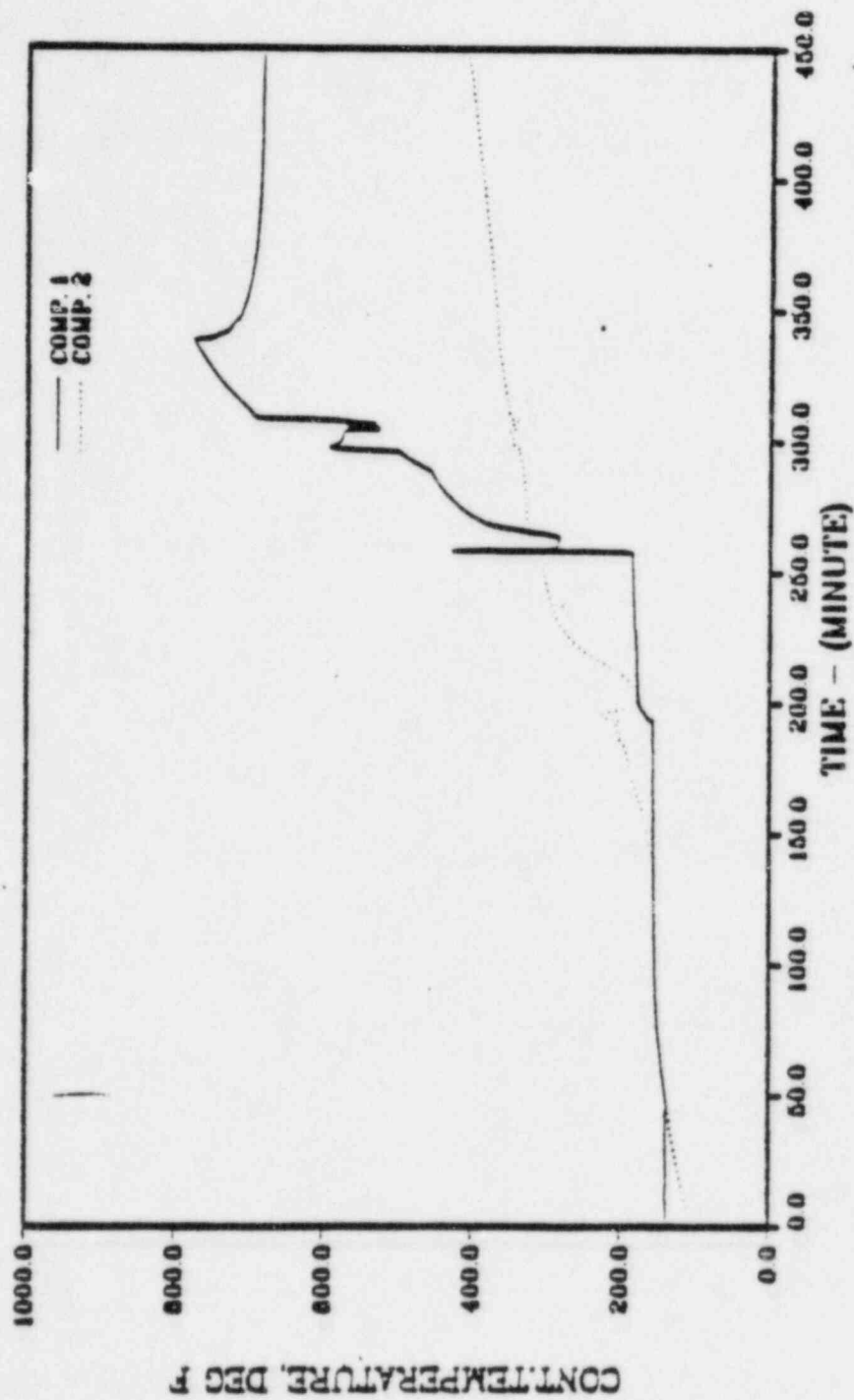


Figure 11.6

MARK I STD PROB, CASE 1C

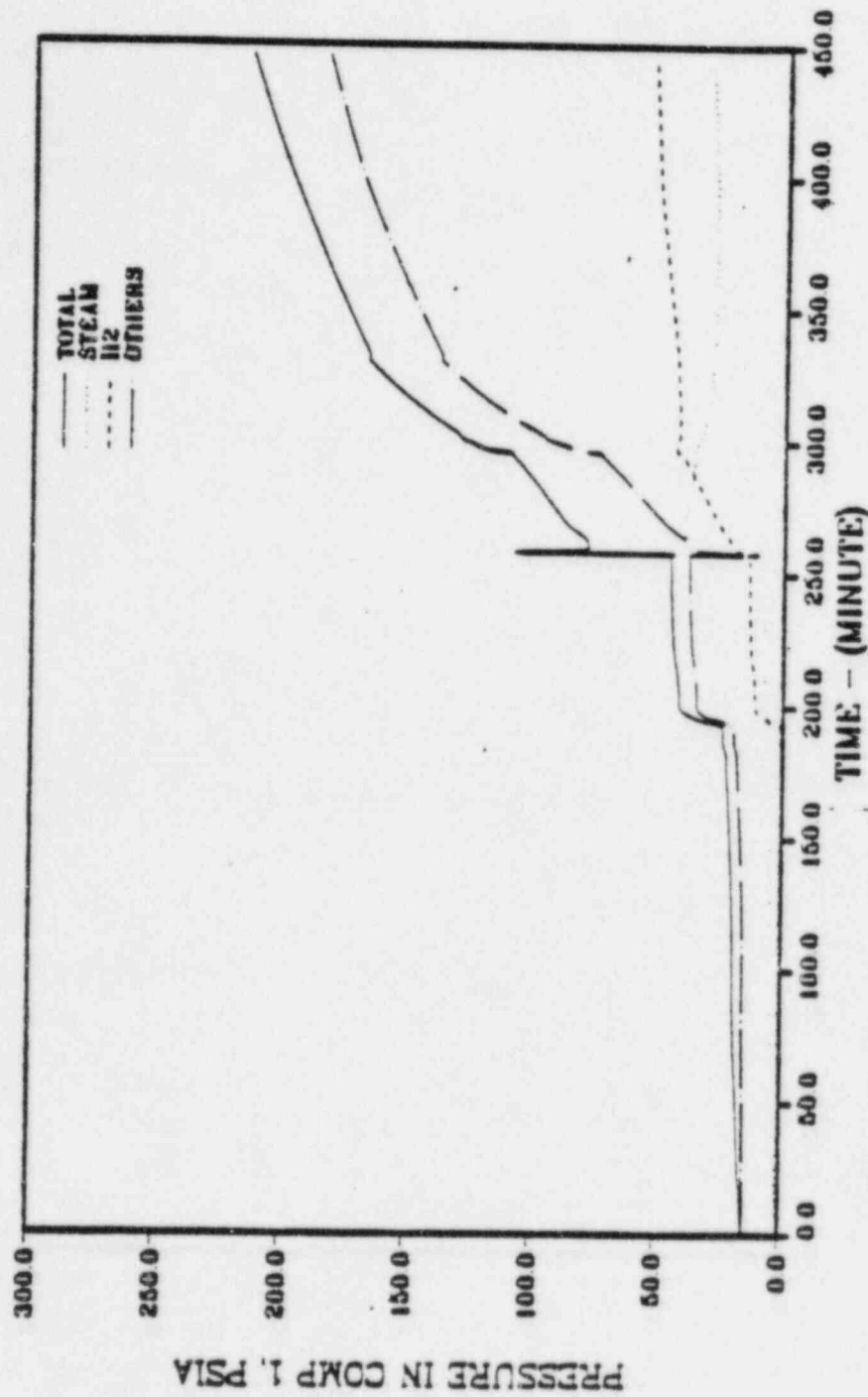


Figure 11.7

MARK I STD PROB, CASE 1C

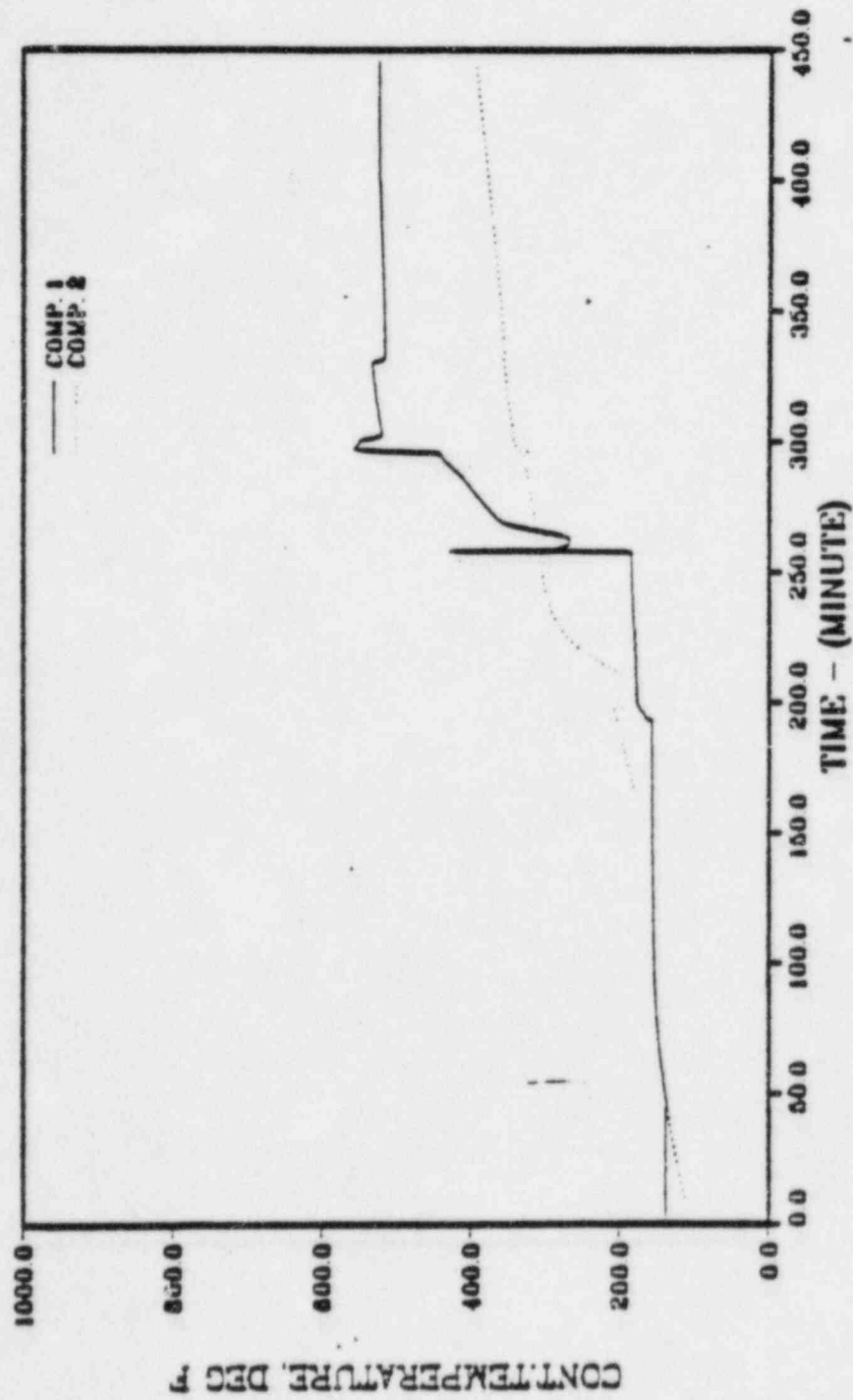


Figure 11.8

MARK I STD PROB, CASE 2

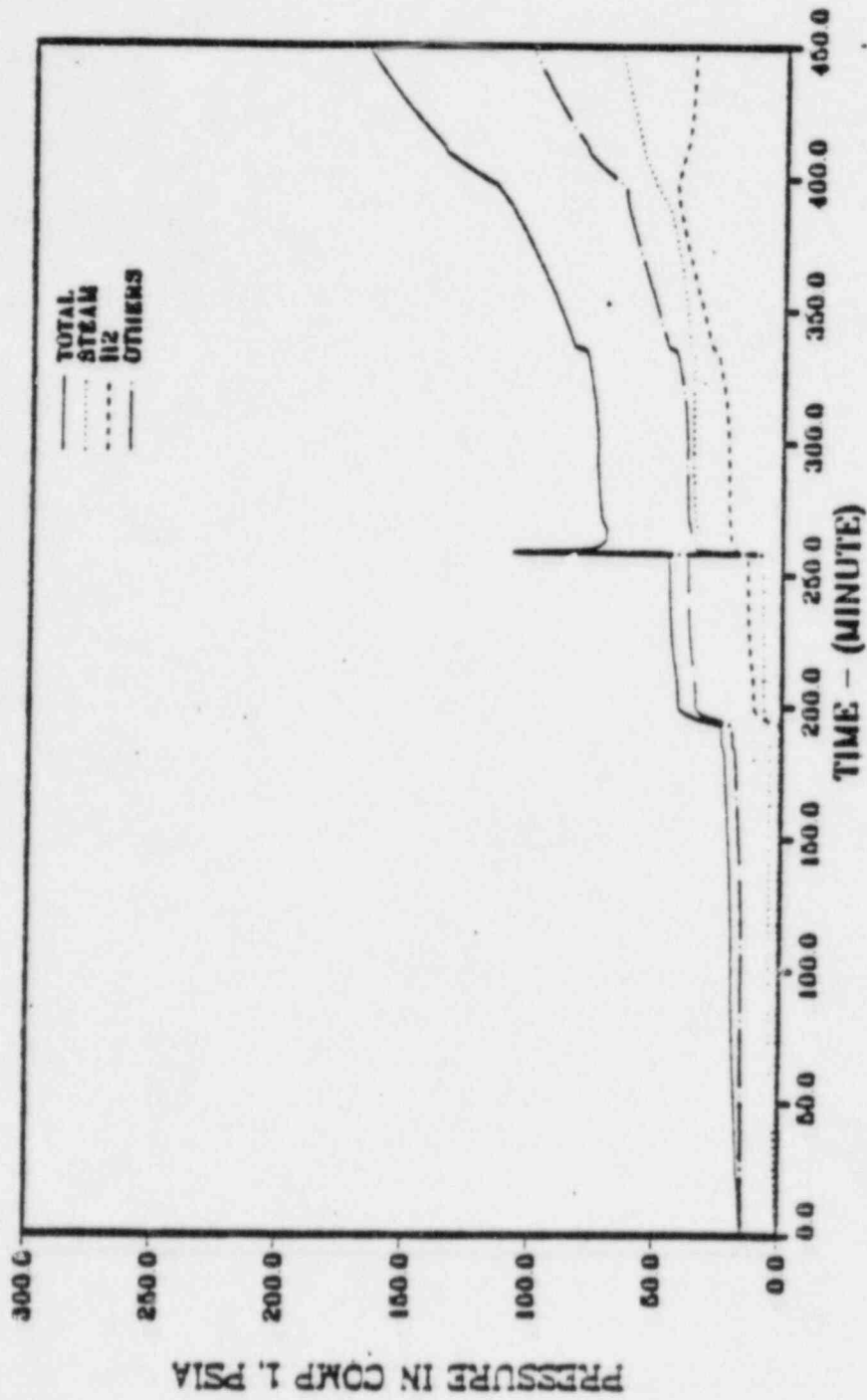


Figure 11.9

MARK 1 STD PROB, CASE 2

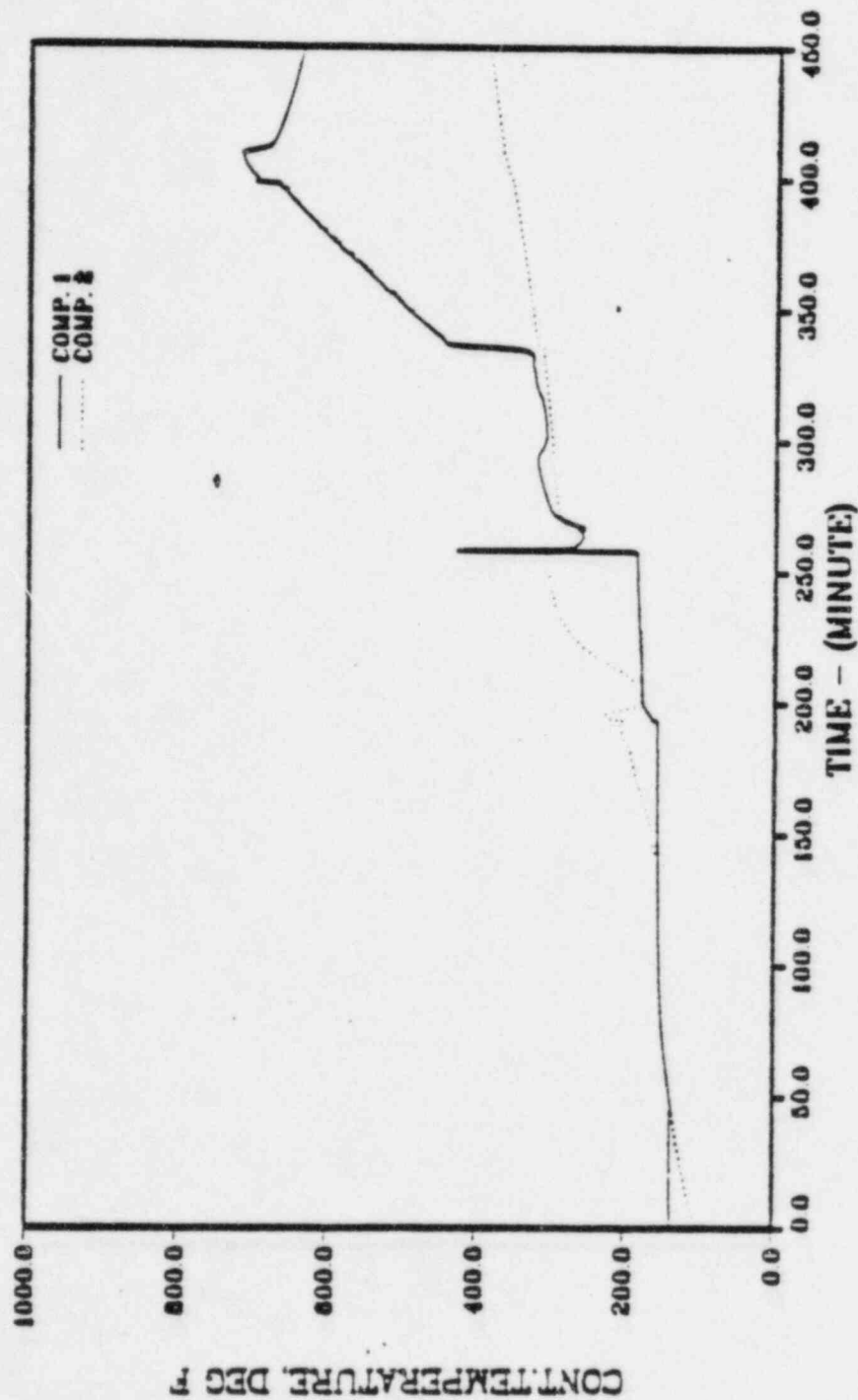


Figure 11.10

MARK I STD PROB, CASE 3

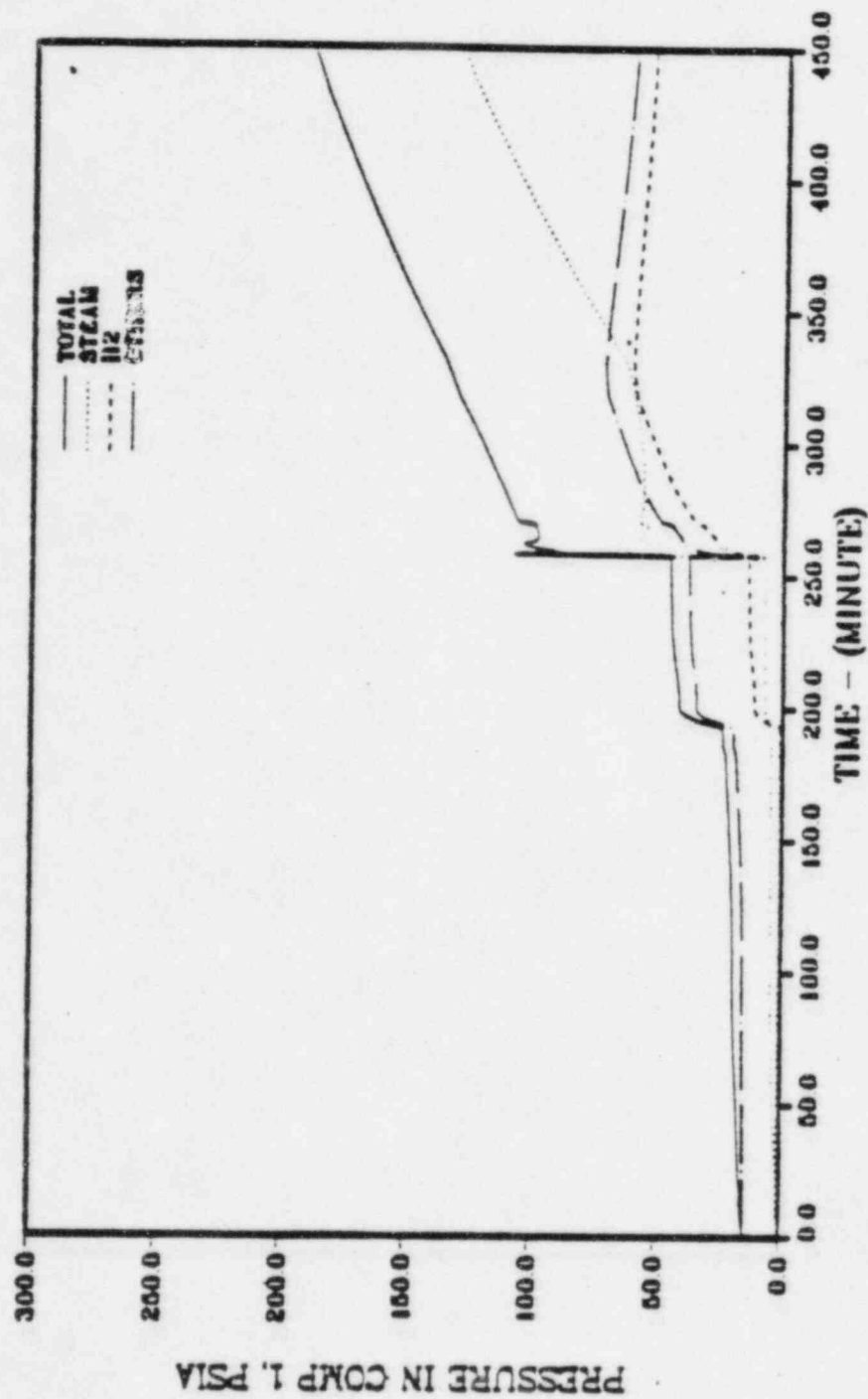


Figure 11.11

MARK I STD PROB, CASE 3

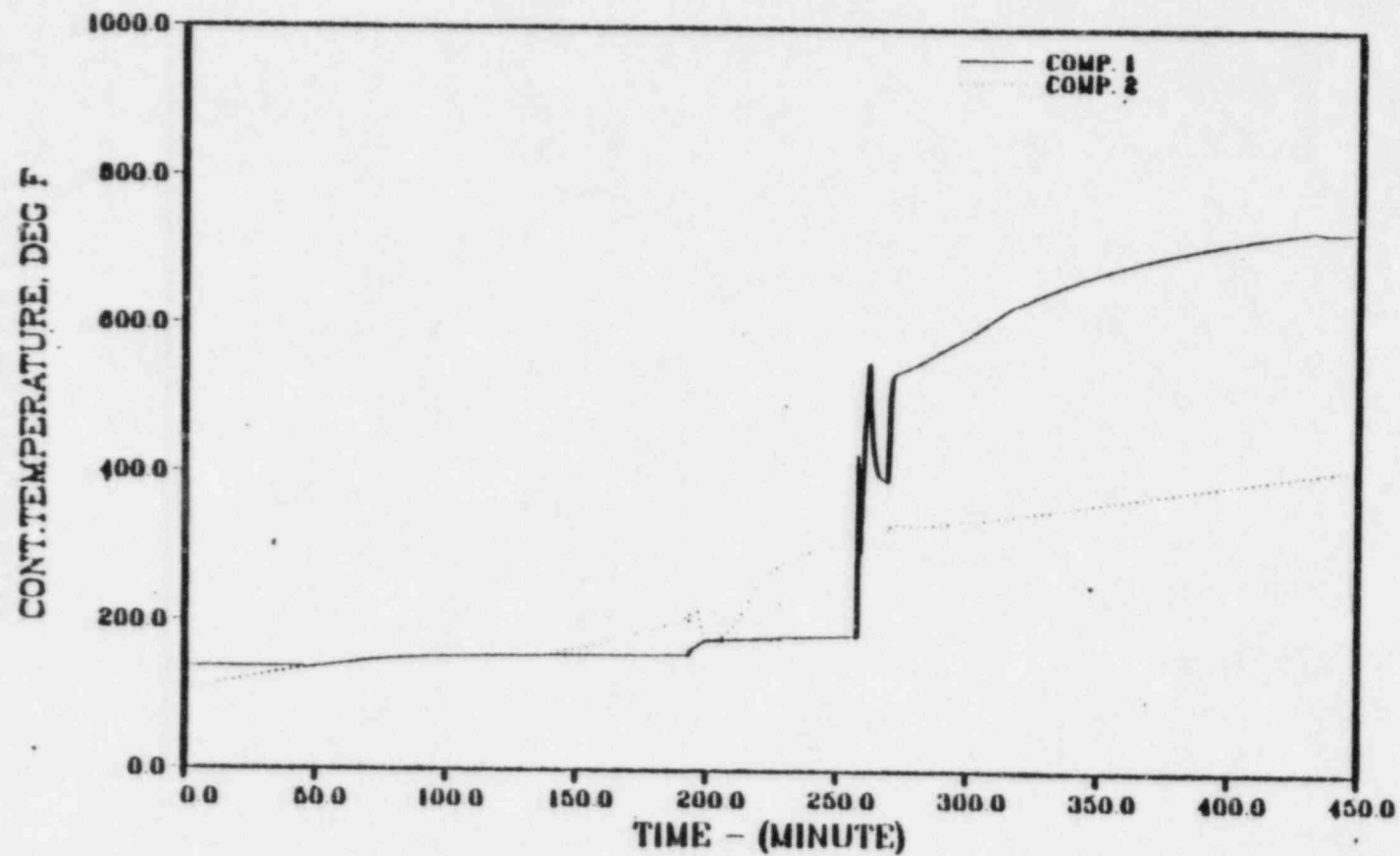


Figure II.12

MARK I STD PROB, CASE 3A

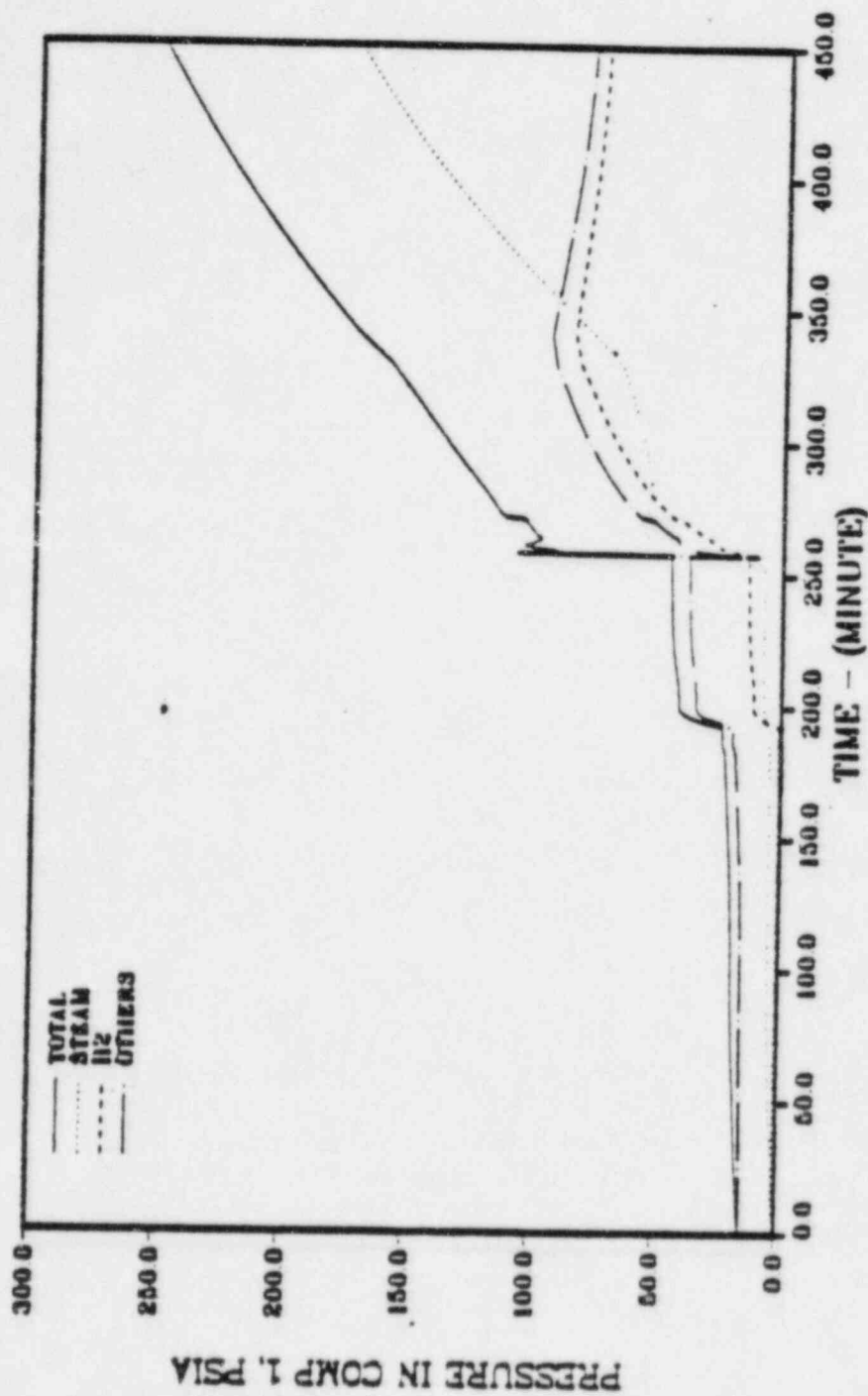


Figure 11.13

1 F F

MARK I STD PROB, CASE 3A

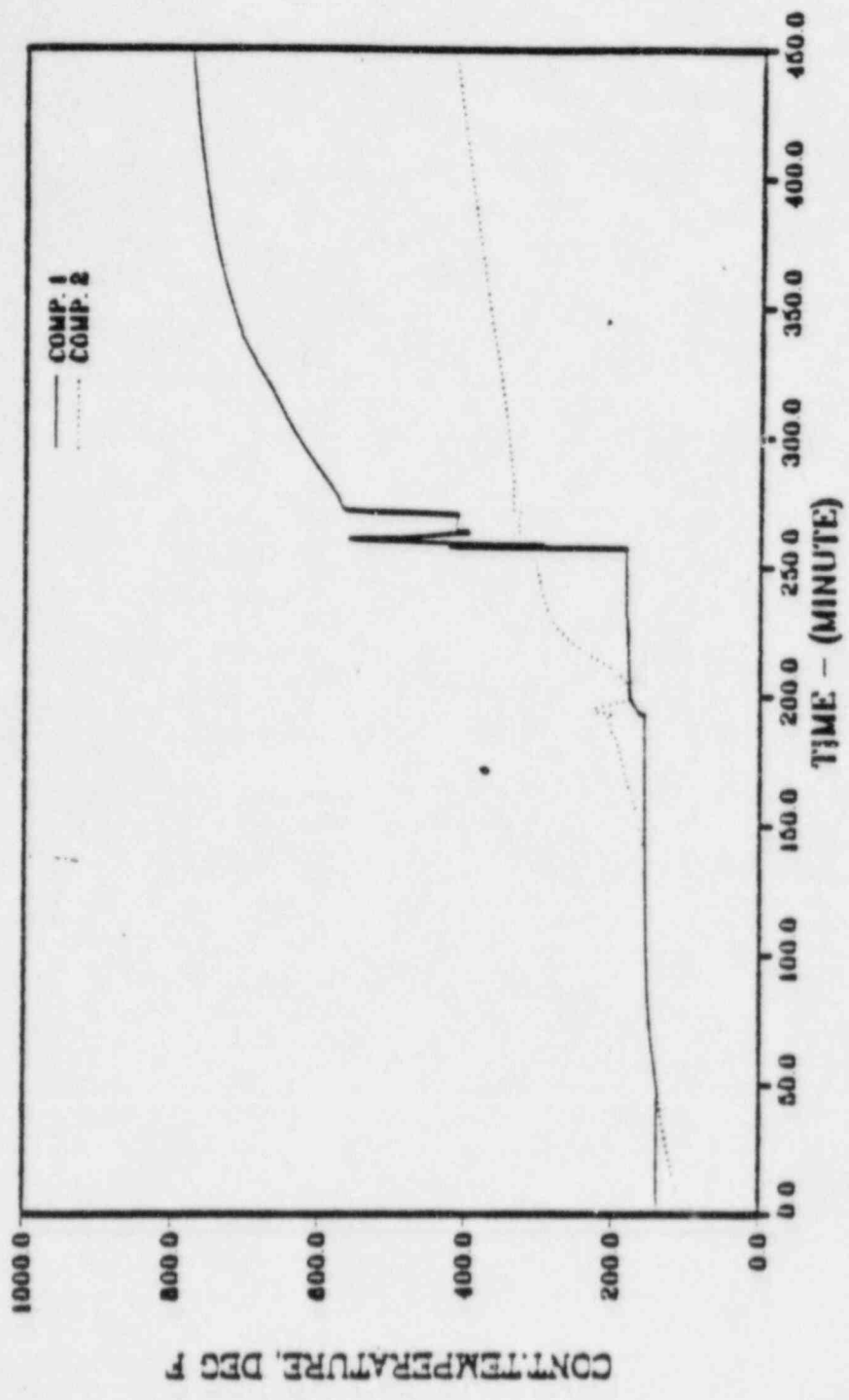


Figure 11.14

MARK I STD PROB, CASE 4

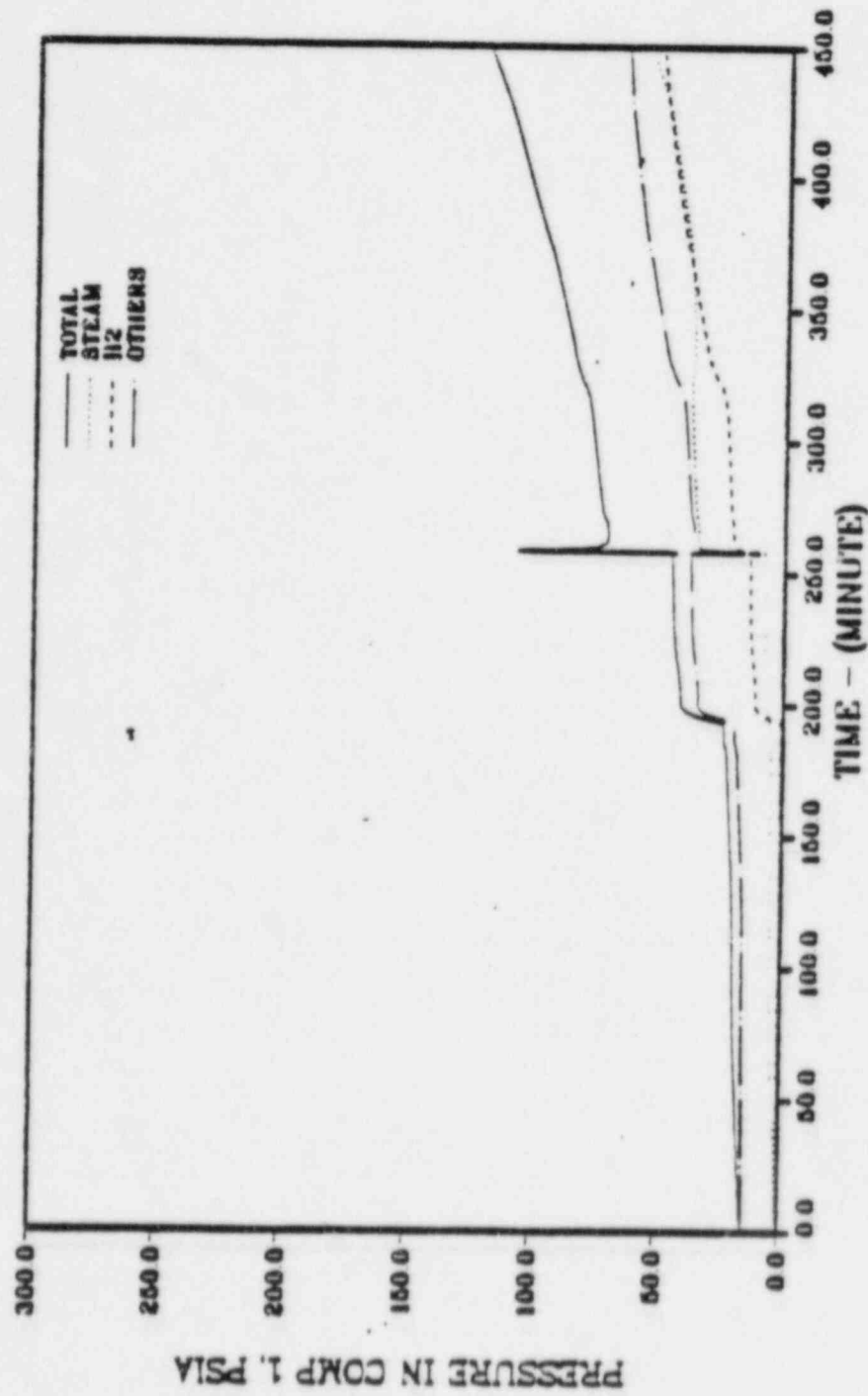


Figure 11.15

MARK I STD PROB, CASE 4

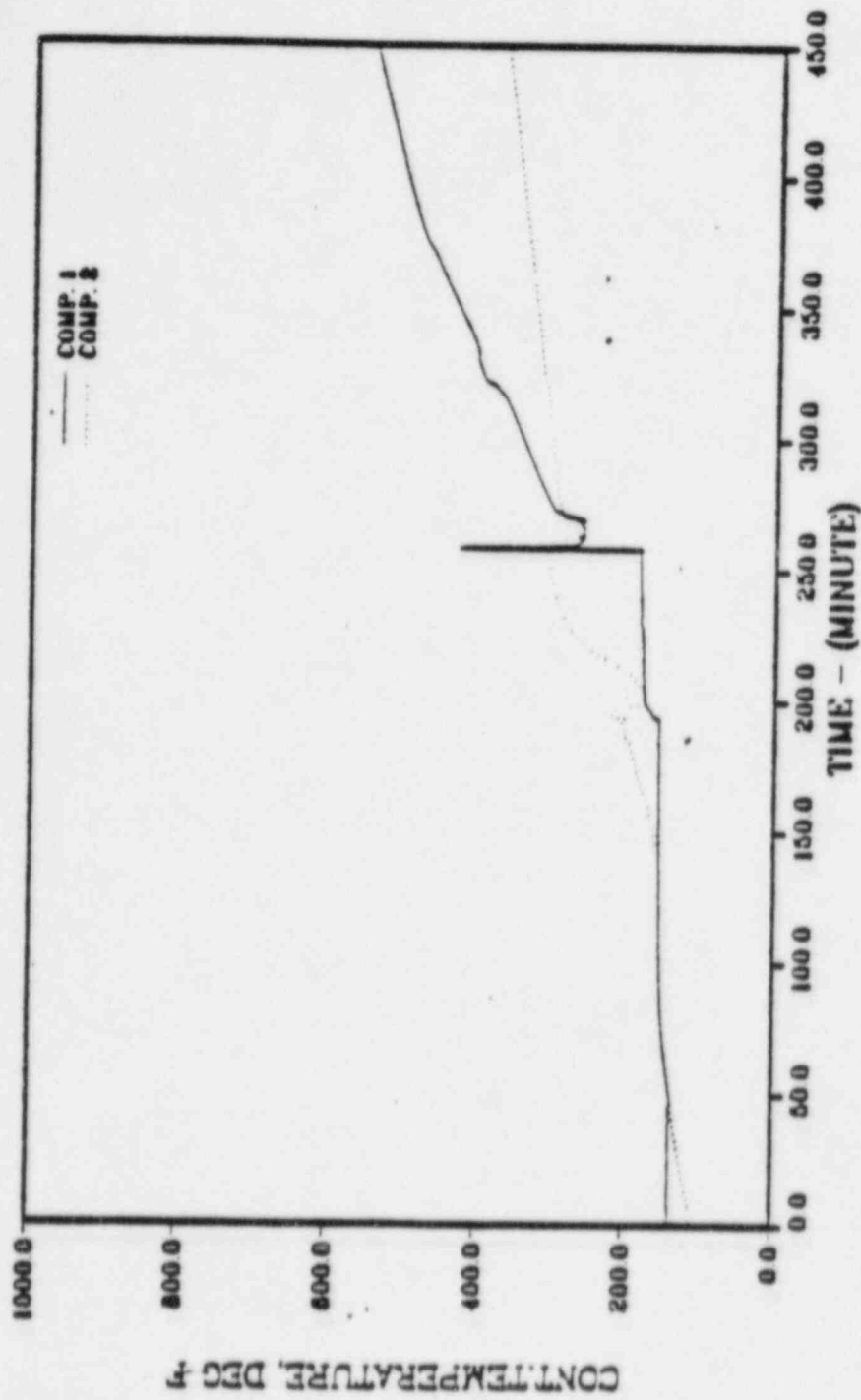


Figure 11.16

MARK I STD PROBLEM

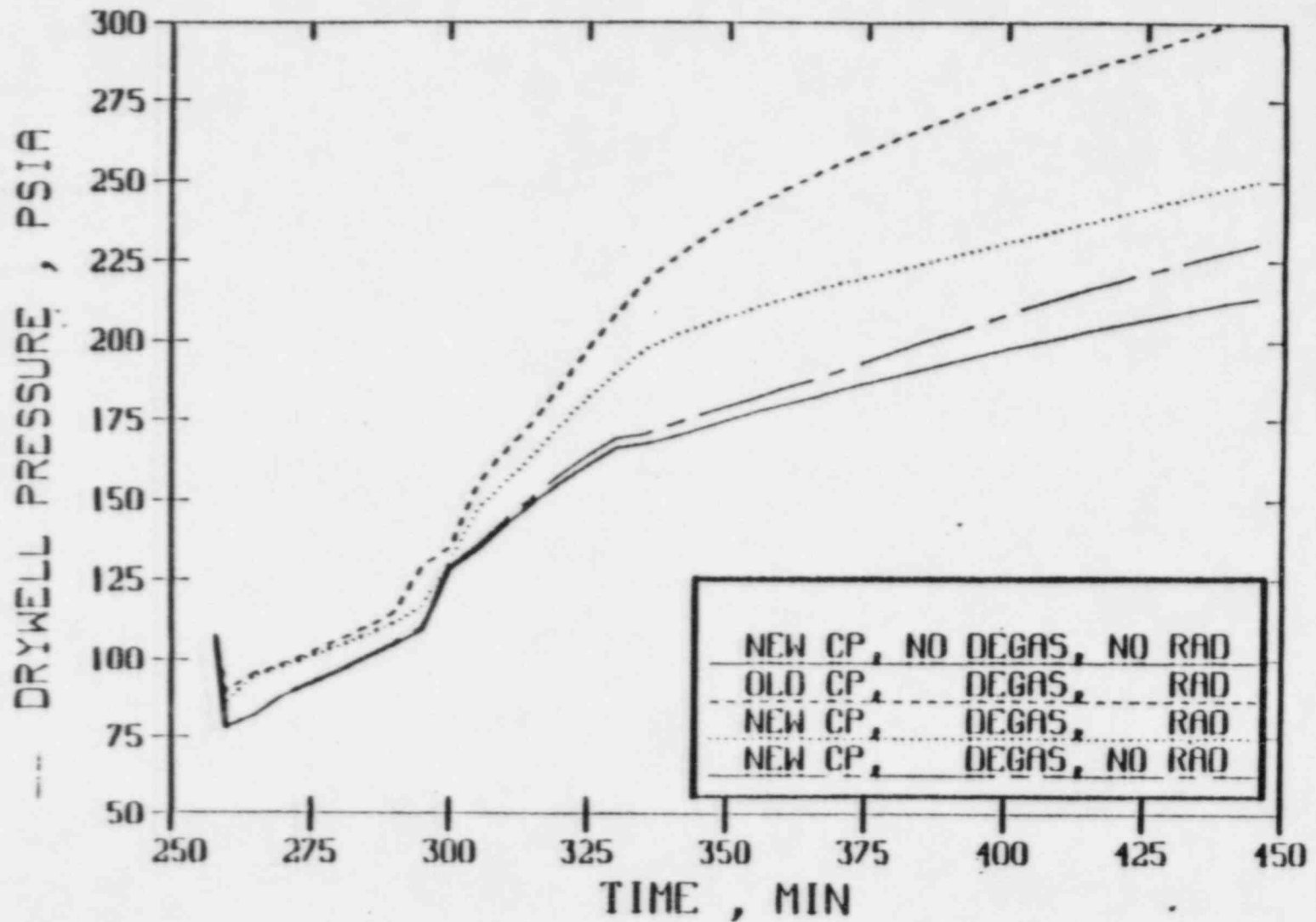


Figure 11.17

MARK I STD PROBLEM

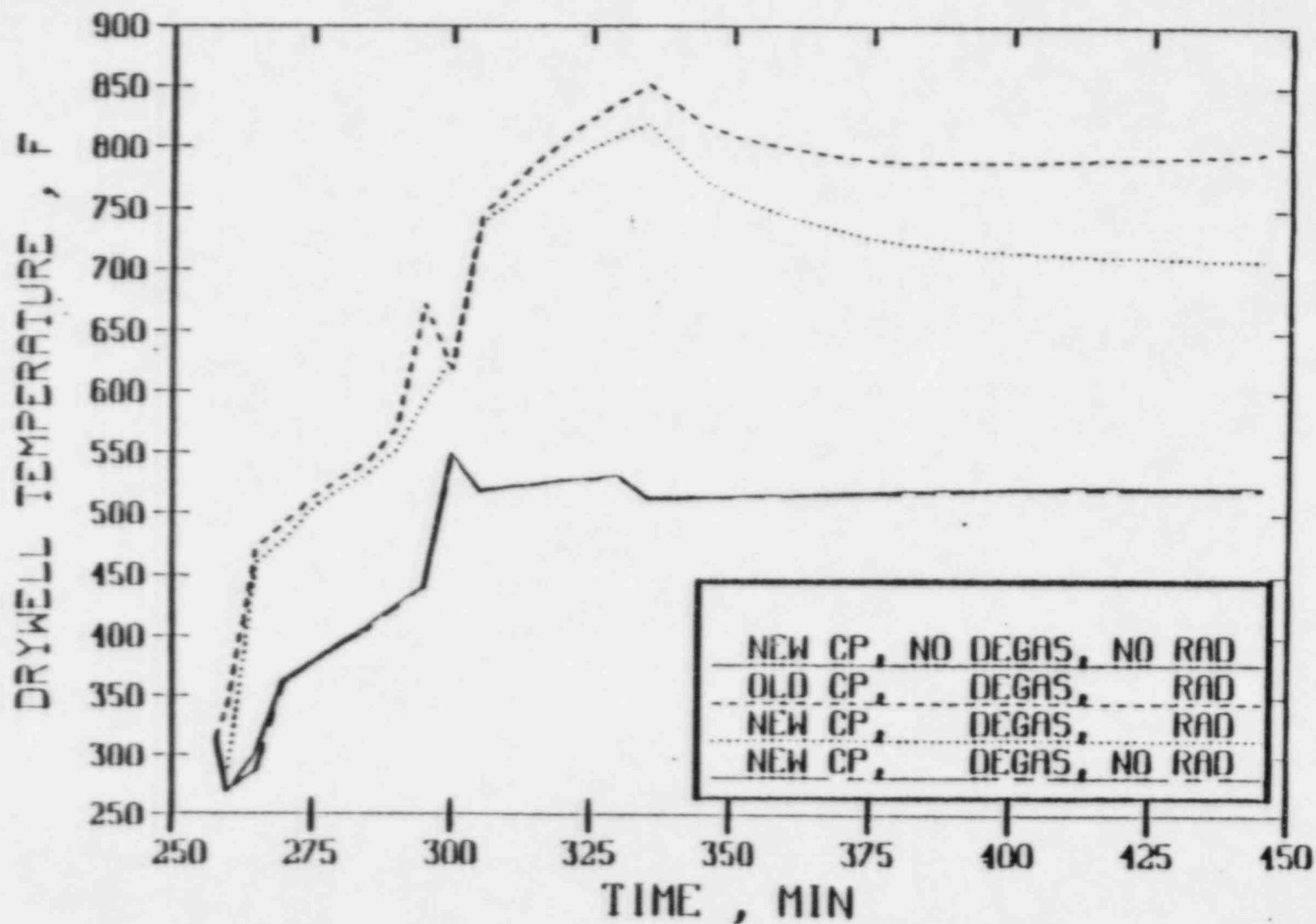


Figure II.10

III. MARK II RESULTS

A summary of results for each case is presented in Table III.1. Shown are the drywell temperature and pressure, steam pressure fraction, containment surface temperatures, and the concrete penetration distances. The data was taken at both 2 and 3 hours after the vessel failed. The peak drywell temperature is also shown. Case 5 was also run using MARCON's PWR models described in the summary attachment. The PWR calculation which will be discussed later was done to test the impact of the BWR assumption that all the thermal radiation goes directly to the drywell atmosphere. Also listed are calculations in which there was no thermal radiation from the debris surface ($c = 0$) for Case 7. This was done to create a consistent calculational approach for comparison with other laboratories.

Several specific comparisons are presented in Table III.2. The drywell pressure at 3 hours, the peak drywell temperature, and the vertical concrete penetration at 3 hours are compared.

1. Type of concrete - Higher drywell temperatures and pressures are encountered with the limestone concrete while the deepest vertical penetration is found with basalt concrete.
2. Free H_2O - A higher percentage of free H_2O leads to higher drywell temperatures and pressures, and higher vertical concrete penetration for both types of concrete.
3. Corium temperature and spread - The higher temperature corium which spreads further leads to higher drywell temperatures and pressures but lower concrete penetration.
4. Steel in corium - Reducing the steel in the corium reduced the pressure slightly and reduced the drywell peak temperature but increased the concrete penetration.

Case 5

The containment pressures for compartments 1 (drywell) and 2 (wetwell) are shown in Figures III.1 and III.2, respectively, and the compartment temperatures in Figure III.3. The lower vessel head failed at 258 minutes. The pressures increase after head failure with a change in slope at about 340 minutes. This change in slope corresponds to a reduction in the drywell temperature shown in Figure III.3. This reduction in temperature is caused by a reduction in the debris surface heat transfer. Figure III.4 shows the rates of energy added to the containment atmosphere. The total radiative and convective heat transfer from the debris surface is shown with the solid line. Also shown are the gas enthalpy rates for the gases released by the debris, the gases released by the wall degassing model, and total rate of energy added to the containment.

The pressure plots also show the partial pressures for steam, hydrogen gas, and non-condensable gases. Steam contributes roughly one third to the drywell pressure while the wetwell is dominated by non-condensable gases.

The left surface node temperatures for concrete, lined concrete, and miscellaneous steel slabs are shown in Figure III.5. The surface temperatures encountered in the steel and steel lined slabs are higher than the concrete surface temperatures.

The temperatures of the melt surface, the melt upper layer bulk, and the drywell atmosphere are shown in Figure III.6. The melt rapidly develops a surface crust which lowers the temperature of the melt surface, and the surface heat transfer. The top and bottom melt surface crusts are shown in Figures III.7 and III.8. CORCON calculates a layer flip at about 301 minutes (18050 seconds) in which the heavy oxide layer on the bottom changes place with the metallic layer above it. The heavy and light oxide layers then combine to form one layer on top of the metallic layer. This layer flip is illustrated with the melt layer density plot shown in Figure III.9. The density plot shows the density of the heavy oxide (HOX) decreasing until it equals the density of the metallic layer, then the flip occurs. After the flip, the surface temperature is about equal to the bulk temperature of the upper oxide layer. The temperatures remain equal until a new surface crust is able to form at about 340 minutes (20400 seconds).

The melt in this calculation starts out with 45380 kg of metallic Zr. The Zr is oxidized at the rate of about 20 kg/s and is completely oxidized at about 296 minutes (17760 seconds). When the oxidation is complete, the bulk and surface temperatures both start to decrease.

The resulting vertical and radial penetration of the melt into the concrete is shown in Figure III.10. The penetration rates decreased after the layers flipped. At 3 hours after vessel failure, the vertical penetration is continuing at a fairly steady pace.

The rates of CO, CO₂, H₂, and H₂O gases released from the melt are shown in Figure III.11 and the cumulative releases are shown in Figures III.12 through III.15. The released gases are dominated by CO, followed by CO₂, then H₂ and H₂O. The cumulative mass of gases released at a time of 3 hours after vessel failure are 46335, 2637, 1536, and 509 lbm for CO, CO₂, H₂, and H₂O, respectively. The release rates for CO, CO₂, and H₂O are the highest right after the layers flip in CORCON. The highest H₂ rate is before the layer flip.

The H₂O released by the degassing of the unlined concrete in the containment is shown in Figure III.16 in a comparison

with the H_2O released by the melt. The H_2O released by degassing is considerably higher than the H_2O released by the melt and is a significant contribution to the containment pressure.

Calculations were made to determine the disposition of energy within the containment system at 2 and 3 hours after vessel failure. Two sources of energy additions to the containment include the fission product decay heat within the containment and energy transfer into the containment from the melt surface heat transfer and the enthalpies of the released gases. About 20% of the increased energy deposited in the containment comes from fission product decay heat. The largest amount of the energy added to the containment (~90%) goes into heating the containment walls. The next largest amount goes into heating the sump water. Any models involving heat transfer between the drywell atmosphere and the walls such as the new radiative heat transfer model are quite important.

Case 5 MARCON PWR models

Basically the BWR models added to MARCON assume that all the thermal radiation from the top of the debris goes directly to the drywell atmosphere and that the atmosphere is well mixed due to convective flows. In addition, the BWR model allows for the degassing of concrete. To test the impact of these assumptions, the Case 5 calculation was repeated using the MARCON PWR reactor cavity models. With these models, the radiation heat transfer goes into the reactor cavity atmosphere, most of which goes into ablating concrete, and the concrete heat structures in the drywell are not allowed to degass. The results of this calculation show a reduction in the containment pressure (Table III.1) at 3 hours of about 5 psia with a peak drywell temperature of about 456°F (Table III.1). The drywell steam partial pressure is reduced primarily because there is no containment wall degassing. The melt bulk and surface temperatures and the reactor cavity atmosphere temperature are shown in Figure III.17. The reactor cavity atmosphere temperature is in the neighborhood of 2900°F which tends to reduce melt surface heat transfer, keep the melt bulk temperature hotter, reduces the thickness of the surface crust, and results in slightly higher concrete penetration distances. The rates of CO_2 and H_2O gases released by the melt are about twice as high with the PWR models while the CO and H_2 rates remain about the same. The differences in the results between the PWR and BWR models are considerable.

Case 5A

Case 5A is a variation of Case 5 in which the free H_2O in the concrete was increased from 3 to 6%. The result (Table III.1) of the increased H_2O is a pressure increase of about 9%. This pressure increase is due to higher rates of H_2 and

The basaltic concrete causes the CORCON calculation to behave much differently than it did for limestone concrete. The layer flip causing the heavy oxides to merge with the light oxides occurs much earlier at about 268 minutes (16,100 seconds) or about 10 minutes after vessel failure. The metallic Zr in the debris reacts at a slower rate, i.e., about 9 kg/sec initially and 0.6 kg/sec at 3 hours. Only about 50% of the Zr is oxidized at 3 hours after vessel failure. This slower reaction rate allows the debris to cool to a temperature about 500°K colder than Case 5 as shown in Figure III.25 resulting in lower energy rates added to the drywell atmosphere (Figure III.26). The top and bottom crust plots indicate that the debris has frozen at about 320 minutes (19200 seconds). The vertical concrete penetration distance shown in Figure III.27 is significantly larger than the corresponding limestone concrete distance.

The rates of CO, CO₂, H₂, and H₂O gases released from the melt are shown in Figure III.28. The cumulative mass of gases released from the melt at a time of 3 hours after vessel failure are 159, 122, 2128, and 2327 lbm for CO, CO₂, H₂, and H₂O, respectively. The H₂O released by the degassing of the unlined concrete in the containment is higher than the H₂O released by the melt and is a significant contribution to the containment pressure. This is shown in Figure III.29.

Case 7 Without Radiative Heat Transfer

Case 7 was also calculated assuming that there was no thermal radiation from the top surface of the debris (by setting the surrounding emissivity to 1.0E-60) in order to create a consistent calculational approach for comparison with other laboratories. The drywell pressure and temperature, and the concrete penetration distances are presented in Figures III.30, III.31, and III.32, respectively.

Case 7A

Case 7A is a variation of Case 7 in which the free H₂O in the concrete is increased from 4 to 8%. The result (Table III.1) of the increased H₂O is a drywell pressure increase of about 20% and a peak temperature increase of 45°F. This pressure increase is due to higher rates of gases released by melt into the containment which are higher by 28, 38, 72, and 100% for CO, CO₂, H₂, and H₂O than Case 7, respectively.

In Case 7A, the layers in CORCON flipped at about the same time as Case 7, however, the debris froze at about 340 minutes (20400 seconds) or 20 minutes later than Case 7. The debris temperature and surface heat transfer for Case 7A are slightly higher than in Case 7. Case 7A penetrates concrete 13 to 24% faster than Case 7.

Case 8

The initial debris temperature in Case 8 has been reduced from 4130 to 2700°F and the corium spread on the floor has been reduced from 5 to 3 meters. Case 8 is similar to Case 6 with the concrete composition as the only difference. The drywell pressure is down a third and the peak drywell temperature (Figure III.33) is 161°F lower. However, the temperature is steadily increasing.

The debris is initially frozen and starts to melt at around 290 minutes and is completely melted around 310 minutes. The layers flip much later, at about 370 minutes. The debris starts out at a lower temperature than Case 7 but remains fairly constant as shown in Figure III.34 such that at 3 hours it is higher than Case 7. The debris surface heat transfer is about half of Case 7. The concrete penetration distances at 3 hours are roughly 20% higher than Case 7 and steadily increasing.

The average gas release rates for CO, CO₂, H₂, and H₂O are 0.6, 77., 55., and 77.% of the Case 7 rates.

TABLE III.1
SANDER RESULTS FOR DWR NAME II STANDARD PROBLEM

CASE	P ₂	P ₁	T ₂	T ₁	T _P	T _{CON2}	T _{CON1}	T _{at2}	T _{at1}	T _{LIN2}	T _{LIN1}	AR ₂	AR ₁	AR ₂	AR ₁	F _{at2}	F _{at1}
5	129.5	136.1	623	571	832	657	628	650	576	569	494	.38	.38	.38	.42	.35	.37
5 PWB	128.9	130.9	277	389	456	270	270	625	197	360	321	.42	.45	.41	.48	.22	.20
5A	141.1	147.7	660	570	832	655	625	661	580	577	496	.37	.37	.38	.43	.37	.39
5B	129.8	135.4	612	561	788	624	608	631	567	545	482	.38	.38	.41	.46	.32	.32
6	76.4	95.7	563	570	691	304	308	493	603	388	510	.38	.53	.31	.53	.50	.35
7	103.2	109.5	650	616	658	617	640	652	618	554	547	.35	.37	.47	.52	.53	.56
7 PWB	97.4	104.1	395	379	397	253	257	389	382	308	307	.47	.57	.76	.90	.35	.36
7A	121.8	134.7	687	666	703	637	658	689	667	591	575	.41	.46	.53	.61	.49	.53
8	76.2	82.1	655	697	697	271	307	415	688	344	394	.29	.43	.39	.66	.51	.49

P - Containment Pressure (psia)
T - Containment Temperature (°F)
T_{CON} - Concrete Surface Temperature (°F)
T_{at} - Steel Surface Temperature (°F)
T_{LIN} - Steel Lined Concrete Surface Temperature (°F)
AR - Radial Concrete Penetration (in)
AZ - Vertical Concrete Penetration (in)
F_{at} - Mole Fraction of Steam

Subscripts - 2 - Evaluated at 2 Hours
- 1 - Evaluated at 1 Hour
P - Peak Value

MKII STD PROB, MARCON CASE 5

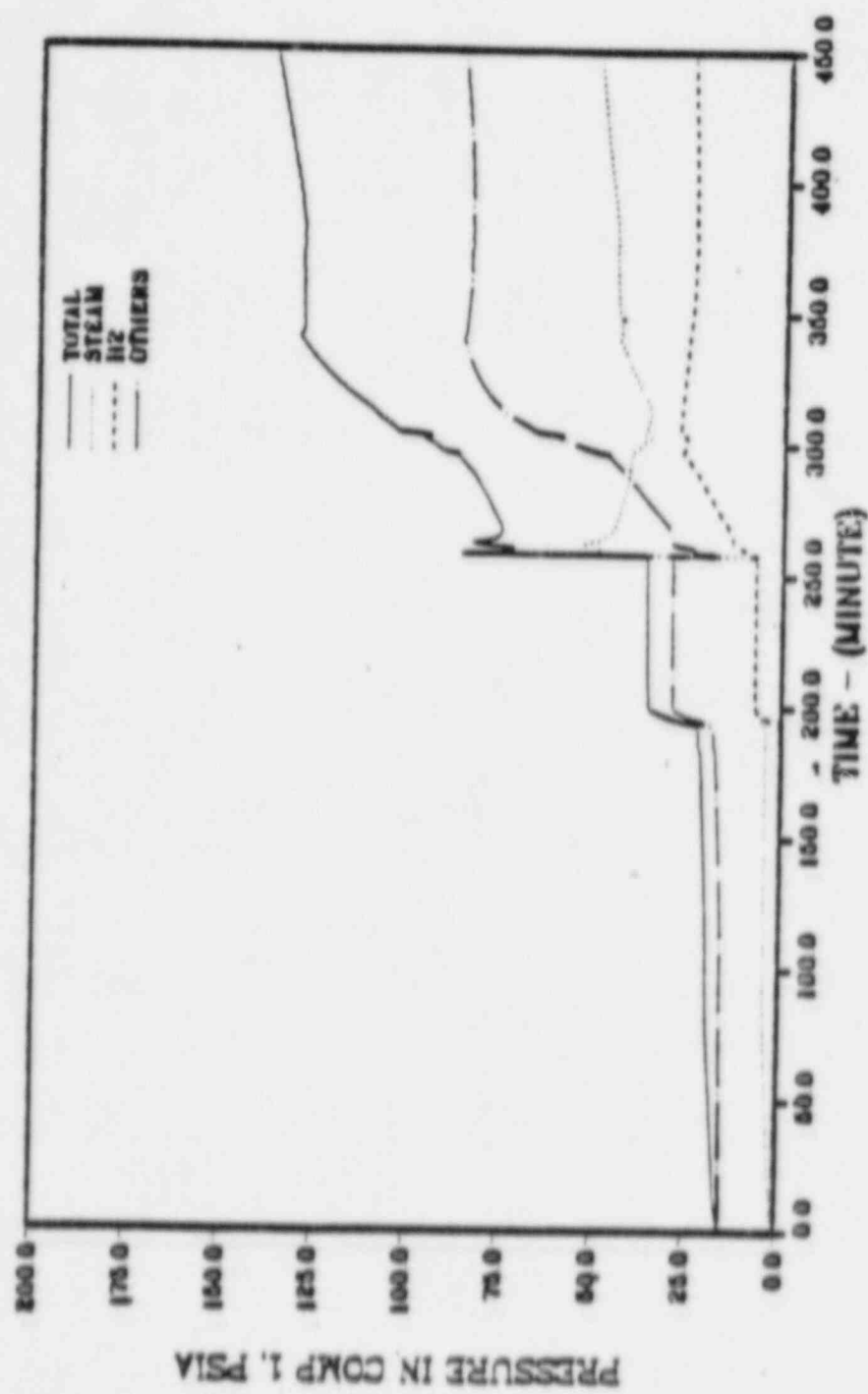


Figure III.1

1 P P

MKII STD PROB, MARCON CASE 5

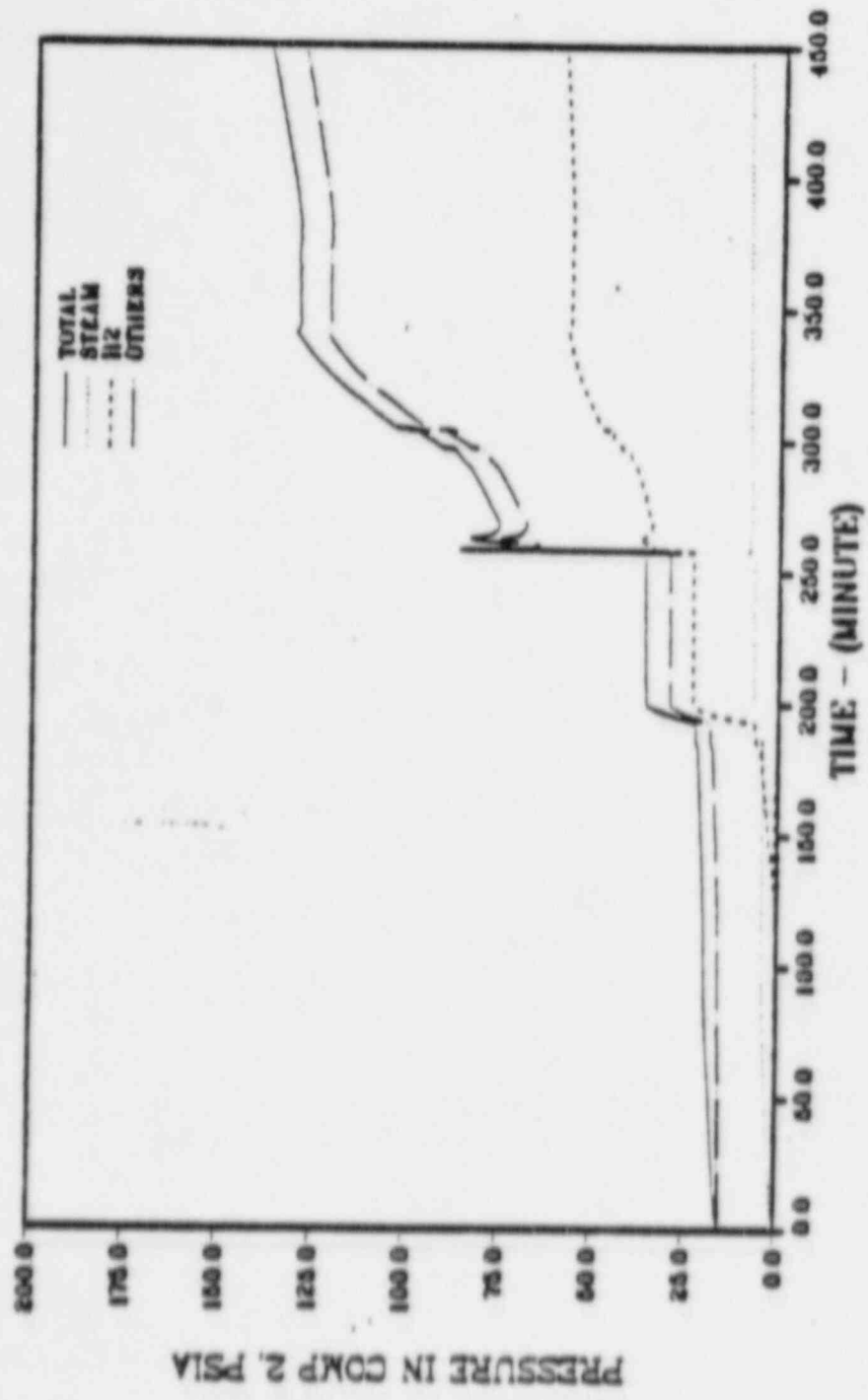


Figure III.2

1 P P

MKII STD PROB, MARCON CASE 5

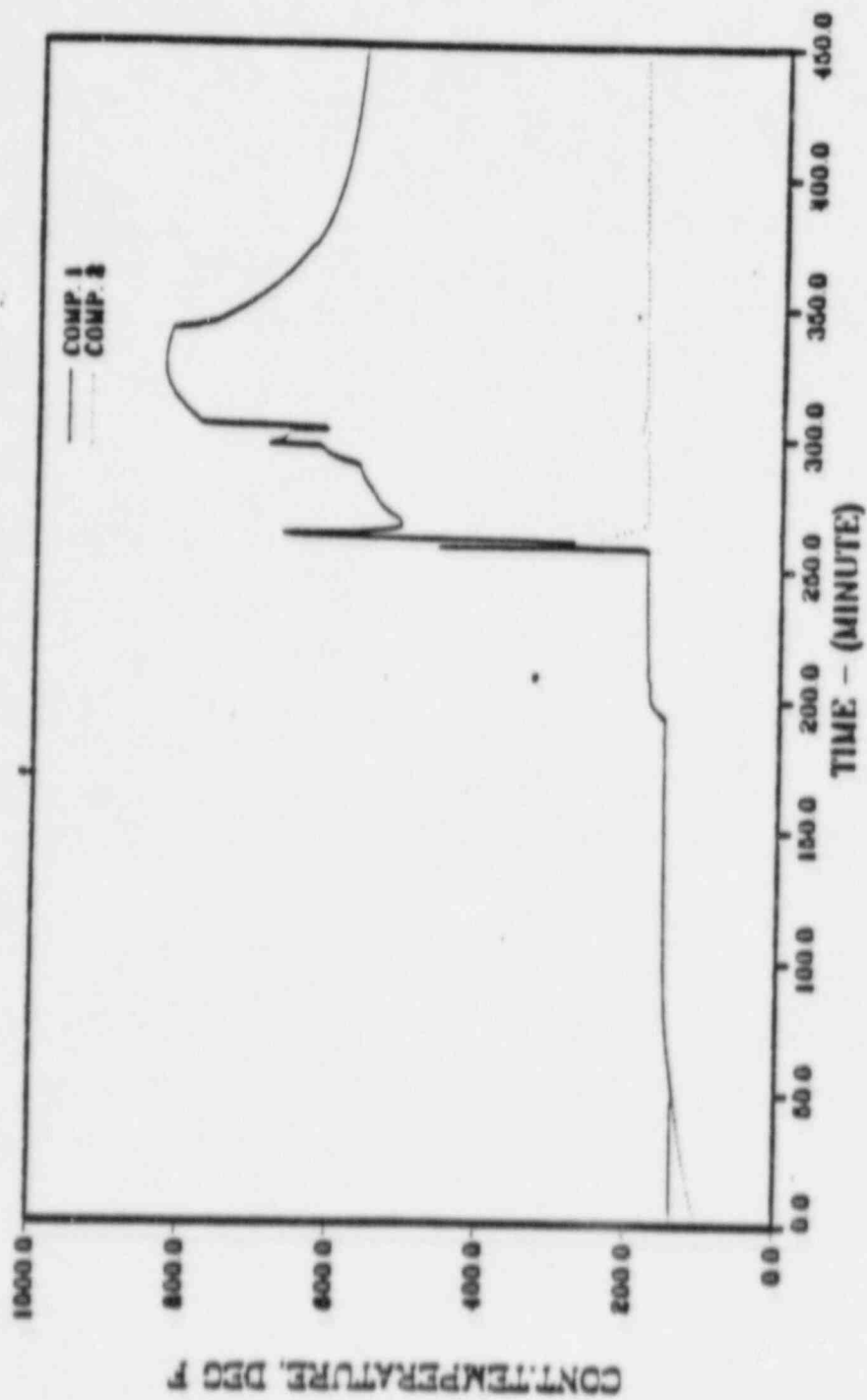


Figure 111.3

MKII STD PROB, MARCON CASE 5

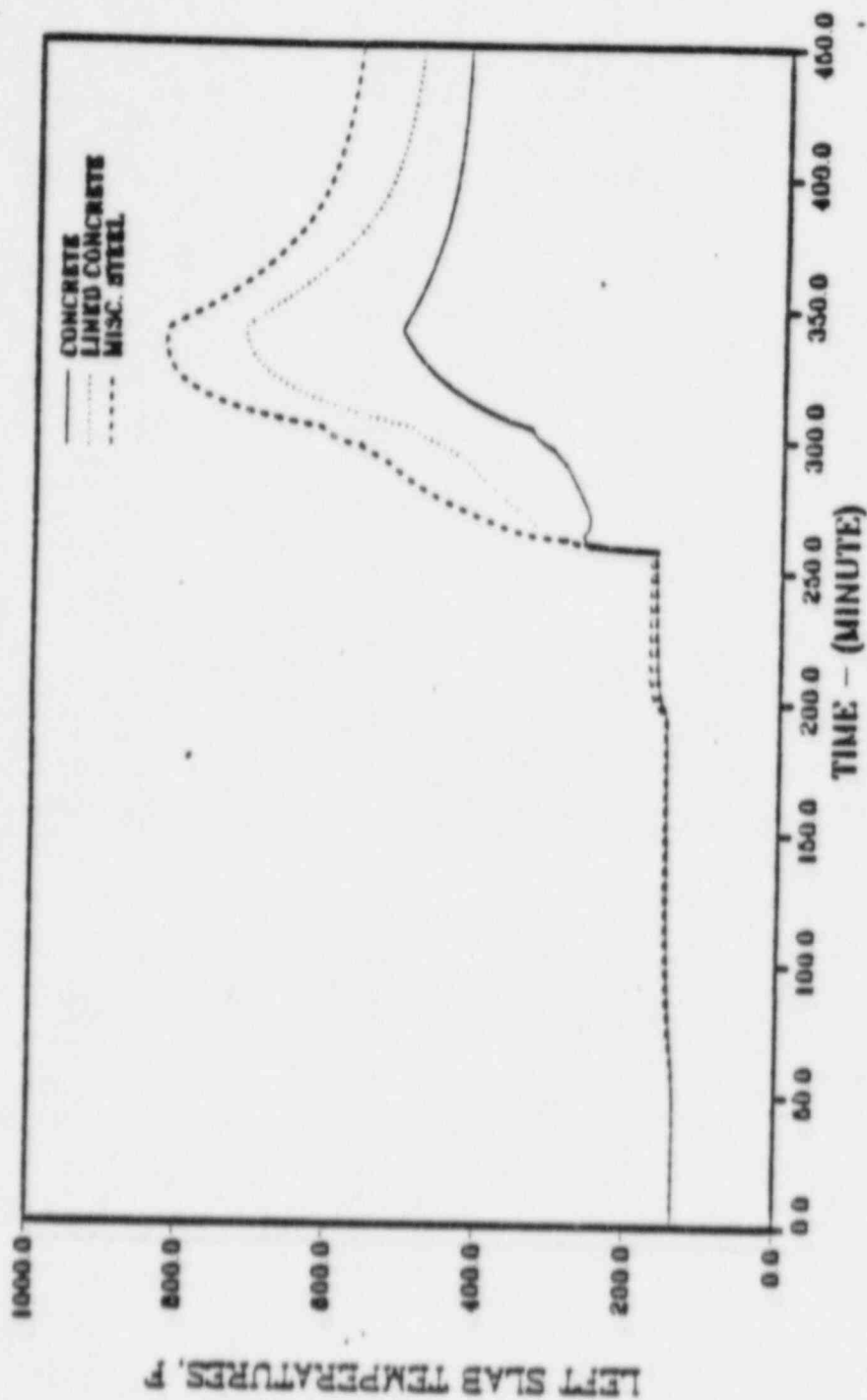
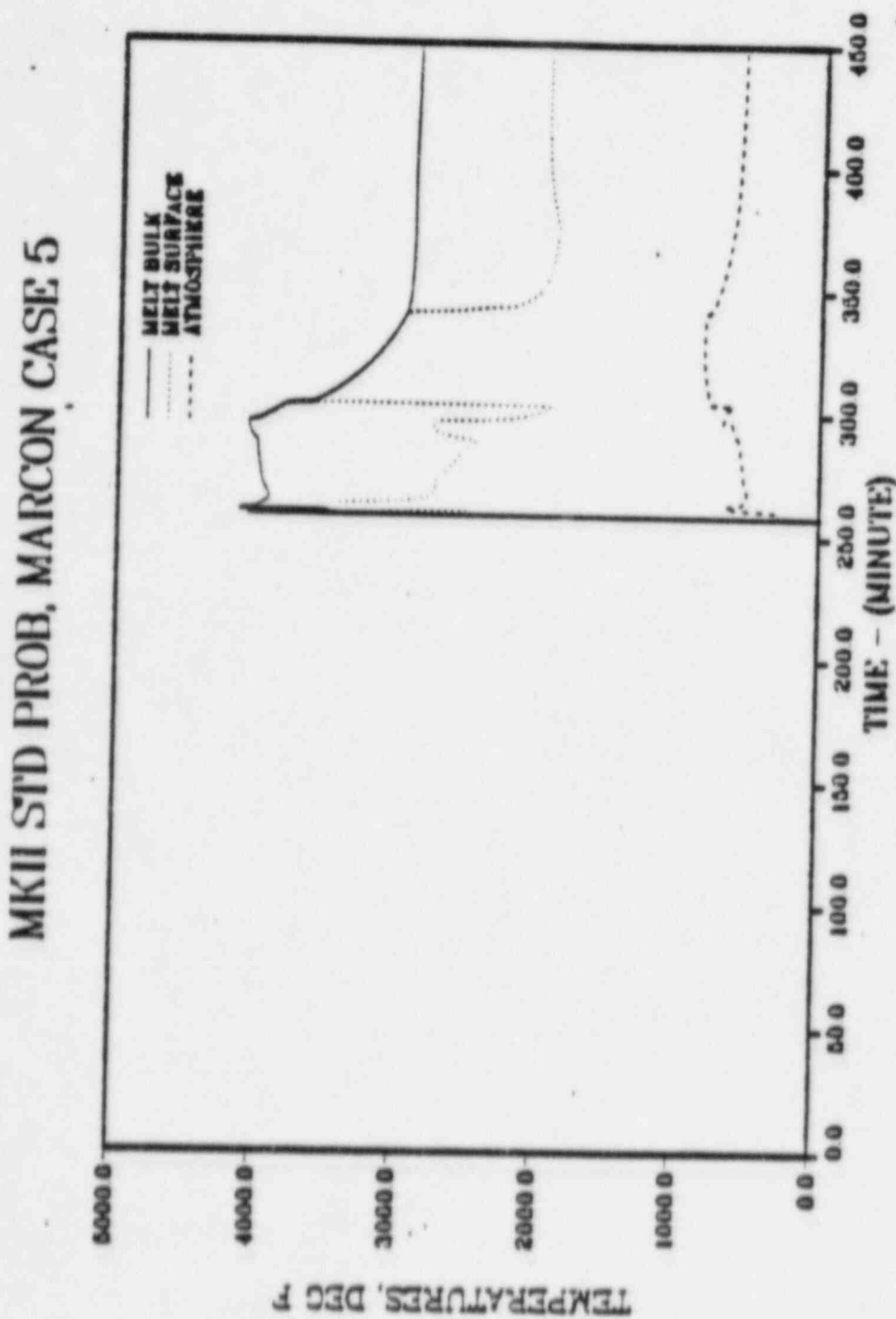
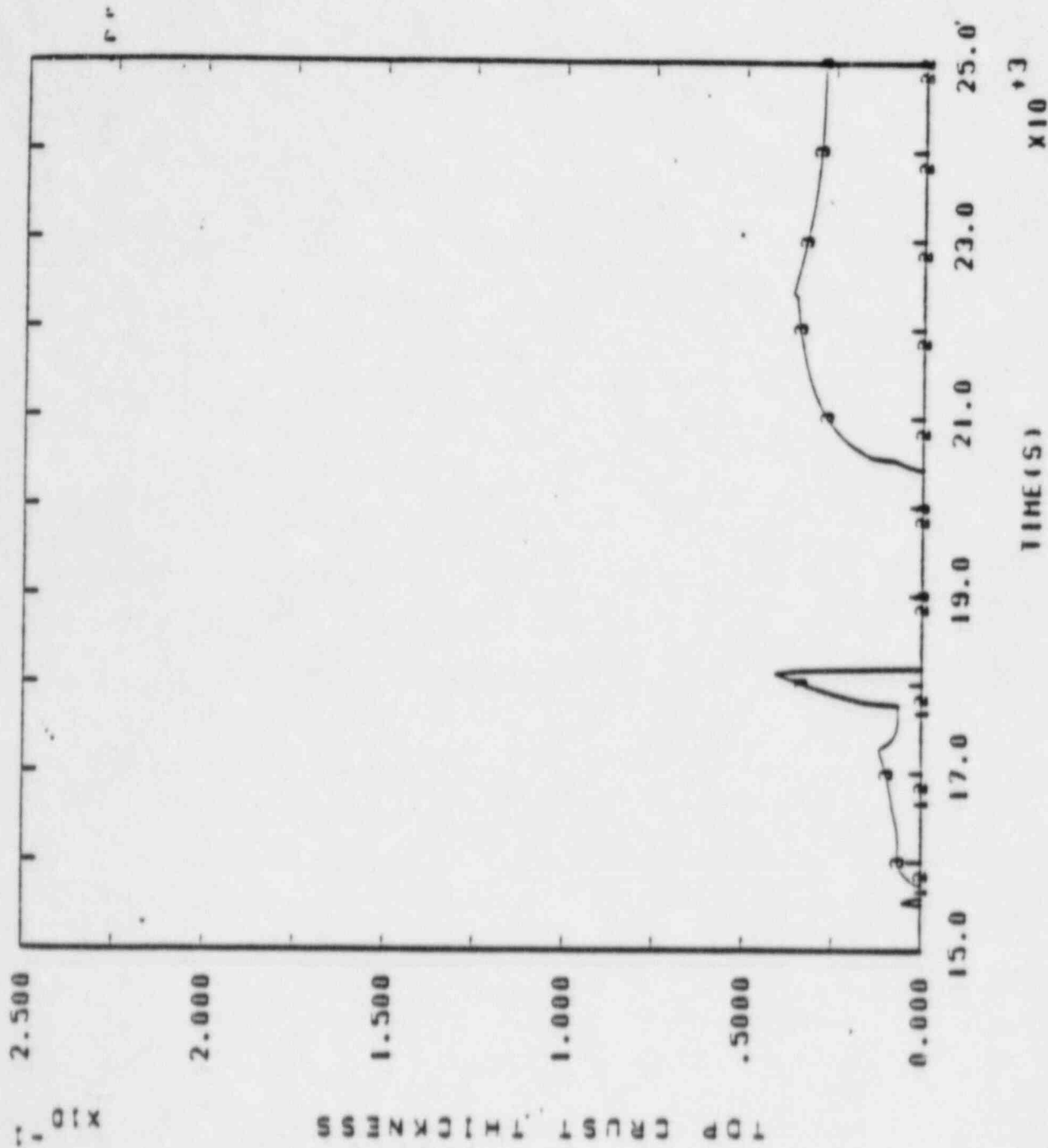


Figure 111.5

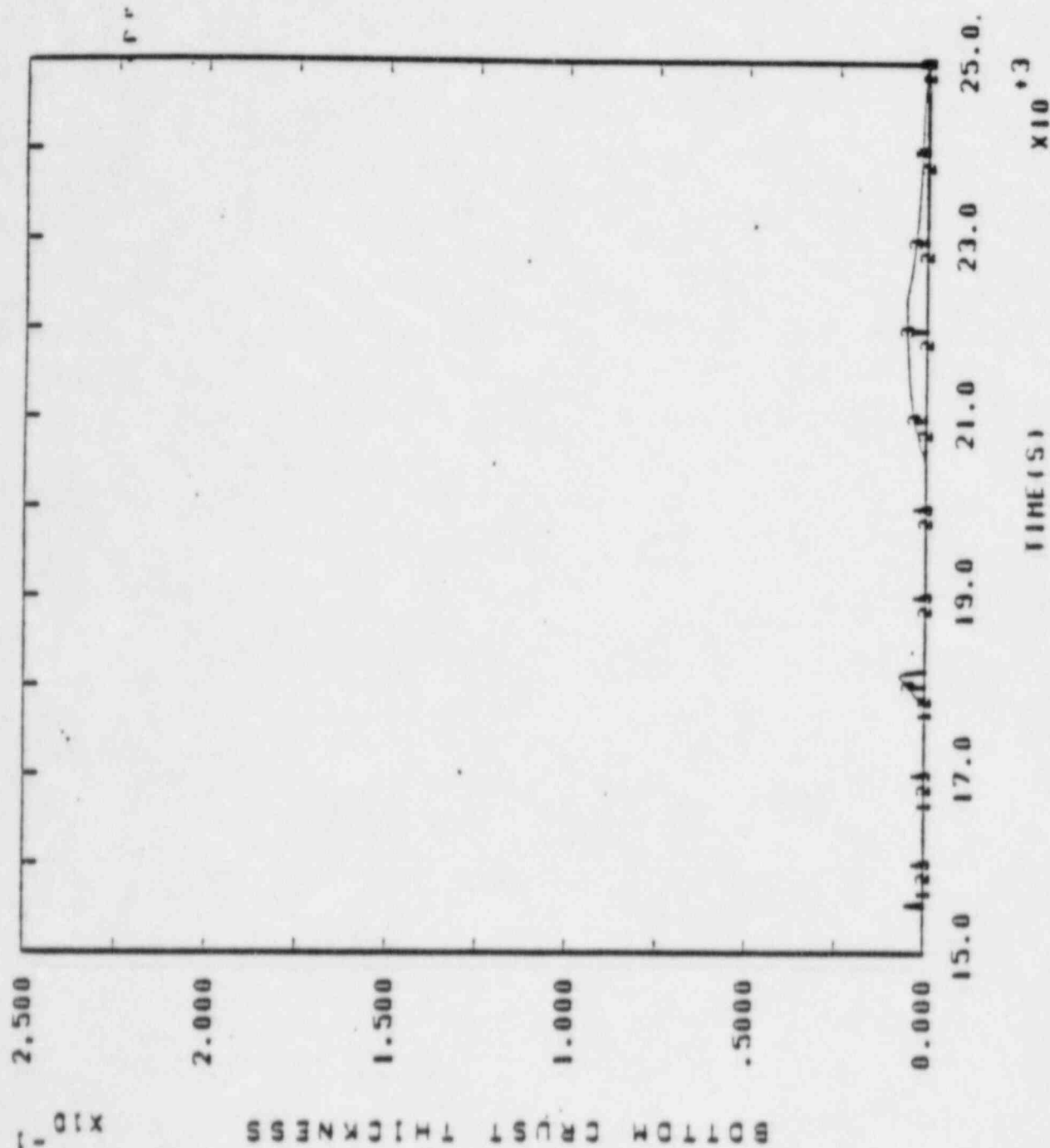




MARK II SID PROB. MARCON CASE 3

Figure III.7



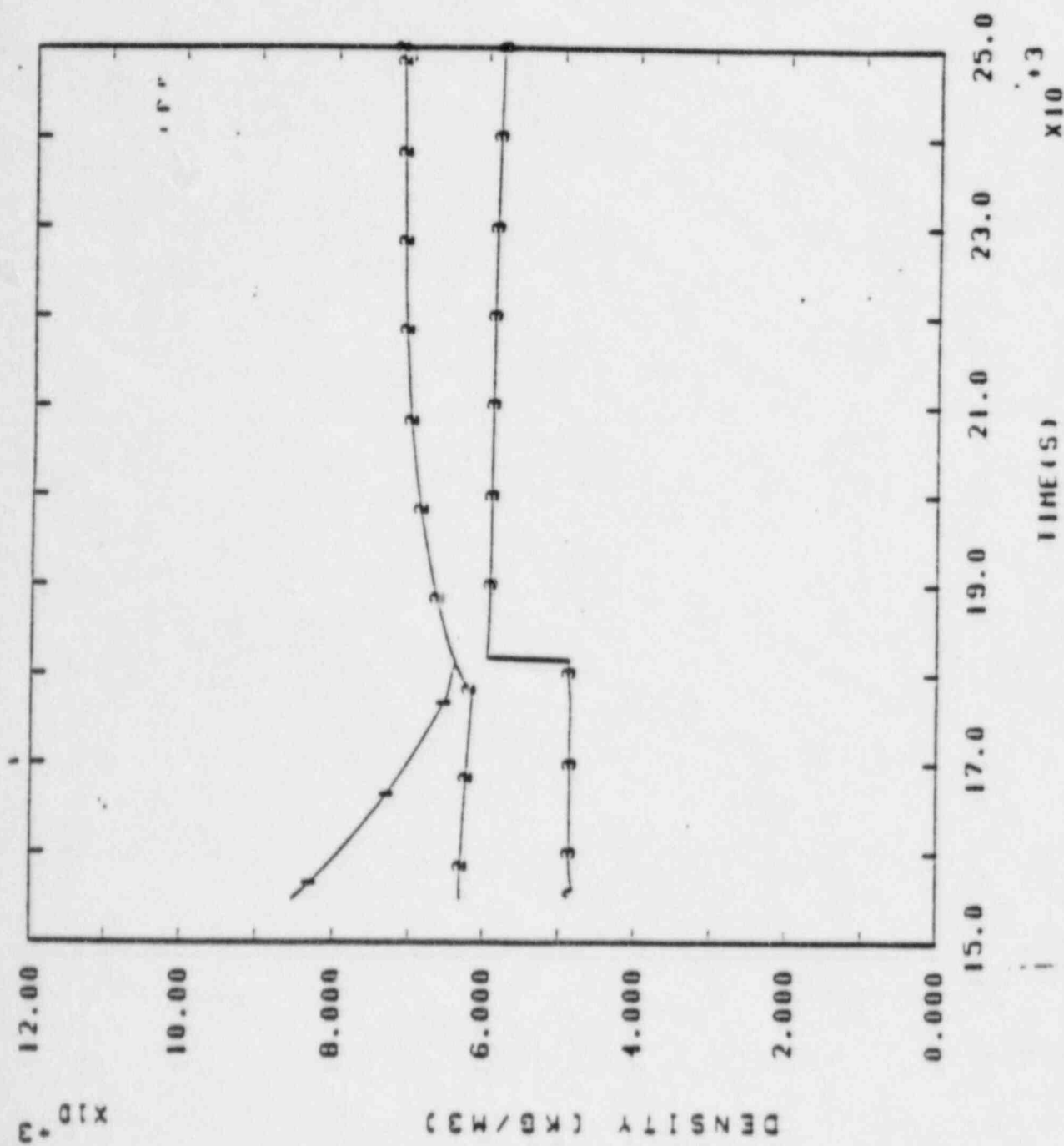


1 - CRUST THICKNESS
2 - CRUST HEIGHT
3 - CRUST LENGTH

MARK II STD PROB. MARCON CASE 3

Figure III.0





1 - DENSI11Y HON
2 - DENSI11Y HEI
3 - DENSI11Y LON

MARK II SID PROB. MARCON CASE 3

Figure III.9



MKII STD PROB, MARCON CASE 5

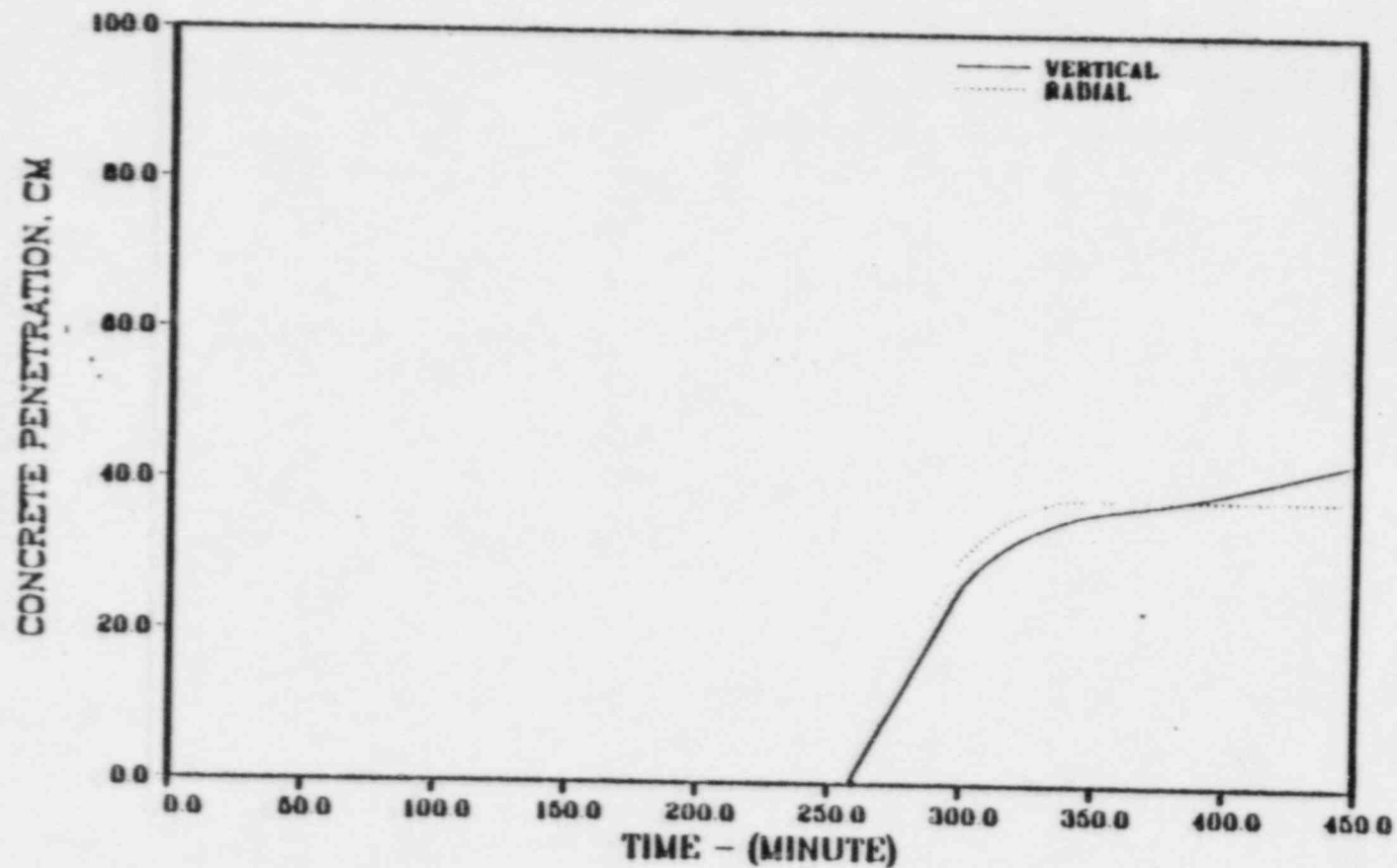


Figure III.10

MKII STD PROB, MARCON CASE 5

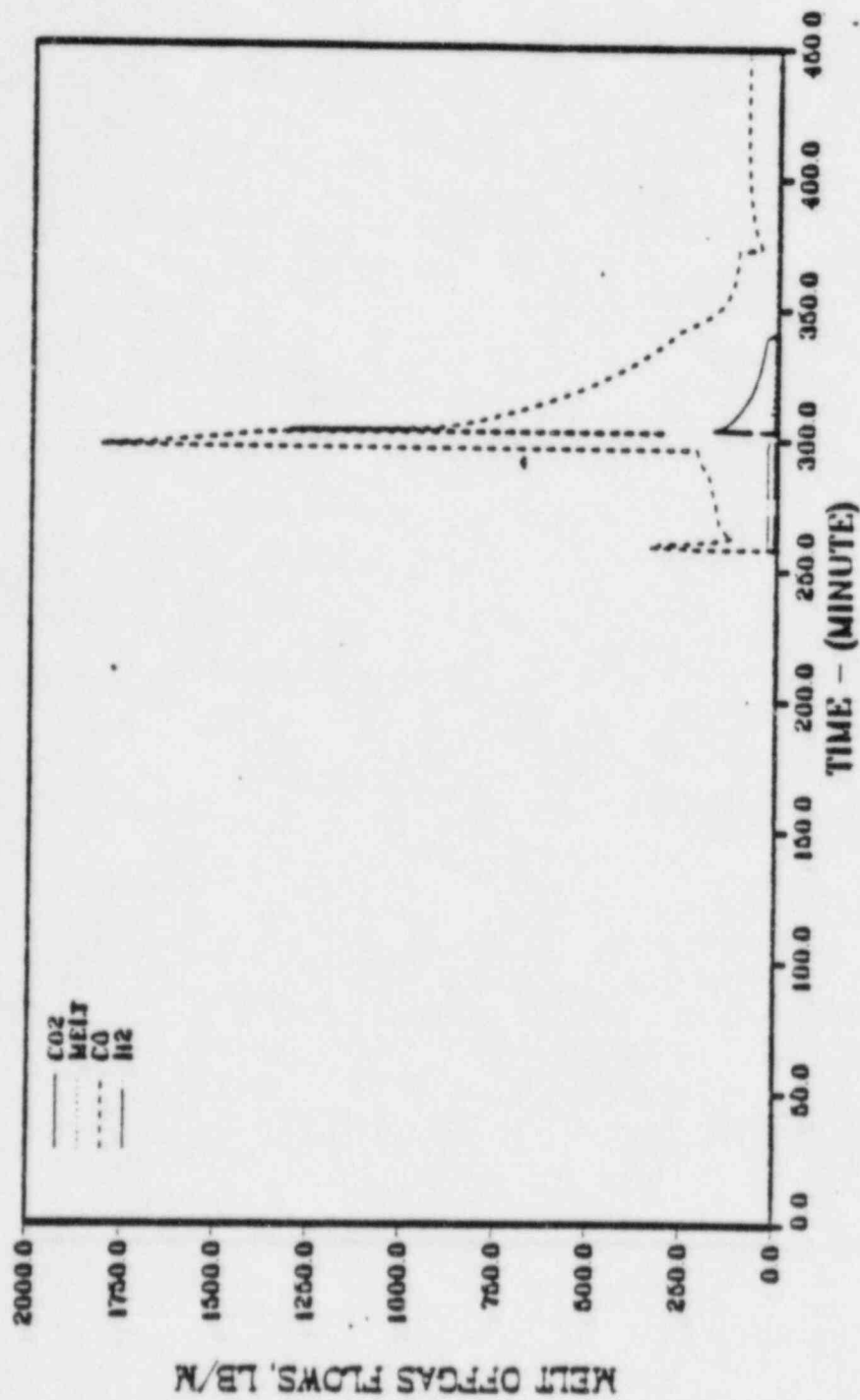
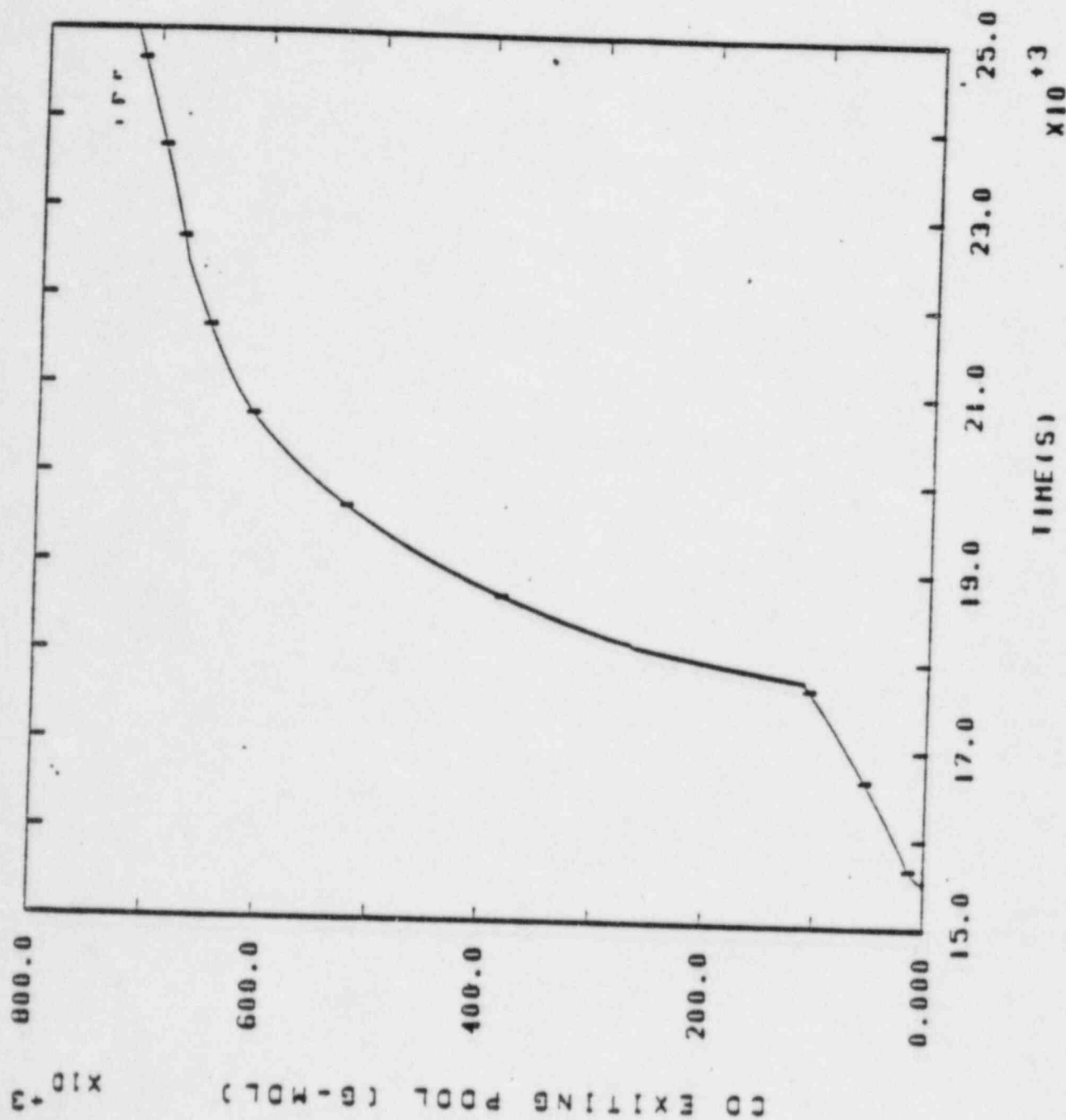


Figure III.11

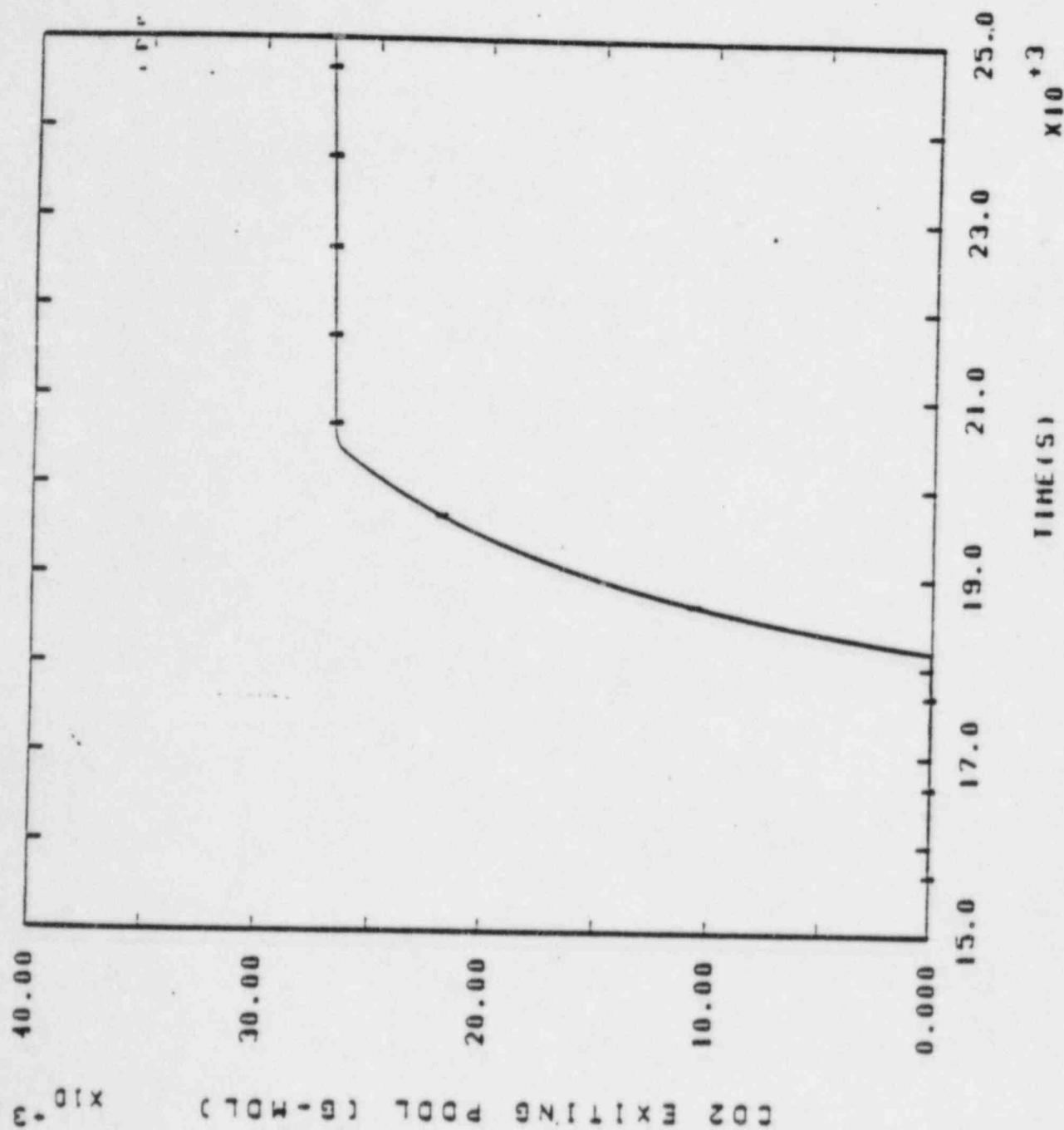


1 - CO GEN

MARK II STD PROB. MARCON CASE 3

Figure III.12



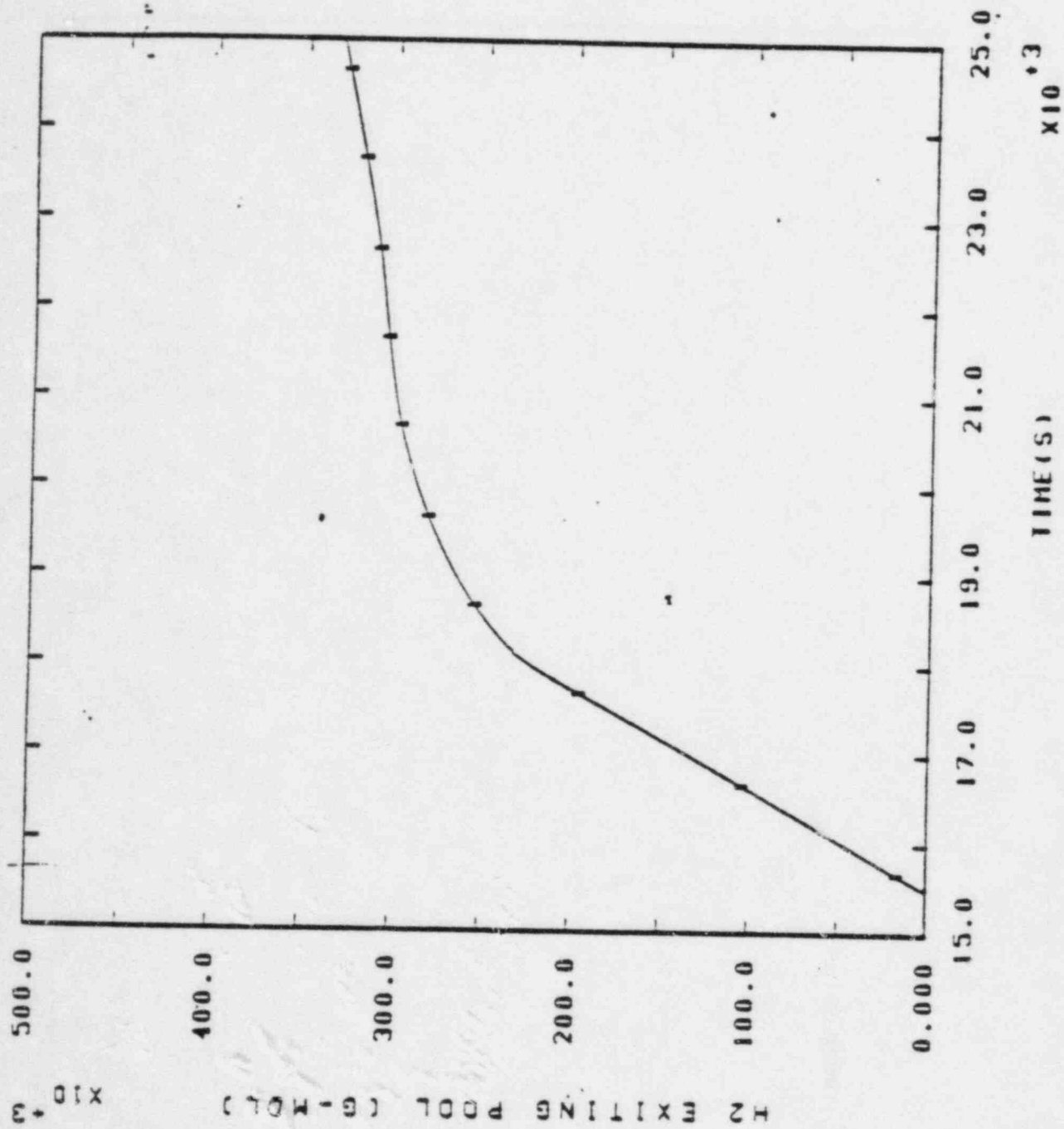


1 - CO2 GEN

MARK II SID PROB. MARCON CASE 3

Figure III.13



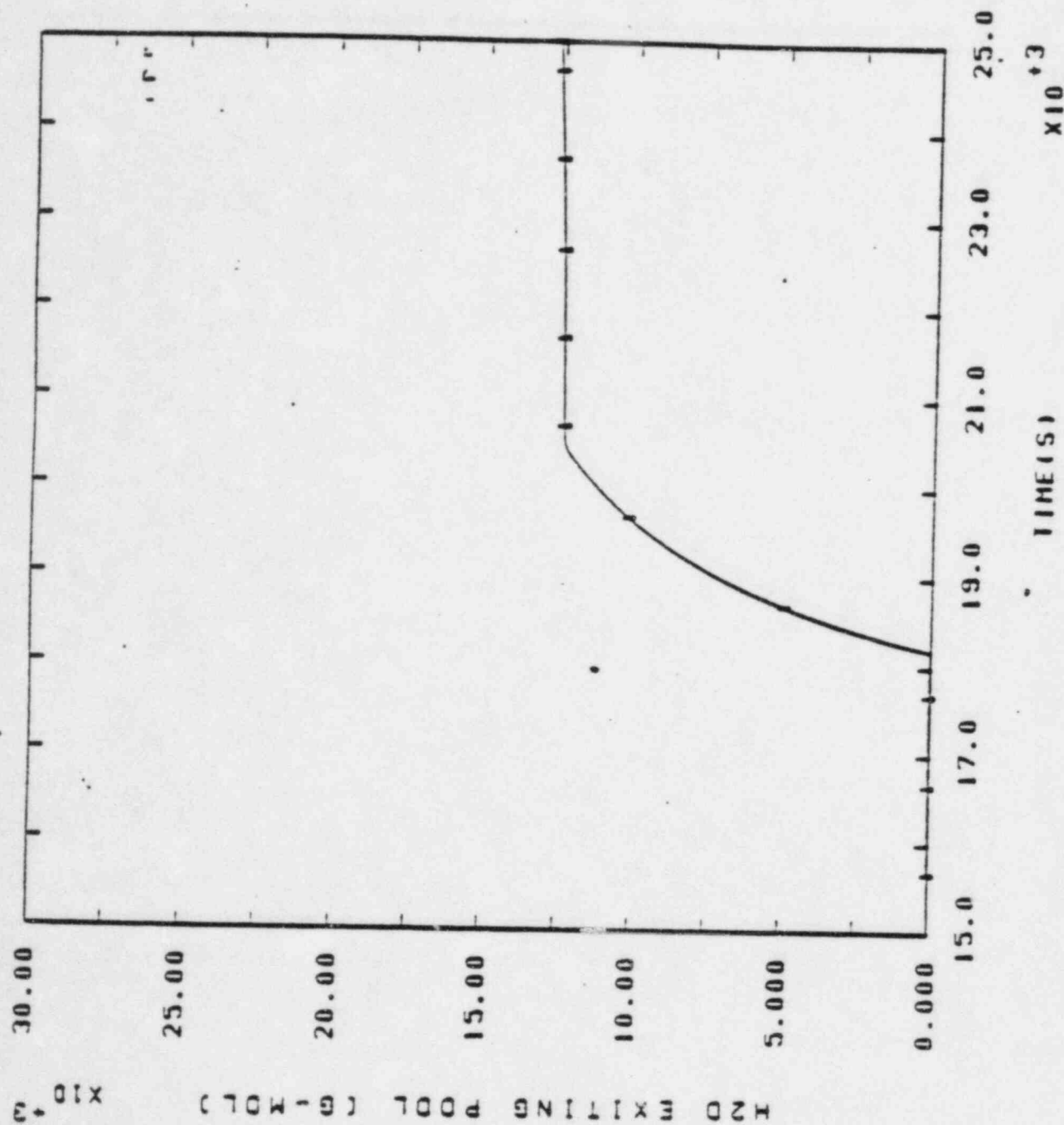


1 - H₂ GEN

MARK II SID PROB. MARCON CASE 3

Figure III.14





1 - H₂O GEN

MARK II SID PROB. MARCON CASE 3

Figure III.15



MKII STD PROB, MARCON CASE 5

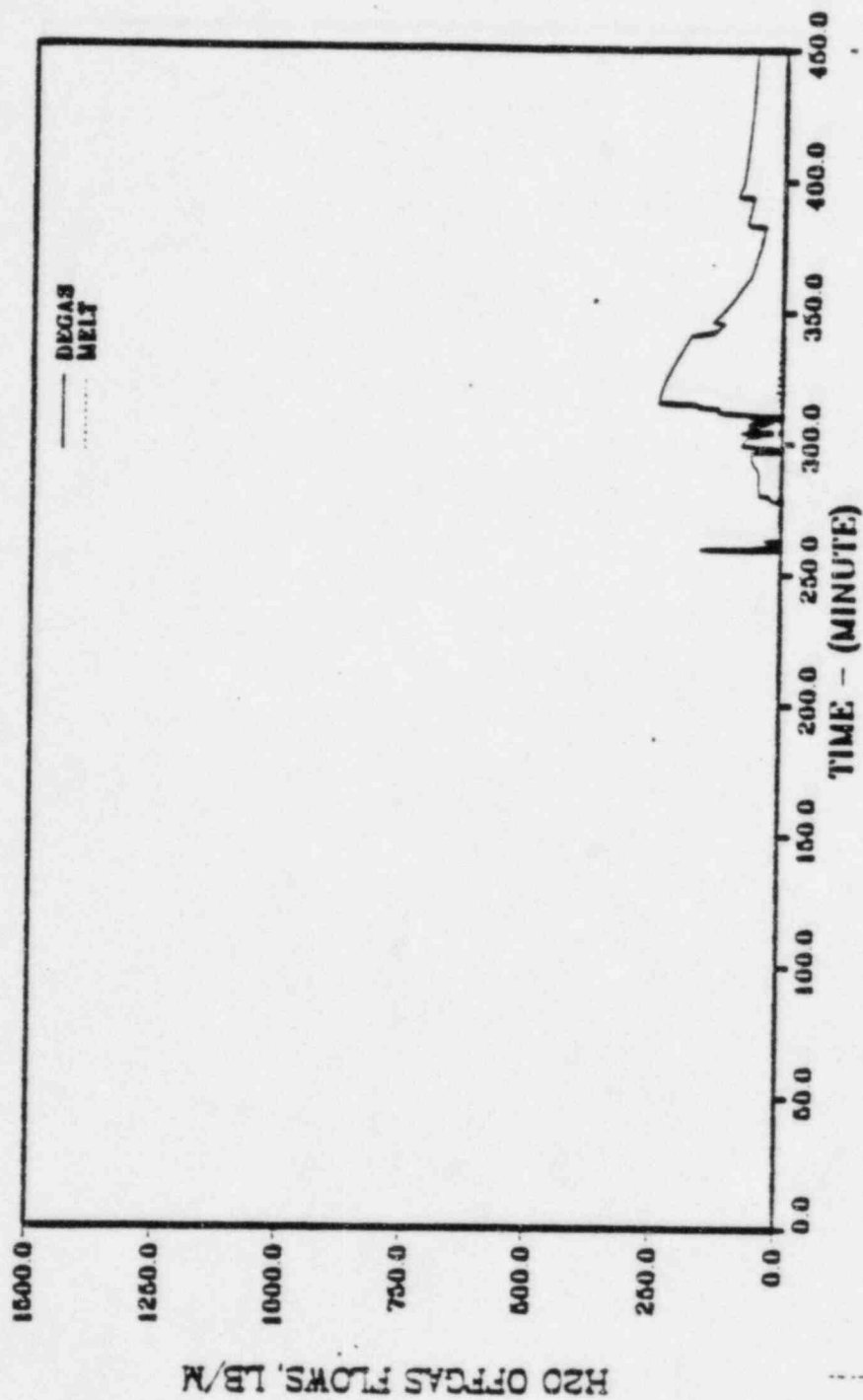


Figure 111.16

177

MKII STD PROB, MARCON CASE 6

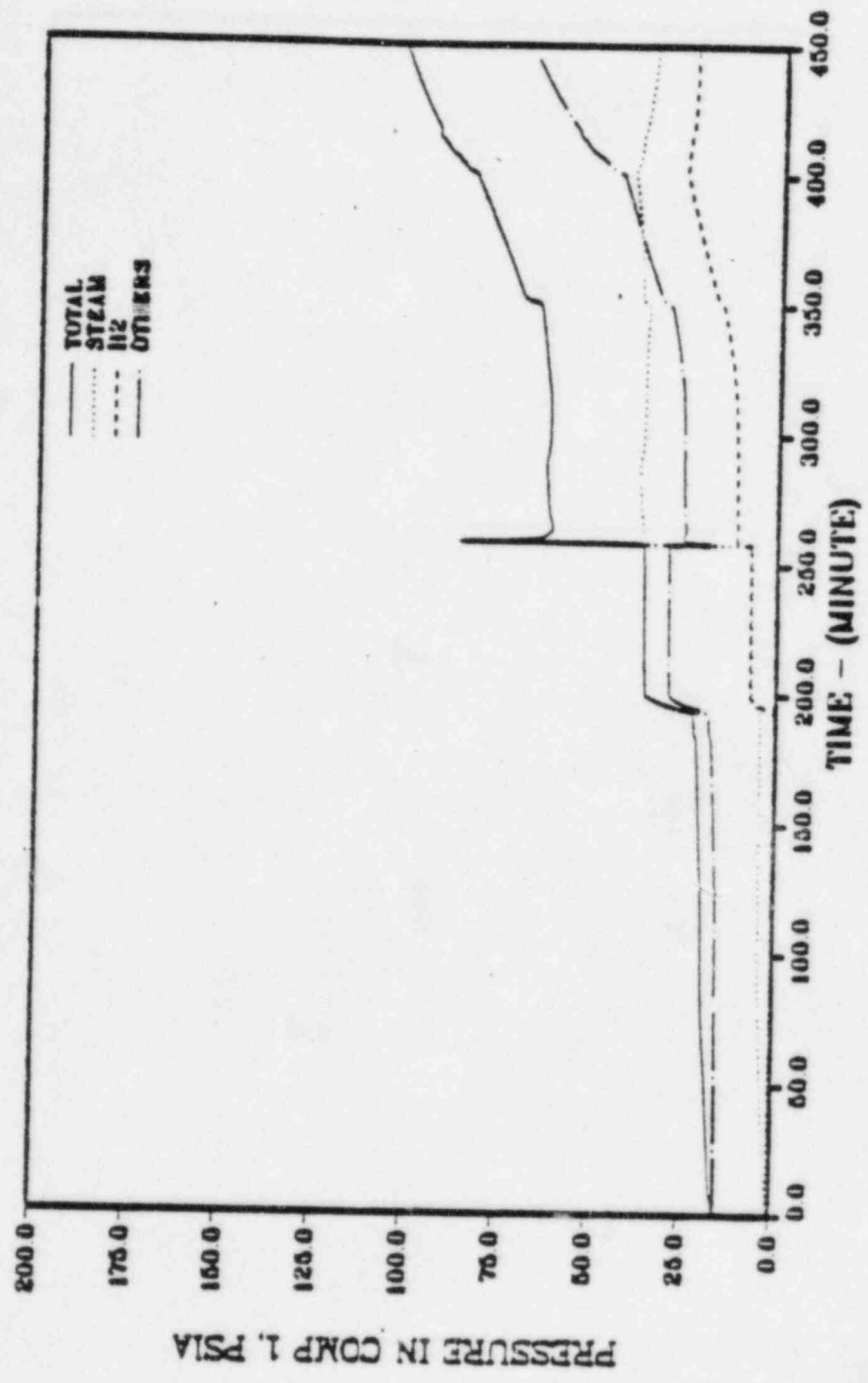


Figure III.18

MKII STD PROB, MARCON CASE 6

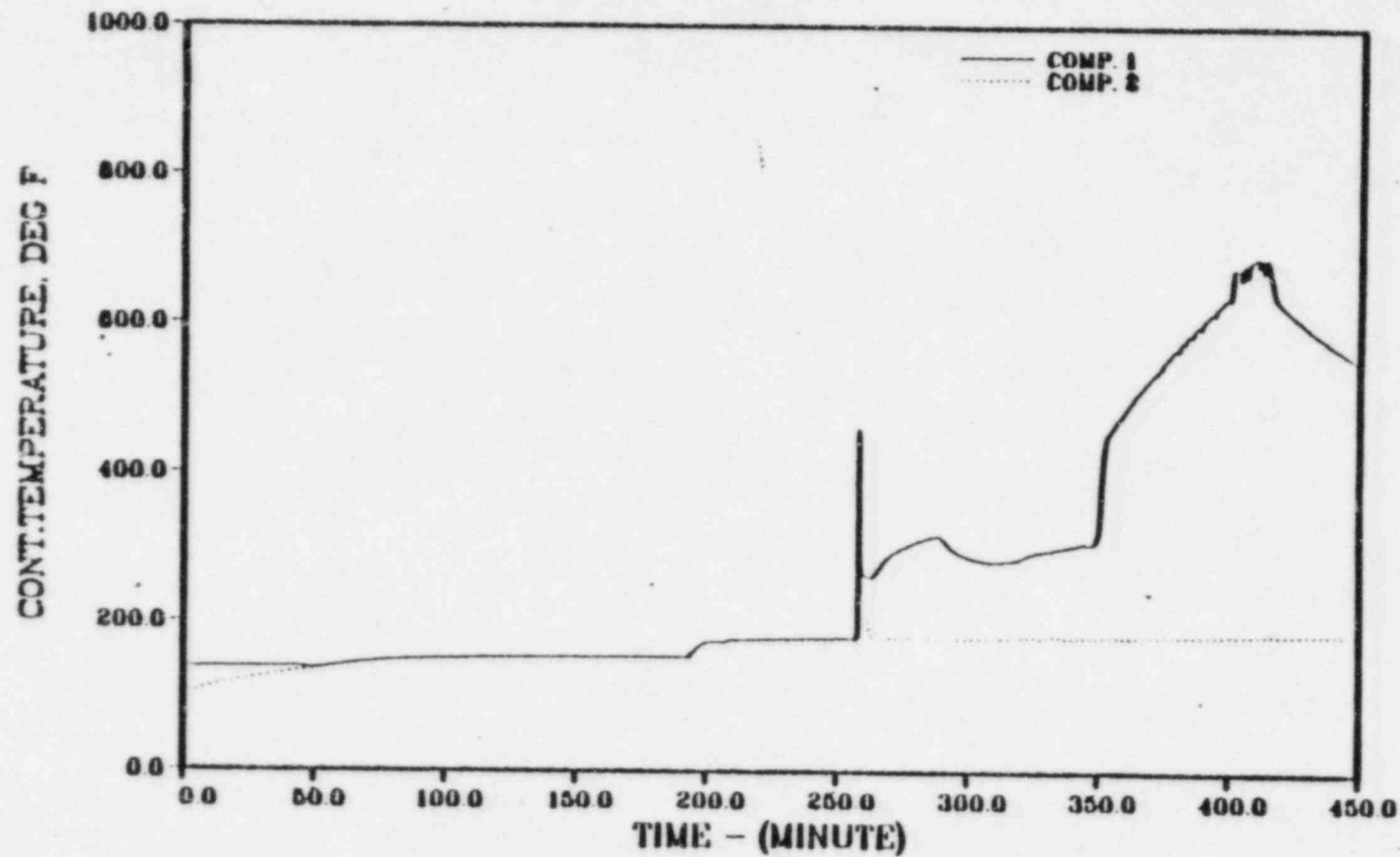


Figure III.19

MKII STD PROB, MARCON CASE 6

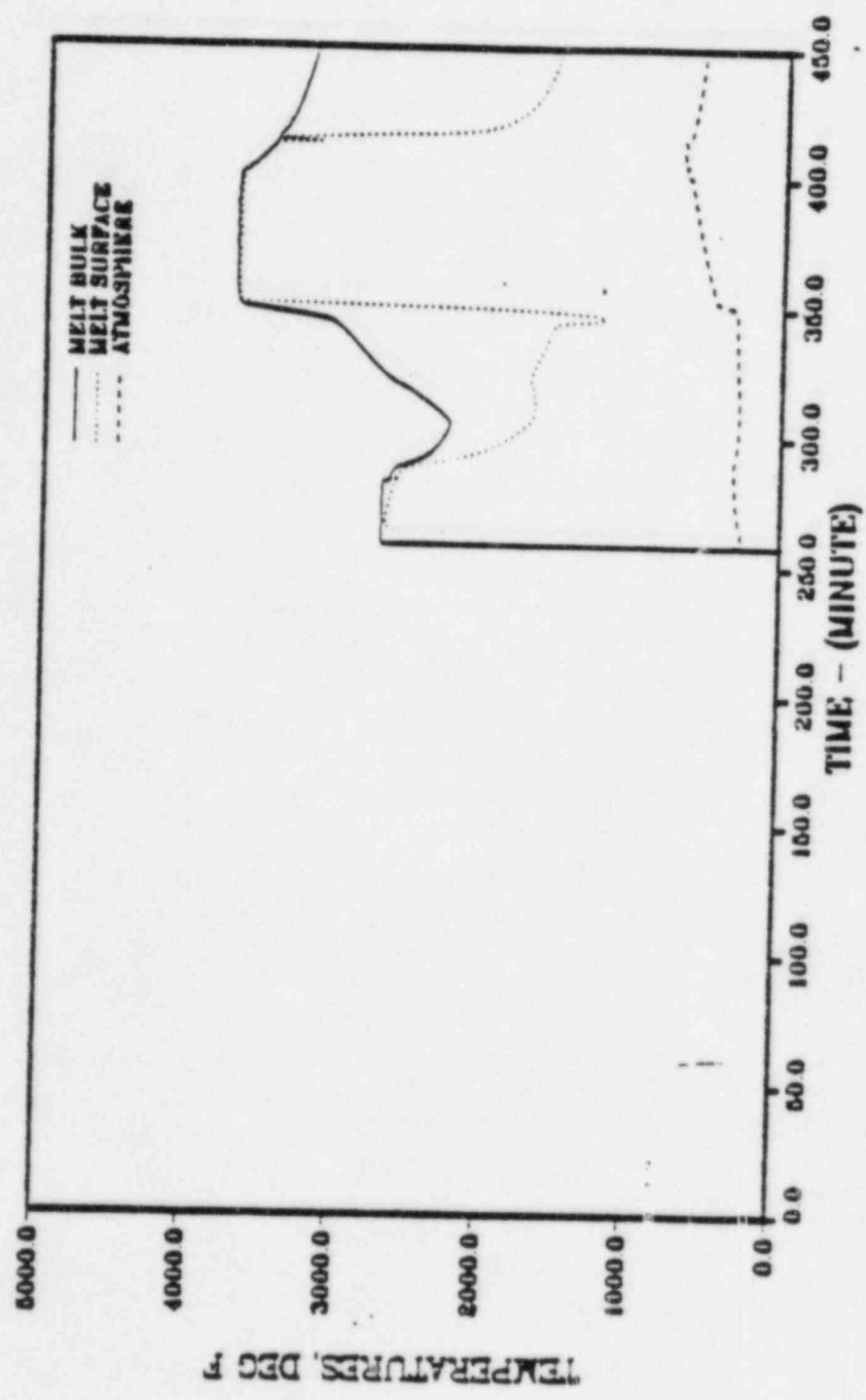


Figure III.20

MKII STD PROB, MARCON CASE 7

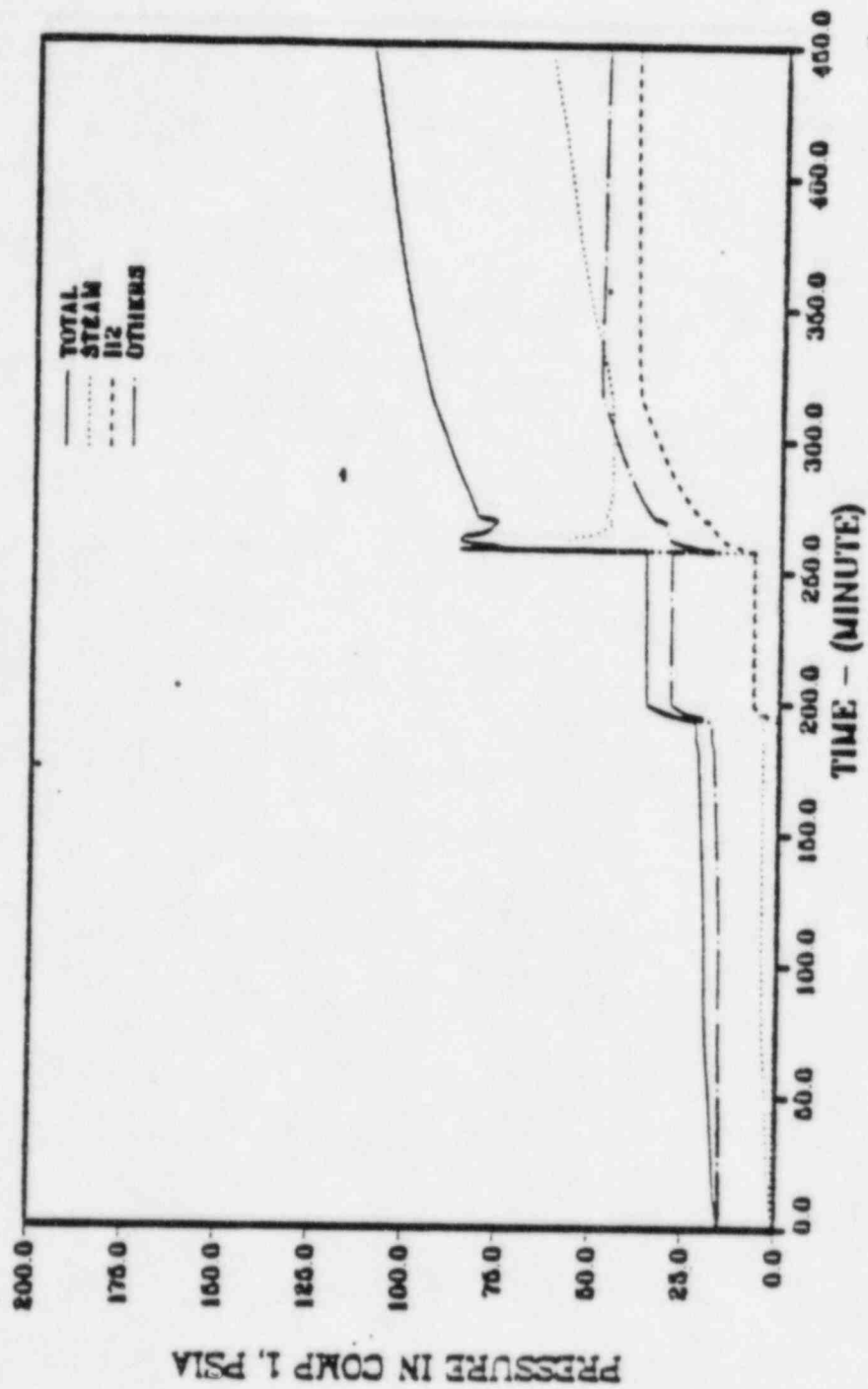


Figure III.22

MKII STD PROB, MARCON CASE 7

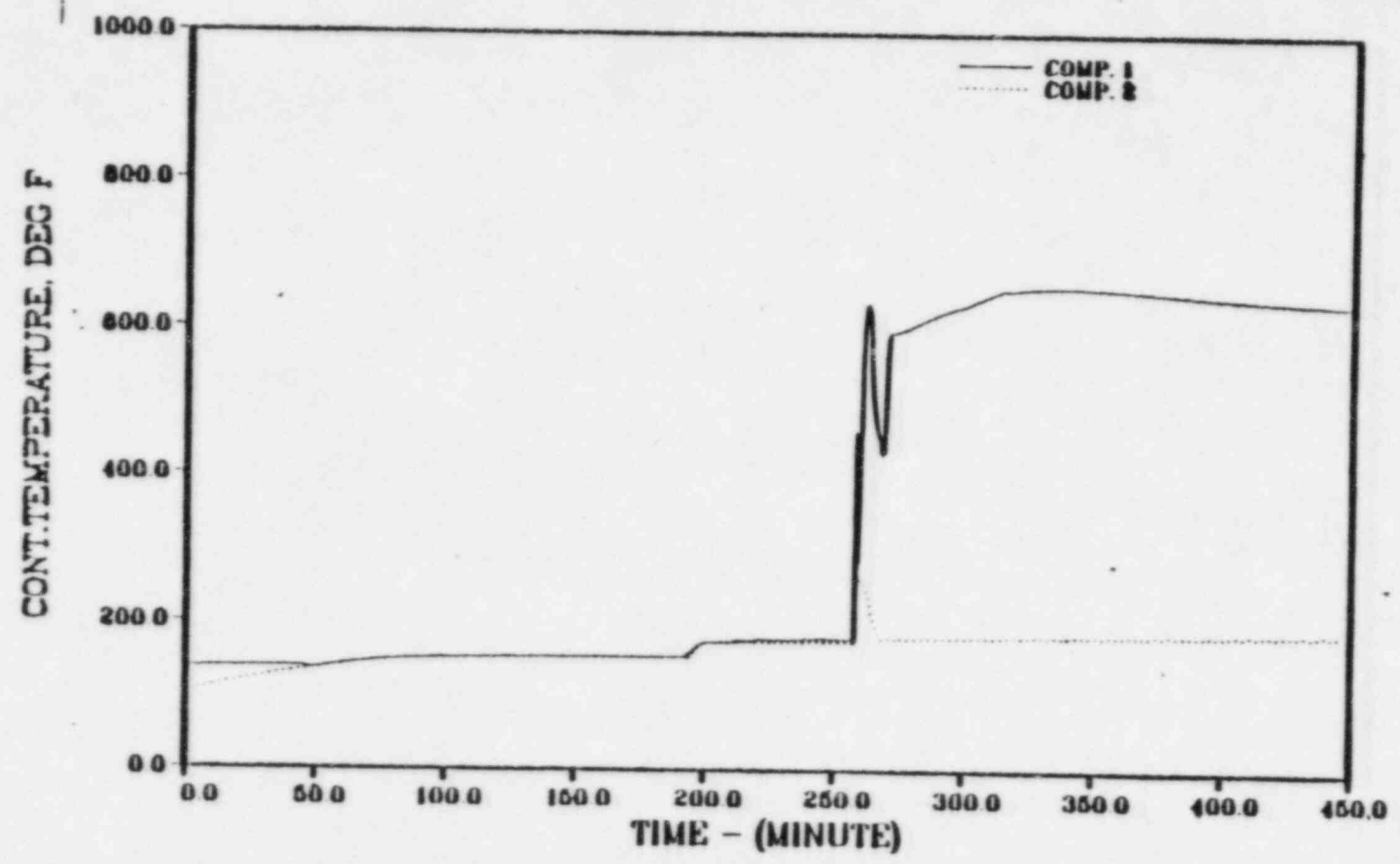


Figure III.23

1 F P

MKII STD PROB, MARCON CASE 7

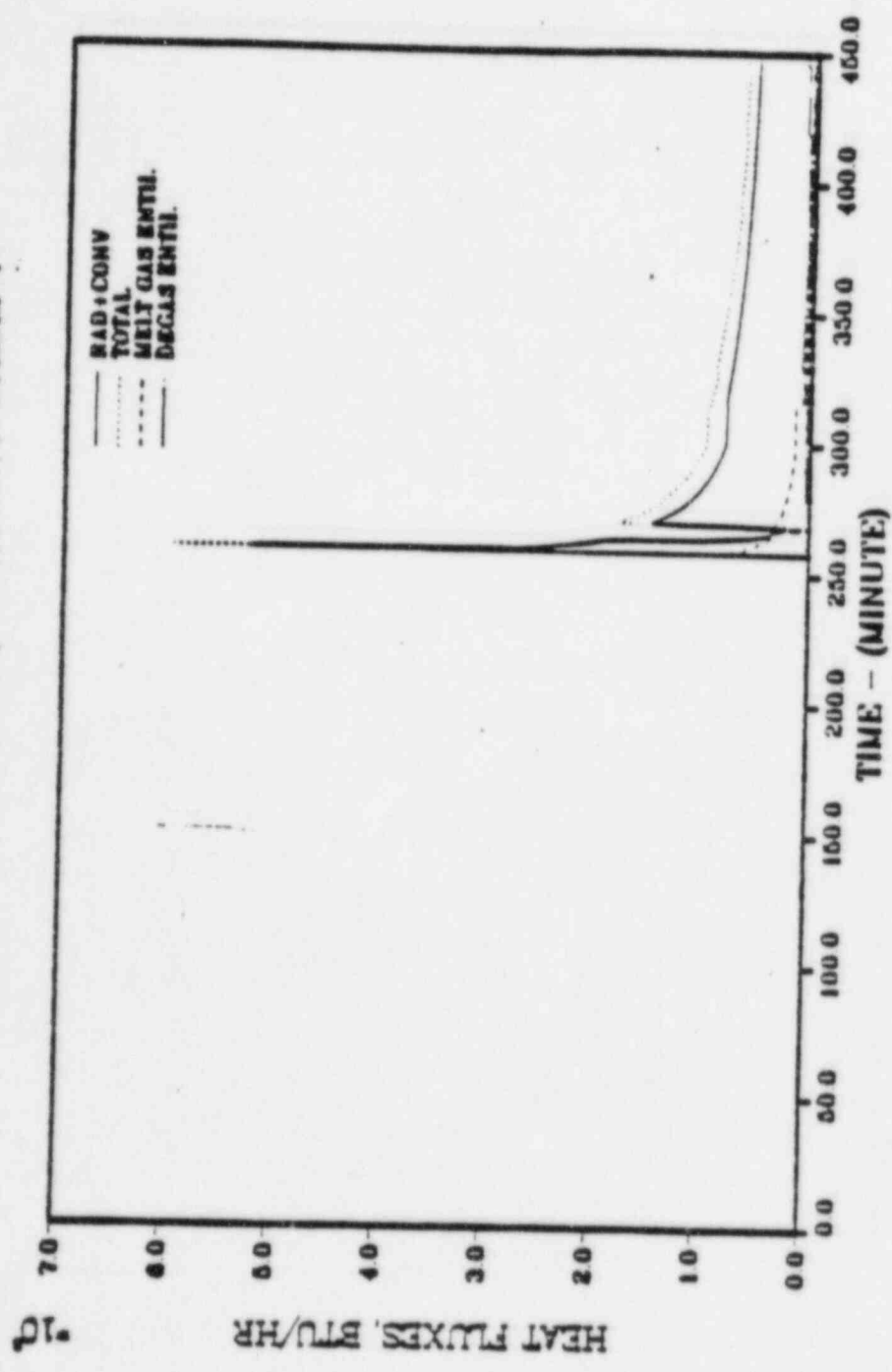


Figure III.26

MKII STD PROB, MARCON CASE 7

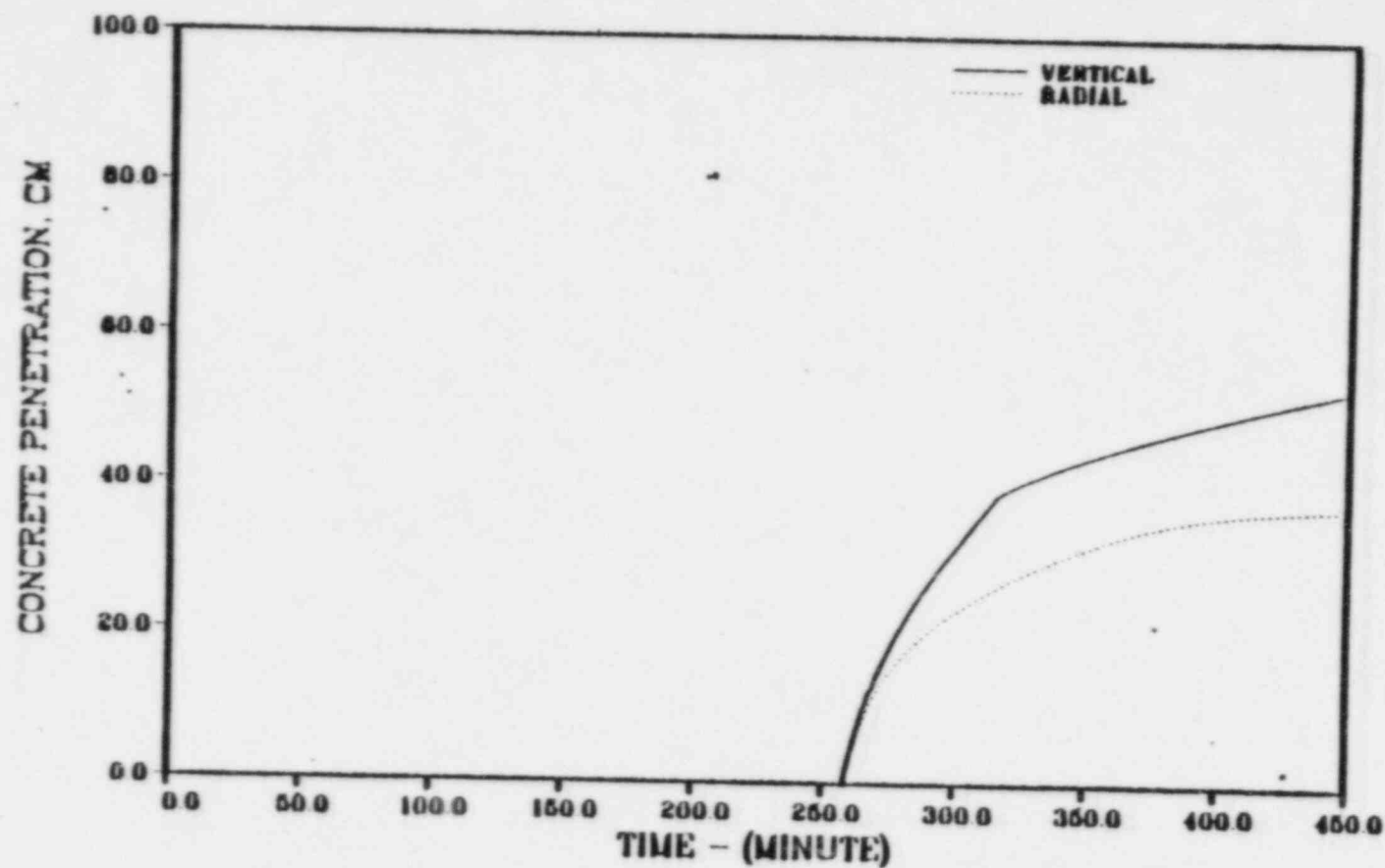


Figure III.27

MKII STD PROB, MARCON CASE 7

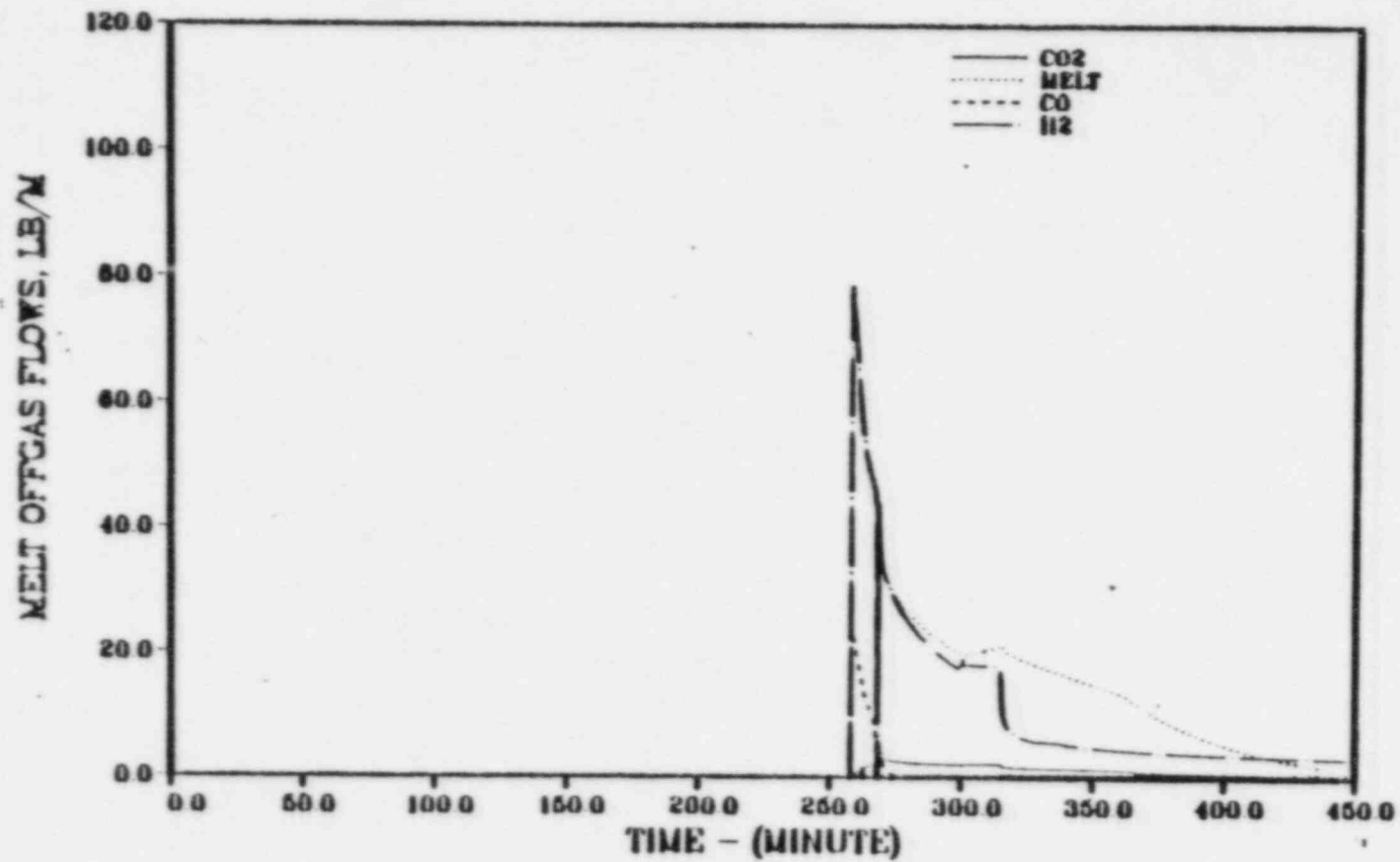


Figure III.28

1 F 4

MKII STD PROB, MARCON CASE 7

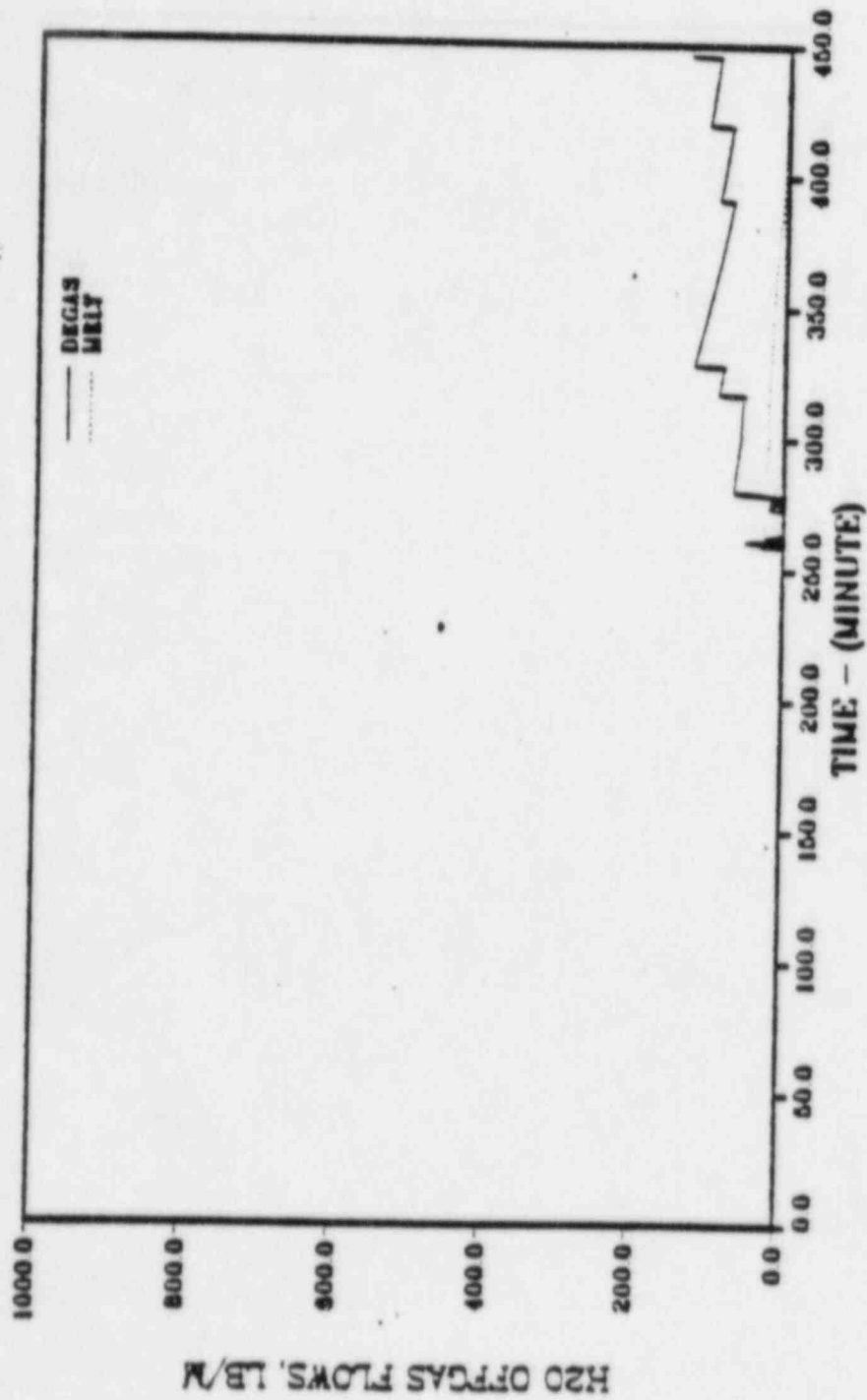


Figure III.29

1 F P

MKII SP MARCON CASE7, NO RHT

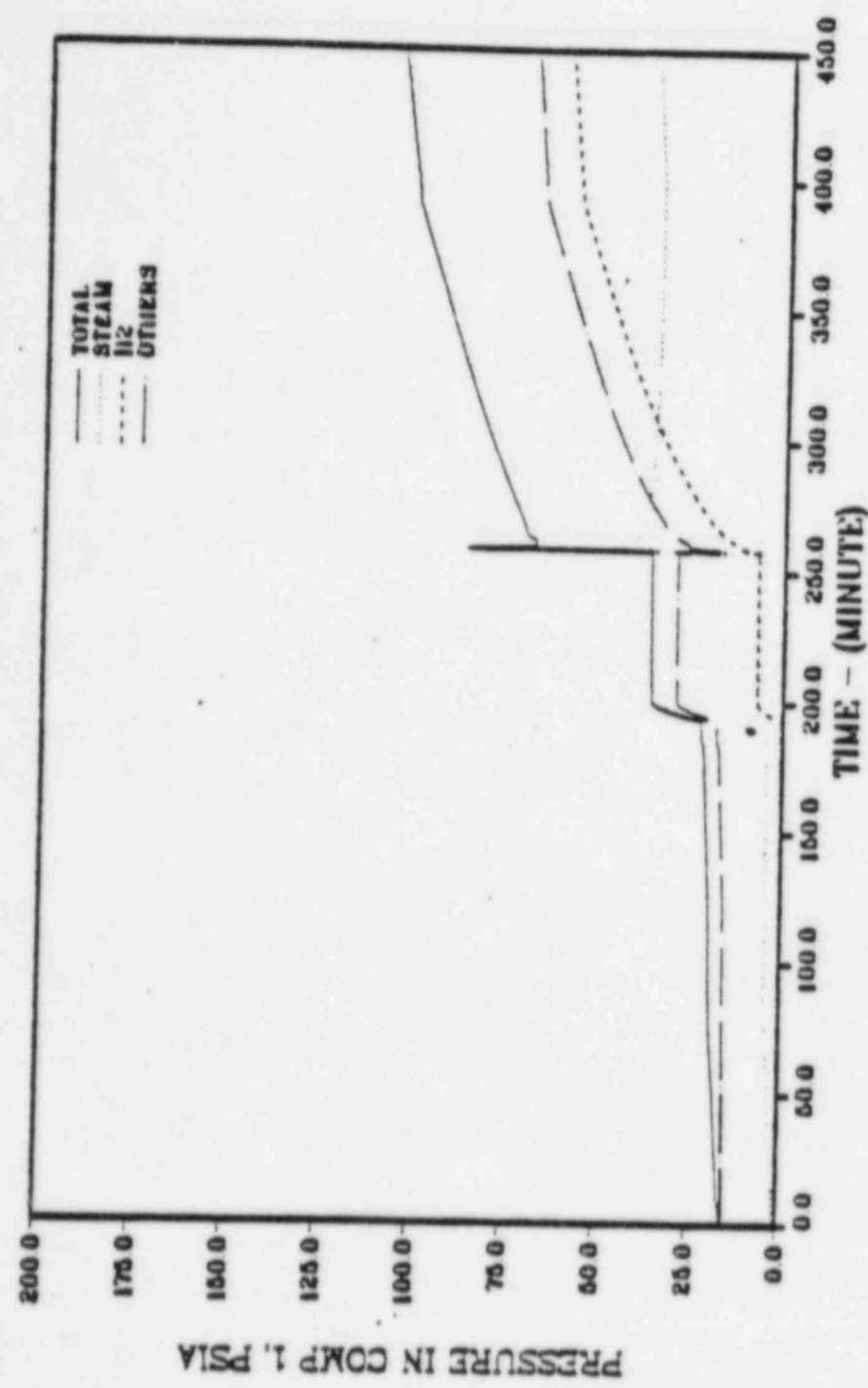


Figure 111.30

1 F F

MKII SP MARCON CASE7, NO RHT

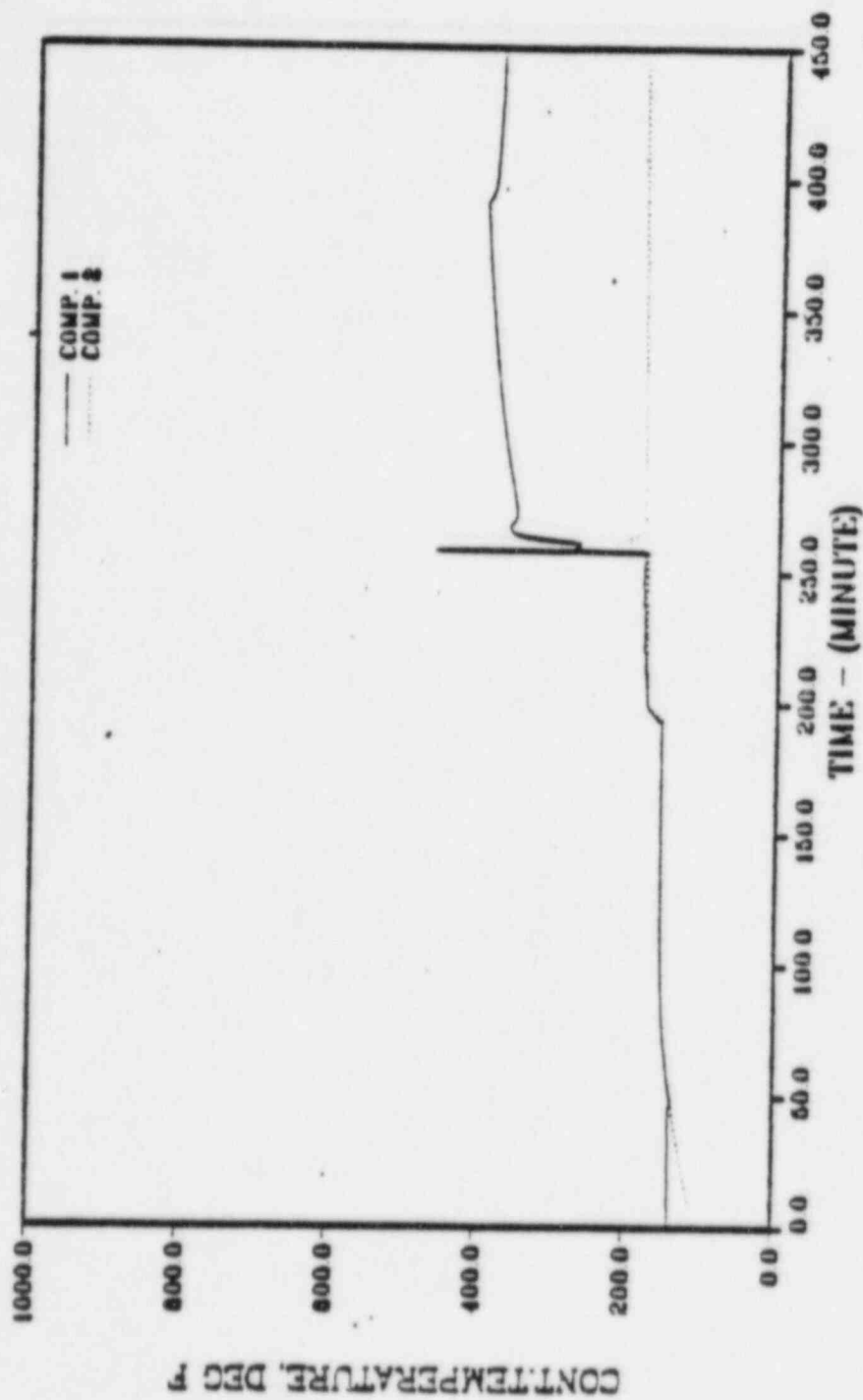


Figure III.31

1 F F

MKII STD PROB, MARCON CASE 8

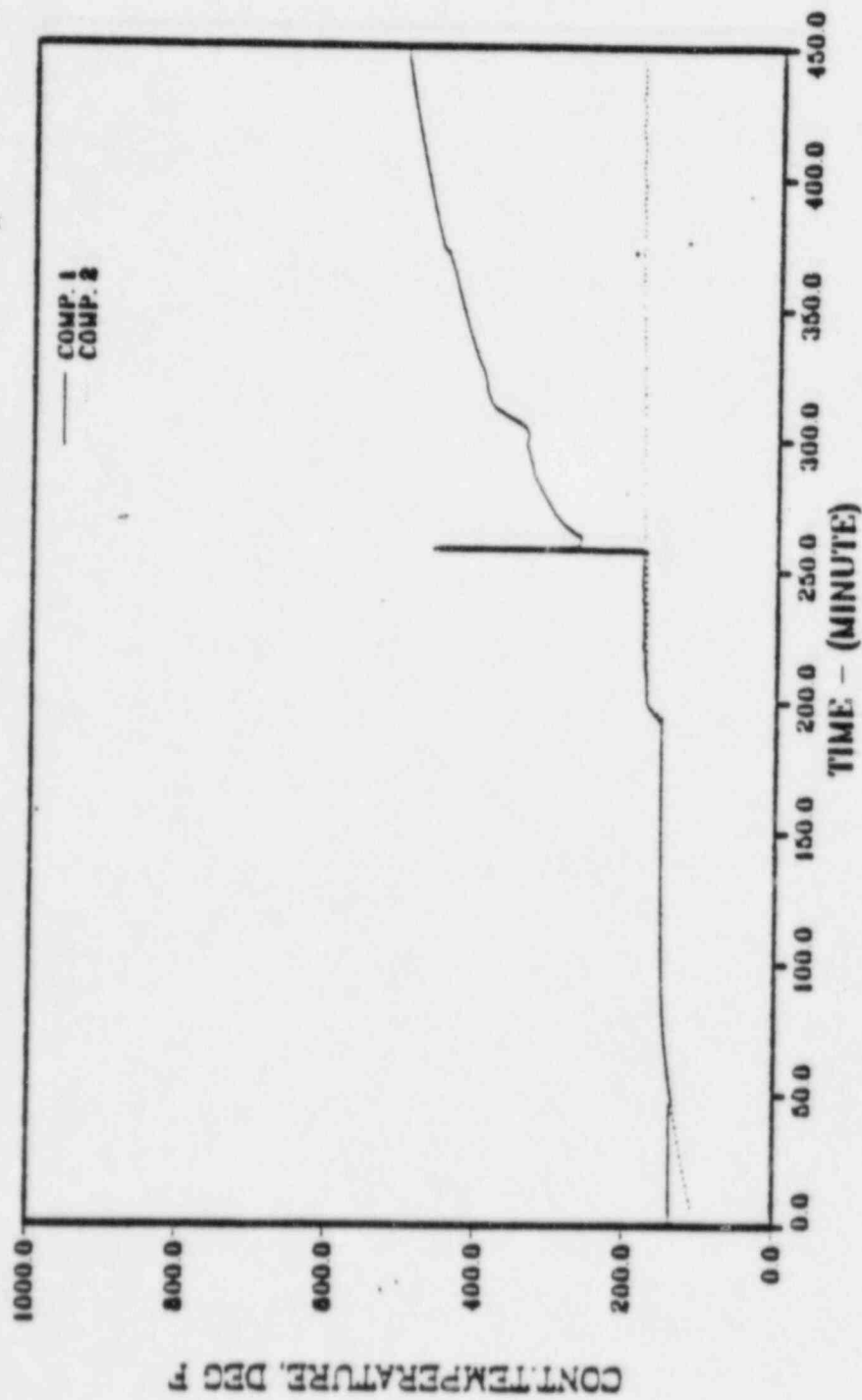


Figure III.33

1 F F

MKII STD PROB, MARCON CASE B

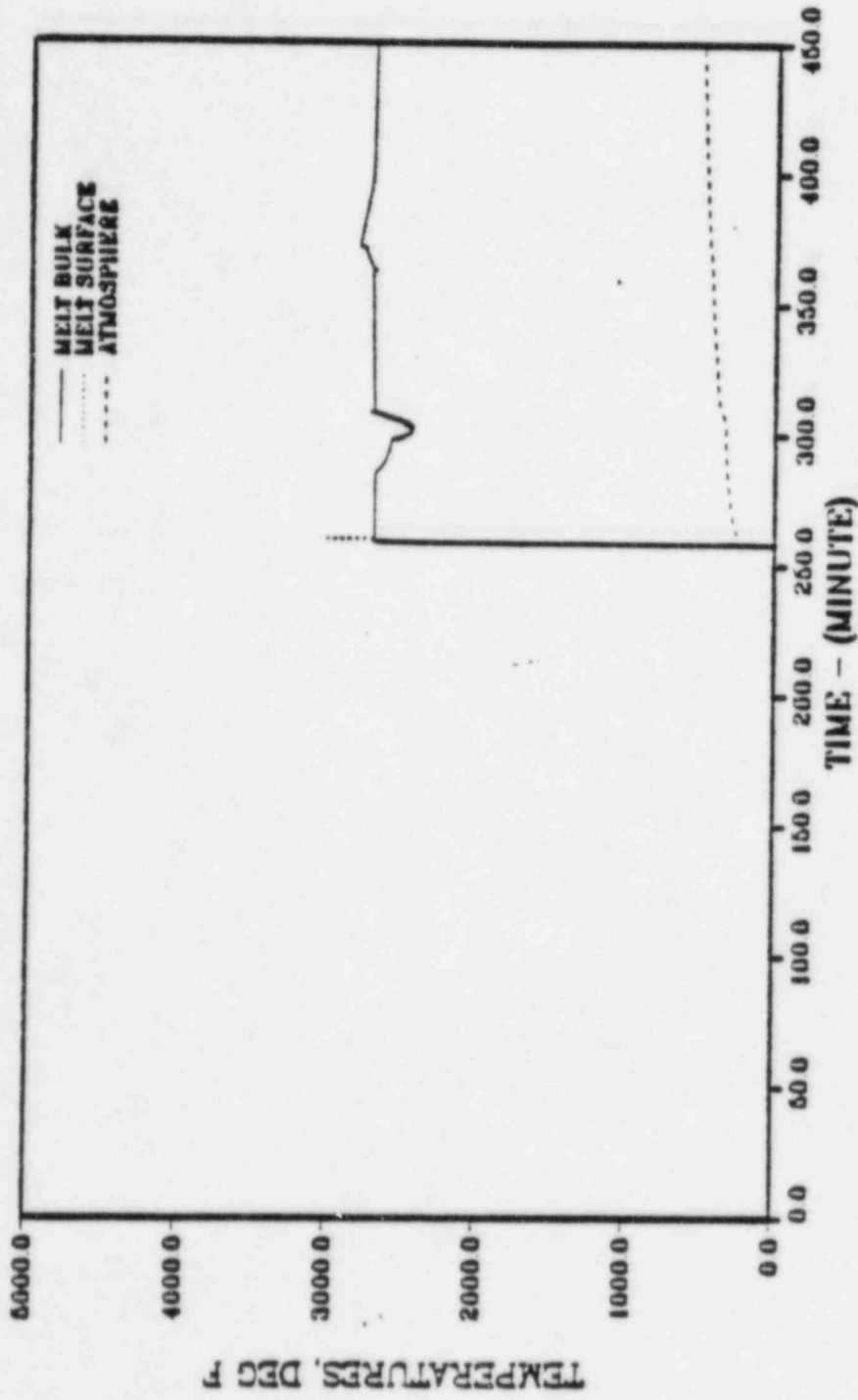


Figure III.34

TABLE III.2: SPECIFIC COMPARISONS

	<u>Drywell*</u> <u>Pressure</u> <u>(psia)</u>	<u>Peak</u> <u>Temperature</u> <u>(°F)</u>	<u>Vertical*</u> <u>Penetration</u> <u>(m)</u>
1. Type of concrete			
Case 5	136.1	832	0.42
Case 7	109.5	658	0.52
Case 6	99.7	691	0.53
Case 8	82.3	497	0.66
2. Free H ₂ O			
Case 5	136.1	832	0.42
Case 5A	147.7	837	0.43
Case 7	109.5	658	0.52
Case 7A	134.7	703	0.61
3. Corium temperature and spread			
Case 5	136.1	832	0.42
Case 6	99.7	691	0.53
Case 7	109.5	658	0.52
Case 8	82.3	497	0.66
4. Steel in corium			
Case 5	136.1	832	0.42
Case 5B	135.4	788	0.46

* 3 hours after vessel failure

REFERENCES

1. M. Silverberg. "Completion of BWR MARK I, MARK II Standard Problems." USNRC Memorandum January 20, 1984.

APPENDIX A

SUMMARY OF MARCON MODELS

The interaction of the core debris with the concrete containment basemat is modeled in the MARCH 2 code using a core concrete interaction code called INTER. The INTER code was developed as a preliminary tool and the more recent and detailed CORCON code has been developed to replace INTER. MARCON is a version of MARCH 2 in which the INTER code has been replaced by CORCON MOD2. CORCON was developed with a larger experimental data base, uses more realistic phenomenology and more mechanistic models, and has improved numerical techniques.

The combined MARCH-CORCON version called MARCON was created by deleting the subroutine INTER from MARCH, inserting CORCON as a subroutine, and adding an interfacing subroutine named MARCON. The containment subroutine MACE in the MARCH code is executed interactively with the CORCON code in the same manner that MACE and INTER are executed in MARCH.

Certain information is passed back and forth between MARCH and CORCON through subroutine MARCON. MARCON converts the data to the correct form and units. The following list of data is passed between the programs through MARCON.

MARCH to CORCON Information

1. CORCON initialization data
 - a. CORCON start time
 - b. Melt temperatures
 - c. Mass of melt by species
 - d. Atmosphere data (not currently used by CORCON)
2. Pressure
3. Atmosphere temperature
4. Effective emissivity and temperature of the surroundings
5. Melt surface heat transfer coefficient

CORCON to MARCH Information

1. Time step size
2. Mass flow rates and enthalpies of the gases released by the melt

3. Melt surface convection and radiation heat transfer rates

4. Concrete decomposition data

The interfacing subroutine MARCON contains models necessary to link the two programs. For PWR calculations, the models include reactor cavity thermal radiative heat transfer, reactor cavity pool boiling, concrete ablation above the melt after the reactor cavity dries out, and heat transfer to the remaining containment. For BWR calculations, the models include a melt surface heat transfer coefficient and a concrete degassing model for concrete structures in the drywell compartment. Fission product loss from the melt is calculated using subroutine FPLOSS from MARCH in the same way that FPLOSS was used in the MARCH-INTER code.

PWR MODELS

After vessel head failure in a PWR meltdown accident the melt will pool in the bottom of the reactor cavity. Any water still in the reactor cavity will collect above the melt pool until it is completely boiled away. After dryout, the reactor cavity atmosphere will heat up until it comes into thermal equilibrium with its surroundings. Since the reactor cavity has a relatively small volume compared to the total containment volume and a small atmospheric heat capacity relative to the melt surface heat transfer rates and the surrounding concrete wall has a low thermal conductivity, the atmospheric temperature will heat up to thermal equilibrium rapidly.

The reactor cavity in MARCON is modeled for conditions when a water pool exists and atmospheric thermal equilibrium after dryout. The transition between these two conditions is assumed to happen instantaneously. The reactor cavity pressure is assumed equal to the MARCH calculated drywell containment volume absolute pressure.

The before-dryout models are relatively simple. The surrounding and atmospheric temperatures needed by CORCON are taken to be the temperature of the water pool. The surrounding emissivity is set equal to 0.9. A film boiling correlation is used for the melt surface heat transfer coefficient. The energy from the melt surface convective and radiative heat transfer and the enthalpies of the gases released by the melt go into heating up and boiling the water pooled above the melt. The released gases are cooled down to the temperature of the water and the water vapor released by the melt will be condensed if the water pool is subcooled. If the water pool is saturated and the reactor cavity depressurizes, then flashing in the water is calculated.

The PWR reactor cavity after dryout is modeled as a right circular cylinder with the bottom surface representing the core melt, the cylinder representing the concrete wall, and the steel reactor vessel lower head is represented by the top surface. These three surfaces and the reactor cavity atmosphere are the four components in the thermal radiation heat transfer model. The atmosphere is assumed at thermal equilibrium with its surroundings. The concrete surface temperature is assumed to be equal to the concrete ablation temperature used by CORCON. The radiative view factor matrix is determined from the diameter and height of the cylinder using a relationship for the view factor between parallel circular disks of the same diameter with centers along the same normal.

Thermal radiation is both absorbed and emitted by the reactor cavity atmosphere. The atmosphere will consist primarily of N_2 , O_2 , H_2 , H_2O , CO , and CO_2 gases and aerosols. The N_2 , O_2 , and H_2 gases with symmetric diatomic molecules are transparent to infrared radiation. The heteropolar gases, H_2O , CO , and CO_2 , absorb and emit significantly. The aerosols are considered to have a significant effect on the absorption and emission characteristics of the atmosphere.

The radiation heat transfer model consists of a system of 10 equations and 10 unknowns. The simultaneous solution of these equations yield the surface heat fluxes for each surface and the temperature of the reactor cavity atmosphere and the steel lower vessel head.

A simple model is included which accounts for thermal radiation leaving the reactor cavity directly through an opening in the concrete wall or vessel to the containment. The user specifies in the input data, an area for this opening. The area is treated as a low temperature black body surface such that all the thermal radiation flux incident upon the area is transferred from the reactor cavity to the drywell atmosphere. The emission by this area is assumed negligible. The model is more valid for small areas.

An option for the radiative heat transfer model is included such that the user can input a constant heat flux for heat conducted through the steel vessel. This input flux specifies the net radiative flux for the vessel and allows the calculation of the steel vessel surface temperature. The conducted energy is added directly to the drywell atmosphere. If this option is not needed, the flux can be input as zero for the adiabatic condition.

The surface heat transfer models in CORCON require an atmosphere temperature and a convective heat transfer coefficient to calculate the surface convective heat transfer

rate, and an effective surrounding temperature and emissivity to calculate the surface radiative heat transfer rate. The atmosphere temperature is the temperature of the reactor cavity as calculated by the radiative heat transfer model. The convection heat transfer coefficient is calculated using a turbulent natural convection correlation. The surrounding emissivity is an effective average of the emissivities of the concrete wall, steel vessel and atmosphere based upon the radiative heat transfer to the melt surface. The surrounding temperature is calculated to give the same net radiative heat transfer flux from the melt surface for the parallel planes model used by CORCON as the flux calculated by the four-component radiative heat transfer model. The drywell atmosphere pressure is used for the reactor cavity pressure.

Energy transferred to the concrete walls above the melt after the reactor cavity dries out is assumed to decompose or ablate the concrete. The model assumes that all the net energy absorbed leads to ablation. The mass of concrete ablated is proportional to the energy absorbed. The gases produced by the concrete ablation include CO_2 and H_2O and are proportional to the amount of concrete ablated. The proportionality constants are obtained from CORCON models. The gases produced are added to the drywell atmosphere at the temperature of the reactor cavity and to the reactor cavity atmosphere at the concrete ablation temperature.

The sump in some PWR calculations will overflow into the reactor cavity after the reactor cavity has dried out. When this happens, radiation heat transfer vaporizes the overflow water and adds the vapor to the gases going into the containment.

The present version of MARCON uses the MARCH code subroutine FPLOSS to calculate the melt fission product loss in the same way that FPLOSS was used in the MARCH-INTER code. Subroutine FPLOSS was written to model the loss of volatile fission products from the melted fuel. The decay heat of the lost fission products is added to the decay heat of the fission product inventory in the containment. There is, however, a mismatch between the fission products added to the atmosphere by FPLOSS and those that are calculated to be lost from the molten debris by CORCON. An appropriate selection of the vaporization release parameter (IFPSV) in the MARCH input has minimized the differences.

BWR MODELS

The melt after vessel heat failure in a BWR meltdown accident will pool on drywell compartment floor. The floor is assumed dry at the time. The spreading of the melted fuel or the diameter of the corium pool will depend upon factors such as the melt temperature and primary system pressure at vessel failure time.

In the BWR models, the thermal radiative and convective heat transfer from the top of the debris is transferred to the drywell atmosphere on the premise that the drywell atmosphere will be opaque due to high aerosol densities, yet well-mixed due to convective flows. This results in significantly higher drywell atmosphere temperatures. The radiative heat transfer from the drywell atmosphere to passive heat sinks is modeled. A model is included for degassing of unlined drywell concrete which will result from the higher structure temperatures.

The surface heat transfer models in CORCON require an atmosphere temperature and a convection heat transfer coefficient to calculate the surface convection heat transfer rate, and an effective surrounding temperature and emissivity to calculate the surface radiation heat transfer rate. The drywell atmosphere temperature is used by CORCON for both the surrounding and the atmosphere temperatures. A turbulent natural convection correlation is used to calculate the convective heat transfer coefficient. The surrounding emissivity is fixed at 0.9. CORCON uses the drywell atmosphere pressure.

A model for degassing unlined concrete is used in the BWR calculations for degassing drywell concrete. This model is contained in subroutine DEGAS which is called from subroutine MARCON and uses data input in namelist NLSLAB and temperatures calculated by subroutine SLAB. The model calculates the H₂O and CO₂ degassing rates for unlined concrete slabs found in the drywell compartment (IVL(I)=NCAV). The gases are then added to the drywell atmosphere with enthalpies corresponding to the slab surface temperatures.

The degassing rates for H₂O and CO₂ gases at each time step are given by the following equations:

$$W_x = \frac{\rho_x}{(T_{xhi} - T_{xlo}) \Delta t} \sum_{k=1}^{NSLAB} k^A \sum_{i=1}^{NN} \Delta T_{i,k} \Delta x_{i,k}$$

$$\Delta T_{i,k} = \begin{cases} T_{i,k} - T_{max_{i,k}} & \cdot T_{i,k} > T_{max_{i,k}} \\ 0 & \cdot T_{i,k} \leq T_{max_{i,k}} \end{cases}$$

W_x = the degassing rate for either H_2O or CO_2 .
lbm/min
 ρ_x = density of releasable H_2O or CO_2 gas in the
concrete. lbm/ft³
 T_{xhi} = the temperature at which all releasable H_2O or
 CO_2 is released. °F
 T_{xlo} = the temperature at which releasable H_2O or
 CO_2 starts to release. °F
 Δt = the time step size, min
 A_k = surface area of slab k, ft²
 $\Delta x_{i,k}$ = node spacing of node i in slab k, ft
 $NSLAB$ = number of slabs
 NN_k = number of nodes in slab k
 $T_{i,k}$ = the temperature of node i of slab k, °F
 $T_{m_{i,k}}$ = the maximum temperature that slab i,k has reached
during the accident sequence. °F

This rather simple model assumes that the degassing occurs uniformly over the temperature range T_{xhi} to T_{xlo} . The gases are released only when a node temperature exceeds its previous maximum temperature. The energy necessary to release the gases must be included in the concrete specific heat.

The loss of volatile fission products from the melted fuel are calculated using subroutine FPLOSS of MARCH. This is the same calculation as was discussed in the PWR models.

MARCON INPUT AND OUTPUT

The MARCON input data consists basically of the usual MARCH input data with the CORCON input data added directly after namelist NLINTR. The usual NLINTR data is still read but not used. However, a few of the NLINTR variables have been redefined and are used by subroutine MARCON. Several variables which are now calculated by MARCH have been deleted from the CORCON data. A new block of output data with a user controlled output frequency is printed by MARCON in both metric and engineering units along with a variable description.

APPENDIX B

Mark I

Standard Problem

Input Deck

Case 1

```

*// .....
*//
*// MAKE UPDATES TO MARCH AND MARCH .....
*// .....

```

```

*COMPILE MARCH.DEGAS
*COMPILE MARCH.VSCRIPT
*IDENT VARPLTS
*F MARCH.129
*CALL INTRPL
*F MARCH.151

```

```

ZPLOTZ(1)=0.0
ZPLOTZ(2)=0.0
ZPLOTZ(3)=0.0
ZPLOTZ(4)=0.0
ZPLOTZ(5)=0.0
ZPLOTZ(6)=0.0
ZPLOTZ(7)=0.0
ZPLOTZ(8)=0.0
ZPLOTZ(9)=0.0
ZPLOTZ(10)=0.0
ZPLOTZ(11)=0.0
ZPLOTZ(12)=0.0
ZPLOTZ(13)=0.0
ZPLOTZ(14)=0.0
ZPLOTZ(15)=0.0
ZPLOTZ(16)=0.0
ZPLOTZ(17)=0.0
ZPLOTZ(18)=0.0
ZPLOTZ(19)=0.0
ZPLOTZ(20)=0.0
ZPLOTZ(21)=0.0
ZPLOTZ(22)=0.0
ZPLOTZ(23)=0.0
ZPLOTZ(24)=0.0
ZPLOTZ(25)=0.0
ZPLOTZ(26)=0.0
ZPLOTZ(27)=0.0
ZPLOTZ(28)=0.0
ZPLOTZ(29)=0.0
ZPLOTZ(30)=0.0
ZPLOTZ(31)=0.0
ZPLOTZ(32)=0.0
ZPLOTZ(33)=0.0
ZPLOTZ(34)=0.0
ZPLOTZ(35)=0.0
ZPLOTZ(36)=0.0
ZPLOTZ(37)=0.0
ZPLOTZ(38)=0.0
ZPLOTZ(39)=0.0
ZPLOTZ(40)=0.0
ZPLOTZ(41)=0.0
ZPLOTZ(42)=0.0
ZPLOTZ(43)=0.0
ZPLOTZ(44)=0.0
ZPLOTZ(45)=0.0
ZPLOTZ(46)=0.0
ZPLOTZ(47)=0.0
ZPLOTZ(48)=0.0
ZPLOTZ(49)=0.0
ZPLOTZ(50)=0.0
ZPLOTZ(51)=0.0
ZPLOTZ(52)=0.0
ZPLOTZ(53)=0.0
ZPLOTZ(54)=0.0
ZPLOTZ(55)=0.0
ZPLOTZ(56)=0.0
ZPLOTZ(57)=0.0
ZPLOTZ(58)=0.0
ZPLOTZ(59)=0.0
ZPLOTZ(60)=0.0
ZPLOTZ(61)=0.0
ZPLOTZ(62)=0.0
ZPLOTZ(63)=0.0
ZPLOTZ(64)=0.0
ZPLOTZ(65)=0.0
ZPLOTZ(66)=0.0
ZPLOTZ(67)=0.0
ZPLOTZ(68)=0.0
ZPLOTZ(69)=0.0
ZPLOTZ(70)=0.0
ZPLOTZ(71)=0.0
ZPLOTZ(72)=0.0
ZPLOTZ(73)=0.0
ZPLOTZ(74)=0.0
ZPLOTZ(75)=0.0
ZPLOTZ(76)=0.0
ZPLOTZ(77)=0.0
ZPLOTZ(78)=0.0
ZPLOTZ(79)=0.0
ZPLOTZ(80)=0.0
ZPLOTZ(81)=0.0
ZPLOTZ(82)=0.0
ZPLOTZ(83)=0.0
ZPLOTZ(84)=0.0
ZPLOTZ(85)=0.0
ZPLOTZ(86)=0.0
ZPLOTZ(87)=0.0
ZPLOTZ(88)=0.0
ZPLOTZ(89)=0.0
ZPLOTZ(90)=0.0
ZPLOTZ(91)=0.0
ZPLOTZ(92)=0.0
ZPLOTZ(93)=0.0
ZPLOTZ(94)=0.0
ZPLOTZ(95)=0.0
ZPLOTZ(96)=0.0
ZPLOTZ(97)=0.0
ZPLOTZ(98)=0.0
ZPLOTZ(99)=0.0
ZPLOTZ(100)=0.0

```

```

*F MARCH.409
ZPLOTZ(70)=TFPLH
*F MARCH.433
ZPLOTZ(20)=TFPLHT
*F MARCH.547
ZPLOTZ(20)=TFPLHT
*F MARCH.1541
ZPLOTZ(3)=WCDO(1)
ZPLOTZ(4)=WCDO(2)
*F MARCH.401
ZPLOTZ(13)=CWMQ
ZPLOTZ(5)=CWDQ
ZPLOTZ(12)=WHRK
ZPLOTZ(28)=WHRK
ZPLOTZ(29)=GWL
ZPLOTZ(16)=GGHA
ZPLOTZ(6)=GTX
ZPLOTZ(7)=TGASF
ZPLOTZ(8)=TINTX
ZPLOTZ(9)=GGINTX
ZPLOTZ(10)=1.80*TA-459.67
ZPLOTZ(11)=WH2OWL
*F MARCH.431
ZPLOTZ(1)=150.0-ORINTR
ZPLOTZ(2)=150.0-OZINTR
ZPLOTZ(14)=FPLKV
*F SLAB.30
*CALL INTRPL
*F SLAB.156
XMIT=0.0
XHOT=0.0

```

YUOTEXHUI-HOT(1)

1 CONTINUE

ZPLOTZ(14)=XHIT

ZPLOTZ(15)=-XHOT

*/

*/ HARDWARE OF INITIAL DERRIS COMPOSITION

IDENT HARDWIR

IDENT MARCON.35

-----TEMPERATURE OF DERRIS

TOI=2550.0

-----WEIGHT OF FE2 (KG)

CONINP(3)=8394.

-----WEIGHT OF UO2 (KG)

CONINP(20)=127000.

-----WEIGHT OF ZRO2 (KG)

CONINP(21)=9150.

-----WEIGHT OF C222

CONINP(22)=2545.

-----WEIGHT OF FE (KG)

CONINP(41)=36974.

-----WEIGHT OF CR (KG)

CONINP(42)=10250.

-----WEIGHT OF NI (KG)

CONINP(43)=6033.

-----WEIGHT OF ZR (KG)

CONINP(44)=45382.

*/

*/ HARDWARE EMISSIVITY FOR THE POOL TO THE SURROUNDINGS

IDENT MARCON.35

ESUR=0.9

```

MILCOON 3.2 MKI STANDARD PROBLEM (TQWV), CASE 1
MILD STEEL CONCRETE
CHTFL 0 DRYWALL EL002 DRYBESTL WETBESTL WETWALL DOWNCOM WWC01
MISC.S.S.
SCHEMATIC
CHECK=0, CPSTP=190., IS=10, PRST=500.00, TRST=450.00,
SEND
$NLHAR
ATTVE=0.0,
DTINTL=0.1, IBLOF=0, IBLOI=1, IBLOP=20,
IBLOK=1, IBLOK=1, IBLOK=1, IBLOK=1,
IECXX=0, IFPSM=3, IFPSV=3, IPOTL=7,
ISOB=0, ITRAV=1, IUE=0, IYD=0, VINTP=1,
NPAIRL=0,
TAP=1.05125,
SEND
$NLMTI
EW(1)=200+0.0,
T(1)=200+0.0,
W(1)=200+0.0,
SEND
$NLSTAR
DXY(1)=490.0,145.0,1+0.0,
OTDY(1)=3+0.0,1.0,
HC(1)=0.1200,0.6500,3+0.0,
WIF(1)=4+0.0,
TW(1)=2+1,2,1,
IVR(1)=2+1,2,1,
MAT1(1)=1,2,1,1,
MAT2(1)=1,2,1,1,
NMAT=2,
NN01(1)=5,7,5,5,
NN02(1)=4+0,
N00(1)=6,7,7,9,38,
NSLAB=4,
PC02WL=0.0,
PC27WL=10.17,
SAREA(1)=18.84,13529.0,17350.3,4040.0,
TC(1)=26.0,0.42,3+0.0,
TCH=1200.0,
TCL0=700.0,
TEMP(1)=32+135.0,3+104.0,5+135.0,
TWHI=500.0,
FWL0=200.0,
Y(1)=0.0,0.01,03.0,05,09175,
Y(6)=0.0,01,02,03,05,06,08,11,14,17,21,25,30,
35,40,45,50,55,60,77,80,10,1.0,1.2,1.4,
1.6,1.8,
Y(33)=0.0,0.01,02,04,0625,
Y(38)=0.0,0.01,02,03,04166667,
SEND
$NLECC
ICMG=10.0, CSPRC=0.144, OTSUBX=-100.0, ECCRC=7.144,
NPUMP=0, P(1)=6+0.0,
PACMG=0.0, PWH=1080.0, PLH=10.0, PSIS=0.0, PUHIO=7, RWSTX=6.1452E6,
PWL0=0.0, PLL0=0.0, PL7(1)=6+0.0, PSL0=0.0,
STR(1)=6+1.56,
STPHH=1.56, STPLH=1.56, STPSIS=1.56,
TACM=3+0.02,
TH(1)=6+1.56,
TWHH=1.56, TWHL=1.56, TWSIS=1.56, TRWSTX=90.0,
TUM(1)=0.0, UHIO=0.0,
WEC(1)=6+0.0,
WHH1=-823.5, WLH1=-6668.8, WSIS1=0.0,

```



```

$NLFCY
EQR=0.0, ETP1R=0.0, ETS1R=0.0, EWPR=0.0, EWSR=0.0,
SEND
$NLCSX
SQR=0.0, STP1R=0.0, STS1R=0.0, SWPR=0.0, SWSR=0.0,
SEND
$NLCOOL
CQR=0.0, CTPR=0.0, CTSR=0.0, CWPR=0.0, CWSR=0.0,
CVAR=0.0,
JC00L=0, NC00L=0, PC00L=0.0, PUFF=0.0, GR00L=0, TC00L=0.0,
SEND
$NLFACE
IPF(1)=1647.3, 10940.3, 0.0, 0.0,
AVBRK=0.0,
C1(1)=1.0F6,
C2(1)=5.83,
C3(1)=4.0,
C4(1)=0.0,
CVBRK=0.0,
OCF=10000., OCFICE=1.0, OTQ=.35, OTPVC=9.0, OTS=5.23,
FALL=1.0, FSPR=0.0, FMAXY=290.0,
IBETA=0, ICECUR=-1, IDRY=-1, IVENT=0, IWET=2,
J2V1=2, J2V2=1, J2V3=2, KT(1,1)=0, KT(1,2)=1,
KT(2,1)=1, KT(2,2)=0,
N=1,
NC(1)=1,
NCAY=1, NCUM=2, NC0V1=1, NC0V2=1,
NC(1)=2,
NCMB=2, NCMB=2,
NT(1)=-7,
OEF35(1,1)=0.0,
PO=14.7, STPEC=1.26, STP3PR=1.26,
TEWPO(1)=135.0, 104.0, 9.0, 0.0,
TICE=20.0, TPOUL=104.0, TSTM=135.0, TVNFI=0.0, TVNIZ=0.0,
TATR=190.0, TATR2=130.0,
VC(1)=159000.0, 119000.0, 0.0, 0.0,
VCAY=133.7, VCRY=933.7, VFLP=470., VTRUG=257700.0,
WICE=0.0, WPOOL=7.79E+6, WMAKS=0.0, WVMAX=612610.0,
SEND
$NLBURN
BK(1,1)=0.0, BK(1,2)=10.5, BK(2,1)=30.5, BK(2,2)=0.0,
CMUN=0.15, CMH=0.157, CMH2=0.133, CMLO=0.0003,
CMQ=0.148, CMUP=0.125, CMXY=7.143,
H2OIST(1)=174.0, 0.0, 0.0, H2ON=0.79,
H2H(1)=0.12, H2H2=0.05, H2LO=1.0701,
H2ON=0.08, H2UP=0.041, H2VJ=352.8,
H2VX=11650.0, H2XY=0.09, H2Z=0.55,
H2OXY=0.05, HUM(1)=0.20, 1.00, 4.0, 0.0,
IBURN=0,
IBURNJ=1, IBURNL=1, IBURNM=0, IGWTE=10.0,
WCO(1)=10.0, 0.0,
WCHO(1)=10.0, 0.0, WHYO(1)=10.0, 0.0,
WNT(1)=10.0, -1.0, WXY(1)=10.0, 0.0,
SEND
$NLRAIL
ARR(1)=16.0, 0.0, ARR(1)=16.0, -1.0,
ARRK=0.0, ACCR=108.7,
ARR(1)=245., 1911., 2700., 18471., 70., 5800., 1000.,
ANSK=0.0,
ARSTR(1)=2.32, 7.56, 3.745., -.75, -33.8, -14.0,
ASR(1)=16.0, -1.0, ASRV=0.0,
ATOT=154.,
CM(1)=2055., 2755., 8363., 6643., 2763., 6636., 23293.,
CLAD=0.04564, D=.34029, DC=15.59,

```

```

OF=.03417, OH=.0459, OPART=.0016,
OTKXXX=10.0, OTPN=-5.0, OTPNTB=5.0,
OWEAT=200.0.0,
OUO2=.03417,
P12=.0.445,
FZ(1)=.47,.55,.64,.74,.85,.97,1.1,1.21,1.29,1.34,1.38,1.4,
1.19,1.16,1.1,1.1,1.15,1.18,1.01,.95,.94,.73,.6,.37,
FCOL=.800, FLD=3.4, FPDV(1)=0.05,0.10,0.20,0.65,
FQO2=.2772, FQOOP=.800, F4=0.7, F3=0.0, F11SG=0.0, F74C3=.177,
FZOCR=.333, FZOS1=.333, H=12.5, 40=52.1, HW=0.0,
F3FDC=1, F3FDS=1, F3FAY=1,
ICOM=0, IFP=2, IMC=0,
TORGMO=0,
IHR=1, IMWA=1, IMZ=100, ISAT=1, ISG=0,
ISTM=0, ISTG=0, KPOSSXX=7, MEL400=-1, MWORNI=1,
NOTM=100000, NOZ=-24, NOZOPP=12, VNT=48896, VR=47363,
VREL(1)=1.5,1.0,1.1,1.1,1.0, VZOL(1)=2.2,2.1,2.1,2.1,2.1,
PF(1)=1.18,1.17,1.15,1.15,1.11,1.06,.99,.98,.69,.62,
QPP=7.4, QSR(1)=16*-1.0,
PSETX=1120.0, PSG=1000., PVSL=1720.0,
Q23QU=200.0,
QPU1P1=0.0, QPU1P2=0.0, QZERQX=8.99259,
QWCCU=68.78, Q1=1, Q2=10, Q23QU=0.3,
TAFW=100.0, TALF1=1.210, TALF2=1.210,
TREL1=16*1.05, TCR4H=10000.0,
TC4V=525.0, TCX=0.0, TFAILX=706.0, TFEON=5+9.0, TFUS=9376.8,
T300=545.0, TAIL2=10000.0,
TM4FV=1.056, TMELT=4130.0,
TMELT(1)=1+1.056,
TMSG1=1.056, TMSG2=1.056, TMUP1=1.056, TMUP2=1.056, TMYBK=1.056, TPM=1.0,
TBM=1.056, TBMV=1.056, TBMV2=1.056, T2S=0.0,
TSR(1)=0.25,3+1.0,
TSGT(1)=0.0,3+1.0510,
TT(1)=4+545.,3+530.,
VEX(1)=10+0.17,
VOLPX=25818., VULSX=11340.,
WAFW=0.0, WATB=X=142710.,
WCST=1.12626, WOEN=5000.,
WFE2=3923.0, WMU1=0.0, WMU2=0.0,
WSETX=13980., WTRSG=0.7, X00=3.29E-6,
YR=0.0, YSRX=65.0, YR2=1.053, YLEG=23., YLEG2=1.053,
YSR(1)=16*-1.0, YSR(1)=16*-1.0, YSRV=65.00, YF=0.0,
SEND
SNLRAO
ECRQSE=.7, ELONG=.215, ESTRUE=.5, EWAT=.99, FAXC=0, ICONV=1,
TBAO=0, TITCH=.04183, W74R=7825.1, VIEW=2.0,
TFAILL=10000.0,
SEND
SNBWRIN
ALCBO=0.40625, OMGXCH=0.014543, F124X=0.1, F12CB=0.1,
F224X=0.1, F22CB=0.1, F22Q=0.1, F4RIV=83.177,
FAROUT=60.666, FBP=0.13, F4XCH=0.25, FRJ4X=0.25,
T4W=0, IMRBOX=1, IM4ROX=1, IM4CB=1, M4QXS=764,
NCBLAO=145, PBOX=1.70497, RHOCPC=56.62, RHOCPC=54.27,
T4ROX=175.0, T4CBO=3409.7, T4ELBX=3369.0,
TMELCB=2600.0, XROX=0.00667, XBOXZ1=8.333E-6,
XROXZ0=8.333E-6, XCB0=0.326, XCB00=3.33E-6,
XCB0SS=0.00675,
SEND
SNLHBAO
CONQ=8.0, CBH=20.915, E1=.8, E2=.5, FOPEN=0.0,
F-EAO=0.9, SIGF=50000.0,
T4ICK=0.713, TMLTXX=4110.0, T4KF=100.0,
WFEQXX=0.0, WGRIOX=66750., WHEAOX=73250.,

```


SEND
SNLWOT

ACAV=845.4,

CCN=5.16,

DB=0.25,

ELBAC=9421.,

THRT=0,

WVS=1,

TPGOLH=135.0,

IOBED=-1,

NSTOP=10003000,

PORO=0.4,

TCORH=120.0,

TMS=2600.0,

TQCH=0.0,

WTR=1.0,

SEND

SNLINTR

CAYCYX=0.135,

CCCYXX=0.394,

DEUSCY=2.52,

DBRTN=1000.0,

HTYXXY=0.5,

EPSI(1)=0.5,0.5,8*0.0,

ECYXX=0.470,

ECYXX=0.150,

ECYXX=0.211,

FC4XXX=0.030,

FIDPEN=0.5,

FRC4=1.0,

HTM=0.01,

WIO=0.01,

T11001,

T12001,

YFOS=2,

QAXXX=25000.,

RBRXXX=0.135,

QOXXX=500.0,

TAUL=0.5,

TAUS=5.0,

TEPS(1)=0.0,3.6E7,8*0.0,

TDC=1750.0,

TIC=140.0,

TE=2.710E4,

TDBTN=300.,

WALL=1.0E3,

ZF=1000.0,

SEND

MARK I STD PROJ, CASE 1

0 0 2 0 0 1 1 0 60 0 0 1 1 0

30.0

27000.

200000.

0.0

0.0

1.5

140.

1750.

0.5

0.1

6.5

1.50

10

10

5

CAC03

0.200

CA(OM)2

0.150

ST03

0.010

H2OEVAR

0.030

AL703

0.010

2520.0

1690.0

1375.0

140.02

3227.

7

TIMETIME

2

2

0.0

.50

1.0E+6

.50

0.0

.50

1.0E+6

.50

APPENDIX B

Mark II

Standard Problem

Input Deck

Case 5

UPDATE

UNLABELED CLOPL

IDENT

VARPLTS

UPDATE

X4IT=0.0

X4DT=0.0

DO 1 L=1, NSLABL

Y4IT=X4IT+HIT(L)

X4DT=X4DT+HDT(L)

1 CONTINUE

ZPLCTZ(14)=X4IT

ZPLCTZ(15)=X4DT

*/

*/

WADNIDE 7F INITIAL DEBRIS COMPOSITION

***** IDENT HAROWIP

***** *INSTRUMENTATION

C-----TEMPERATURE OF OBRIS

TJ1=2550.0

C-----WEIGHT OF PED (KG)

CONINP(3)=12250.

C-----WEIGHT OF UOZ (KG)

CONINP(20)=127000.

C-----WEIGHT OF ZP02 (KG)

CONINP(21)=9180.

C-----WEIGHT OF ZP03

CONINP(22)=2459.

C-----WEIGHT OF PE (KG)

CONINP(41)=41420.

C-----WEIGHT OF CR (KG)

CONINP(42)=4000.0

C-----WEIGHT OF HI (KG)

CONINP(43)=4440.

C-----WEIGHT OF ZP (KG)

CONINP(44)=45360.

*/

*/ HAROWIP SENSITIVITY FOR THE POOL TO THE SURROUNDINGS

*INSTRUMENTATION

***** IDENTIFICATION / CONTROL CARDS

YANK000 *CHECKING CRAY

YANK001 *CHECKING DLT

YANK002 *YANKDECK THRTN

YANK003 *YANKDECK EIGHTN

YANK004 *YANKDECK SIXTN

YANK005 *YANKDECK VTR40

YANK006 *YANKDECK VTR4L

YANK007 *YANKDECK LINRIT

YANK008 *YANKDECK CRRECT

YANK009 *YANKDECK DATA

YANK010 *YANKDECK FORML

YANK011 *YANKDECK MATN

YANK012 *YANKDECK HIC000

YANK013 *YANKDECK HIC001

YANK014 *YANKDECK THRTN

YANK015 *YANKDECK ALL

YANK016 *YANKDECK PASSIN

YANK017 *YANKDECK 4TR400

YANK018 *YANKDECK 4TR401

YANK019 *YANKDECK RAYCRC

YANK020 *YANKDECK RAYJCT

YANK021 *YANKDECK QDOO

YANK022 *YANKDECK CIRCL

YANK023 *YANKDECK PALANC

YANK024 *YANKDECK RAYTOR

YANK025 *CALL TECHLIST

2000 2001 2002 2003 2004 2005 2006 2007 2008 2009 2010 2011 2012 2013 2014 2015 2016 2017 2018 2019 2020 2021 2022 2023 2024 2025 2026 2027 2028 2029 2030 2031 2032 2033 2034 2035 2036 2037 2038 2039 2040 2041 2042 2043 2044 2045 2046 2047 2048 2049 2050 2051 2052 2053 2054 2055 2056 2057 2058 2059 2060 2061 2062 2063 2064 2065 2066 2067 2068 2069 2070 2071 2072 2073 2074 2075 2076 2077 2078 2079 2080 2081 2082 2083 2084 2085 2086 2087 2088 2089 2090 2091 2092 2093 2094 2095 2096 2097 2098 2099 2100 2101 2102 2103 2104 2105 2106 2107 2108 2109 2110 2111 2112 2113 2114 2115 2116 2117 2118 2119 2120 2121 2122 2123 2124 2125 2126 2127 2128 2129 2130 2131 2132 2133 2134 2135 2136 2137 2138 2139 2140 2141 2142 2143 2144 2145 2146 2147 2148 2149 2150 2151 2152 2153 2154 2155 2156 2157 2158 2159 2160 2161 2162 2163 2164 2165 2166 2167 2168 2169 2170 2171 2172 2173 2174 2175 2176 2177 2178 2179 2180 2181 2182 2183 2184 2185 2186 2187 2188 2189 2190 2191 2192 2193 2194 2195 2196 2197 2198 2199 2200 2201 2202 2203 2204 2205 2206 2207 2208 2209 2210 2211 2212 2213 2214 2215 2216 2217 2218 2219 2220 2221 2222 2223 2224 2225 2226 2227 2228 2229 2230 2231 2232 2233 2234 2235 2236 2237 2238 2239 2240 2241 2242 2243 2244 2245 2246 2247 2248 2249 2250 2251 2252 2253 2254 2255 2256 2257 2258 2259 2260 2261 2262 2263 2264 2265 2266 2267 2268 2269 2270 2271 2272 2273 2274 2275 2276 2277 2278 2279 2280 2281 2282 2283 2284 2285 2286 2287 2288 2289 2290 2291 2292 2293 2294 2295 2296 2297 2298 2299 2300 2301 2302 2303 2304 2305 2306 2307 2308 2309 2310 2311 2312 2313 2314 2315 2316 2317 2318 2319 2320 2321 2322 2323 2324 2325 2326 2327 2328 2329 2330 2331 2332 2333 2334 2335 2336 2337 2338 2339 2340 2341 2342 2343 2344 2345 2346 2347 2348 2349 2350 2351 2352 2353 2354 2355 2356 2357 2358 2359 2360 2361 2362 2363 2364 2365 2366 2367 2368 2369 2370 2371 2372 2373 2374 2375 2376 2377 2378 2379 2380 2381 2382 2383 2384 2385 2386 2387 2388 2389 2390 2391 2392 2393 2394 2395 2396 2397 2398 2399 2400 2401 2402 2403 2404 2405 2406 2407 2408 2409 2410 2411 2412 2413 2414 2415 2416 2417 2418 2419 2420 2421 2422 2423 2424 2425 2426 2427 2428 2429 2430 2431 2432 2433 2434 2435 2436 2437 2438 2439 2440 2441 2442 2443 2444 2445 2446 2447 2448 2449 2450 2451 2452 2453 2454 2455 2456 2457 2458 2459 2460 2461 2462 2463 2464 2465 2466 2467 2468 2469 2470 2471 2472 2473 2474 2475 2476 2477 2478 2479 2480 2481 2482 2483 2484 2485 2486 2487 2488 2489 2490 2491 2492 2493 2494 2495 2496 2497 2498 2499 2500 2501 2502 2503 2504 2505 2506 2507 2508 2509 2510 2511 2512 2513 2514 2515 2516 2517 2518 2519 2520 2521 2522 2523 2524 2525 2526 2527 2528 2529 2530 2531 2532 2533 2534 2535 2536 2537 2538 2539 2540 2541 2542 2543 2544 2545 2546 2547 2548 2549 2550 2551 2552 2553 2554 2555 2556 2557 2558 2559 2560 2561 2562 2563 2564 2565 2566 2567 2568 2569 2570 2571 2572 2573 2574 2575 2576 2577 2578 2579 2580 2581 2582 2583 2584 2585 2586 2587 2588 2589 2590 2591 2592 2593 2594 2595 2596 2597 2598 2599 2600 2601 2602 2603 2604 2605 2606 2607 2608 2609 2610 2611 2612 2613 2614 2615 2616 2617 2618 2619 2620 2621 2622 2623 2624 2625 2626 2627 2628 2629 2630 2631 2632 2633 2634 2635 2636 2637 2638 2639 2640 2641 2642 2643 2644 2645 2646 2647 2648 2649 2650 2651 2652 2653 2654 2655 2656 2657 2658 2659 2660 2661 2662 2663 2664 2665 2666 2667 2668 2669 2670 2671 2672 2673 2674 2675 2676 2677 2678 2679 2680 2681 2682 2683 2684 2685 2686 2687 2688 2689 2690 2691 2692 2693 2694 2695 2696 2697 2698 2699 2700 2701 2702 2703 2704 2705 2706 2707 2708 2709 2710 2711 2712 2713 2714 2715 2716 2717 2718 2719 2720 2721 2722 2723 2724 2725 2726 2727 2728 2729 2730 2731 2732 2733 2734 2735 2736 2737 2738 2739 2740 2741 2742 2743 2744 2745 2746 2747 2748 2749 2750 2751 2752 2753 2754 2755 2756 2757 2758 2759 2760 2761 2762 2763 2764 2765 2766 2767 2768 2769 2770 2771 2772 2773 2774 2775 2776 2777 2778 2779 2780 2781 2782 2783 2784 2785 2786 2787 2788 2789 2790 2791 2792 2793 2794 2795 2796 2797 2798 2799 2800 2801 2802 2803 2804 2805 2806 2807 2808 2809 2810 2811 2812 2813 2814 2815 2816 2817 2818

[illegible]

2	2				
2	2	2	2	2	2
2	2	2	2	2	2